Politecnico di Torino

MSc. Mechanical Engineering

A.a 2024/2025

23 July 2025

Ply-Level Damage Localization in Composite Structures Using Machine Learning

MSc. Thesis

Supervisors:
Dr. Marco Esposito
Prof. Marco Gherlone

Candidate:
Melih Eren Genç

Acknowledgements

Vorrei ringraziare sinceramente i miei supervisori, il Dott. Marco Esposito e il Prof. Marco Gherlone, per avermi introdotto al campo del monitoraggio strutturale(SHM) e per il prezioso supporto fornito durante tutto il percorso della tesi. Senza il loro sostegno questo lavoro non sarebbe stato possibile.

I would like to express my gratitude to my university, an institution that provided not only academic knowledge, but also a well-rounded education in patience, improvisation, and the noble struggle of securing a spot in the perpetually full study rooms.

From battling endless queues at the mensa (only to discover that the day's special is, once again, the infamous fish fingers), to navigating surprise public transport strikes and embracing last-minute all-nighters, the journey has been nothing short of eventful.

This thesis is not just the product of academic effort, but also of hallway brainstorming sessions, caffeine-powered nights, and mastering the delicate timing required to find a free desk before the library fills up at 8:01 a.m.

I am sincerely thankful for the education, the experiences, the insightful professors, and even the fish fingers. Without them, and without this university, this work would never have come to life.

Tüm yüksek lisans sürecim boyunca beni destekleyen ve yanımda duran aileme teşekkür etmem gerekiyor. Sabırlı bir şekilde bu uzun süreç boyunca desteklerini hiç esirgemediler. Tüm arkadaşlarıma, uzak veya yakın, birlikte geçirdiğimiz vakit ve bana kattıkları için teşekkür ederim. Ayrıca, dostum Yüksel Altay Aksoy'a geçtiğimiz üç yılda, en hafif tabirle bana yoldaşlık ettiği için müteşekkirim. Tez sürecimde yanımda bulunan, beni destekleyen ve bu sürecin çok daha kolay geçmesini sağlayan sevgilim Irmak'a da ne kadar teşekkür etsem azdır.

Son olarak, büyük saygı duyduğum, idolüm olan ve en çaresiz anlarımda karanlığın içinde bana yol gösteren; fiziksel olarak yanımda olmasa da her daim kalbimde ve ruhumda var olan kişiye de sonsuz minnet borçluyum. Borcunu asla ödeyemeyeceğimi bilsem de, minnettarlığımı ifade etmek ve herkese bir kez daha hatırlatmak adına buraya bir sözünü bırakıyorum.

"Umutsuz durumlar yoktur, umutsuz insanlar vardır. Ben hiçbir zaman umudumu yitirmedim."
— Mustafa Kemal Atatürk

Abstract

This study proposes a novel structural health monitoring (SHM) approach for detecting and localizing damage in composite materials. The developed system integrates spatial coordinate-based localization with ply-level damage identification. Sensor data are collected from the composite structure and processed through an ensemble of machine learning models designed to detect and localize damage with high precision. Three numerical case studies are presented to evaluate and compare the performance of different machine learning models. Additionally, a two-stage framework is introduced to improve robustness, allowing different models to be trained on distinct datasets and specialize in damage detection at various ply levels. The proposed SHM system demonstrates significant potential for real-time damage monitoring and localization, accurate remaining service life prediction, and integration with emerging smart material technologies.

Contents

List of Figures **3**

List of Tables **5**

1 Introduction **6**
1.1 Problem Statement 6
1.2 Aim and Scope of the Study 8
1.3 Structure of the Thesis 8

2 Literature Review **10**
2.1 Structural Health Monitoring (SHM) Systems 10
2.1.1 Concept of Structural Health Monitoring 10
2.1.2 Modal-driven and Data-driven SHM 11
2.1.3 Various Applications of Structural Health Monitoring 12
2.1.3.1 Displacement-Based Approach 13
2.1.3.2 Strain-Based Approach 13
2.1.3.3 Vibration-Based Approach 14
2.1.4 Summary of Relevant Work 18
2.2 Damage Detection with Machine Learning 20
2.2.1 Fundamentals of Damage Detection and Assessment 20
2.2.2 Supervised and Unsupervised Machine Learning 21
2.2.3 Applications of Machine Learning in Damage Detection 23
2.2.4 Summary of Relevant Work 26
2.3 Laminated Composite Structures 28
2.3.1 Defects and Damage Modes in Laminate Structures 28
2.3.2 Common Defects and Damage Detection 30
2.3.2.1 Delamination 30
2.3.2.2 Matrix Cracking 32
2.3.2.3 Fiber Breakage 34
2.3.2.4 Porosity 36
2.3.2.5 Fiber-Matrix Debonding 38
2.3.3 Summary of the Relevant Work 40

3 Theoretical Background and Methodology **42**

3.1 Displacement, Strain, and Stress Fields . . . 42
3.1.1 Displacement Field . . . 42
3.1.2 Strain Field . . . 44
3.1.3 Stress Field . . . 49
3.2 Ensemble Methods in Machine Learning . . . 52
3.3 Structure of Selected Machine Learning Models . . . 54
3.3.1 Neural Networks . . . 54
3.3.2 Random Forest . . . 56
3.3.3 Extreme Gradient Boosting (XGBoost) . . . 59

4 Development and Application 62
4.1 Test Case . . . 62
4.2 Data Generation . . . 65
4.3 Numerical Case 1 . . . 66
4.3.1 Feature Engineering and Data Preparation . . . 66
4.3.2 Modeling and Training Process . . . 71
4.4 Numerical Case 2 . . . 72
4.4.1 Feature Engineering and Data Preparation . . . 73
4.4.2 Modeling and Training Process . . . 78
4.5 Numerical Case 3 . . . 80
4.5.1 Feature Engineering and Data Preparation . . . 80
4.5.2 Modeling and Training Process . . . 85

5 Results and Discussion 86
5.1 Custom Scoring Function . . . 86
5.2 Results of Numerical Case 1 . . . 89
5.3 Results of Numerical Case 2 . . . 90
5.4 Results of Numerical Case 3 . . . 91
5.5 Interpretation and Comparison of Results . . . 92

6 Conclusion and Implications 94
6.1 General Conclusions . . . 94
6.2 Practical Implications . . . 95
6.3 Suggestions for Future Work . . . 96

7 References 97

8 Appendix 116
8.1 Appendix A . . . 117
8.2 Appendix B . . . 119
8.3 Appendix C . . . 121
8.4 Appendix D . . . 123

List of Figures

2.1 Speckmann and Henrich's Analogy[1] 11
2.2 Hierarchical Structure of Damage Detection[2] 21
2.3 Comparison of Supervised and Unsupervised Machine Learning[3, 4] . . 22
2.4 Delamination and Debonding[5] 30
2.5 Matrix Crack and Delamination Coupled[6] 33
2.6 Fiber Breakage and Progressive Damage[7] 35
2.7 Different Type of Porosities[8] 37
2.8 Fiber-Matrix Debonding in Different Orientations[9] 38

3.1 Initial and Deformed Configurations 43
3.2 Simple Beam in Unidirectional Loading 44
3.3 Strain on a Infinitesimal Element 46
3.4 Forces on a 2D Infinitesimall Element 50
3.5 Forces Resolved into Components 50
3.6 Stresses in 2D Element 51
3.7 Stresses on a Infitesimal Element 51
3.8 Working Principle of Stacking Technique 53
3.9 A Simple Neural Network 55
3.10 Simplified Mathematical Background of a Neuron 56
3.11 Working Principle of Classification Random Forest 57
3.12 Working Principle of XGBoosting 59

4.1 Isometric Projection of Model 1 62
4.2 Top View of Model 1 Including Mesh Numbers 63
4.3 Isometric Projection of Model 2 63
4.4 Top View of Model 2 Including Mesh Numbers 64
4.5 Selected Elements for Defects 65
4.6 X Component of Strain in Undamaged Condition of Model 1 66
4.7 GNN Neighborhood Structure with 8 Neighbors 67
4.8 PCA Projection of the Initial Data 68
4.9 PCA Projection after Feature Engineering and SMOTE 68
4.10 t-SNE Projection of the Initial Data 69
4.11 t-SNE Projection after Feature Engineering and SMOTE 69
4.12 UMAP Projection of the Initial Data 70

4.13 UMAP Projection after Feature Engineering and SMOTE 70
4.14 Y Component of Strain in Undamaged Condition of Model 1 72
4.15 Feature Importance for L1Spc 74
4.16 PCA Projection of the Initial Data 75
4.17 PCA Projection after Feature Engineering and SMOTE 75
4.18 t-SNE Projection of the Initial Data 76
4.19 t-SNE Projection after Feature Engineering and SMOTE 76
4.20 UMAP Projection of the Initial Data 77
4.21 UMAP Projection after Feature Selection and SMOTE 77
4.22 Developed Ensemble Structure 78
4.23 X Component of Strain in Undamaged Condition of Model 2 80
4.24 Feature Importance for L2Spc 81
4.25 PCA Projection of the Initial Data 82
4.26 PCA Projection after Feature Engineering and SMOTE 82
4.27 t-SNE Projection of the Initial Data 83
4.28 t-SNE Projection after Feature Engineering and SMOTE 83
4.29 UMAP Projection of the Initial Data 84
4.30 UMAP Projection after Feature Engineering and SMOTE 84

5.1 Definition of Neighborhood on FEM 87
5.2 Prediction Equivalent to 1 Point 87
5.3 Prediction Equivalent to 1 Point 88
5.4 Prediction Equivalent to -1 Point 88
5.5 Prediction Equivalent to -1 Point 88
5.6 Prediction Equivalent to 0.5 Point 89

List of Tables

2.1 Comparison between Model-driven and Data-driven SHM Approaches . 12
2.2 Comparison of SHM Methods with Localization and Severity Detection Capabilities 18
2.3 Comparison of Studies on Machine Learning Approaches for Damage Detection 27
2.4 Defects and Damage Types in Composite Materials[10] 29
2.5 Comparison of Various Studies on Damage Detection in Composite Structures 40

4.1 Material Properties of CFRP 64
4.2 Layer Properties 71
4.3 Training Parameters and Details 72
4.4 Employed Machine Learning Models 73
4.5 Hyperparameter Settings Used for Each Random Forest Model 79
4.6 Important Hyperparameters of the PlyDetector 79
4.7 Employed Machine Learning Models for Numerical Case 3 85
4.8 Important Hyperparameters of the ML Models 85

5.1 Results with 30 Samples 89
5.2 Results with 50 Samples 89
5.3 Damage Localization Results with 30 Samples 90
5.4 Damage Localization Results with 50 Samples 90
5.5 Ply-Level Identification Results with 30 Samples 90
5.6 Ply-Level Identification Results with 50 Samples 91
5.7 Damage Localization Results with 30 Samples 91
5.8 Damage Localization Results with 50 Samples 91
5.9 Ply-Level Identification Results with 30 Samples 92
5.10 Ply-Level Identification Results with 50 Samples 92

8.1 Comparison of SHM Methods Based on Sensor Type, Damage Type, and Layer Detection Capability 117
8.2 Comparison of Studies on Machine Learning Approaches for Damage Detection 119
8.3 Comparison of Studies on Damage Detection in Composites 121

Chapter 1

Introduction

1.1 Problem Statement

As user demands evolve over the years and the performance criteria expected from the final products by the manufacturers increase, composite materials managed to meet these complex industrial requirements thanks to their multi-functional and innovative nature. In particular, the use of fiber-reinforced composites (FRC) has grown continuously for the last 50 years due to their low density with high stiffness and strength rendering them a unique combination for industrial applications[11]. The application area of the composites is quite wide, including construction, automotive industry, aeronautics, housing and industrial parts (storage tanks, bathtubs, etc.), and even to the extent of the medical field[12, 13]. Naturally, just like other materials, composite materials are also prone to damage. Unlike other engineering materials such as steel, composite materials frequently have anisotropic behavior. Since the damage generation process is complex and the composite materials are inherently non-homogeneous and anisotropic, detecting the damages becomes a unique challenge[14]. Detecting these damages during quality control is essential whether a destructive or non-destructive testing method is employed. Equally, detecting these damages in real-time as they occur and propagate is important, since it has significant advantages in terms of safety and cost minimization. Live identification and interpretation of the damages allow early intervention and more efficient management decisions.

In this sense, monitoring the state of a structure is crucial to identify the early and progressive damage[15]. Numerous studies have been conducted on damage detection and localization in composites materials. According to a comprehensive review by Hassani et al.[16], the heterogeneous nature of composites leads to multiple nonlinear damage modes — such as impact damage, delamination, matrix cracking, and fiber breakage — which necessitate early damage detection to prevent catastrophic failures like aircraft crashes.

Structural health monitoring (SHM) is clearly one of the most important tools to

achieve this surveillance over the structure, as it implements the monitoring of the structure with periodic measurements. This is achieved by extracting the useful features from these periodic measurements and,by analyzing them the current state of the system is determined[17]. Various sensing approaches and sensor types have been developed in the field of SHM. These include traditional non-destructive testing (NDT) techniques such as ultrasonic, radiographic, acoustic emission, and thermographic testing, as well as vibration-based techniques like modal analysis and irreversible deformation measurements. However, the need for real-time and in-situ monitoring has increased interest in SHM systems that utilize sensors distributed on the surface. Common measurement devices used in SHM include strain gauges, fiber optic (FBG) sensors, acoustic emission sensors, and accelerometers, while techniques such as statistical pattern recognition (SPR) and vibration analysis are utilized for damage detection[18].

Among these sensors, strain gauges are particularly regarded as powerful tools in experimental deformation analysis and are preferred for their high sensitivity in composite structures. However, since these sensors are surface-mounted, monitoring each individual ply becomes challenging; the use of many sensors may be required, potentially leading to electrical connectivity issues. Therefore, optimal sensor network placement and efficient data acquisition strategies have also been topics of research in the literature.

Fiber-optic-based approaches are also common in SHM. For example, Ding et al.[19] embedded fiber Bragg grating sensors inside composite laminates to detect damage. Non-contact methods like digital image correlation (DIC) have also been employed for ply-level strain measurements to support damage analysis[20]. Additionally, acoustic methods and Lamb wave analyses are utilized for damage localization[21]. Nevertheless, each of these techniques requires specialized equipment or advanced signal processing, and some only indicate the presence of damage without providing precise localization, often at high cost.

In studies involving structural sensors such as strain gauges, the collected data are typically processed using machine learning or statistical analysis. For instance, Ručevskis et al.[22] employed eight strain gauges on CFRP plates and applied AI algorithms on both numerical and experimental vibration modes to detect the presence and location of damage, achieving accurate localization using a k-NN classifier. Similarly, Li and Sharif[23] proposed a damage index based on distributed fiber-optic strain measurement, Delaunay triangulation, and Hausdorff distance, successfully detecting both visible and barely visible impact damages with high accuracy. Fikry et al.[24], on the other hand, focused on ply discontinuities (e.g., resin pockets) in unidirectional laminates and analyzed localized strain increases and delamination progression using surface-mounted strain gauges positioned directly above these regions.

These studies collectively demonstrate the versatile potential of sensor-based methods for damage detection in composite structures. In summary, while a wide range of methods exist in the literature for general damage detection and the investigation

of specific mechanisms in CFRP composites, a strain gauge-based methodology that can directly identify the precise coordinates of damage at the ply level has not yet been thoroughly explored. Most existing approaches either classify broad damage zones (e.g., delamination regions) or utilize alternative sensing techniques for damage identification. The proposed approach aims to address this gap by using sensor measurements to directly compute the damage coordinates within the composite structure.

1.2 Aim and Scope of the Study

Current SHM approaches typically rely on global structural responses or simple surface level inspections, which may fail to detect internal or inter laminar damages commonly occur in composite materials. Moreover, the detection of damage at the specific layer within a laminate structure remains a significant challenge. Conventional techniques are often unable to accurately identify which layer is compromised, limiting the diagnostic power of the SHM system, which limits future visions. This research aims to fill this gap by combining strain gauge-based sensing with machine learning models to detect, localize, and identify damage at the layer level within composite laminates, and validate the idea of advanced localization of the damages within composite materials is possible by the use of strain gauges.

This study presents the development of a sensor-based methodology for detecting and localizing damage at a ply-wise level in composite structures. By analyzing data from distributed strain gauges, the proposed approach tries to predict the exact damage location and exact ply using data-driven techniques. As told, this work adresses directly a gap in literature by focusing on damage localization on ply-level. This exact localization of the damage is useful for future applications of the SHM methodologies which may result in better understanding of damage mechanics in composite materials, more prompt early interventions, more precise remaining lifetime estimates, and better administrative decisions.

Main emphasis is placed on developing a data-driven methodology for advanced damage detection. While core topics regarding to this study is completely defined, other related topics are described briefly, since damage detection and localization are already challengingly complex. The methodology is completely developed with simulated data and has not been tested for experimental application. The study does not consider environmental degregation and temperature variations. Although the methodology yields results and provides insights for future work, so told limitations must be considered.

1.3 Structure of the Thesis

This paper is organized in order to facilitate easier understanding of the topic and developed methodology. Contents, list of figures, tables, and abbreviations are given preceding the work. Chapter 1: Introduction, provides the problem statement, aim and

scope of the study, and the structure of the work. The motivation of this study and a brief explanation of current state of damage detection in composite structures are given. Chapter 2: Literature Review, provides a comprehensive review of the literature divided into several sections. Some fundamental concepts about damage detection and localization, SHM, and machine learning (ML) are included as well. This section is quite heavy in terms of information, therefore most of the sections are supported frequently with figures and tables. Some sections include a summary table at the end of the section, in which relevant previous work is compared. It is highly encouraged to make use of these summary tables. Chapter 3: Methodology, explains the feasibility of the proposed idea. Definition of strain, stress, displacement fields, and some procedures to obtain them are given. The motivation for the use of ML is presented along some different methods. This chapter is crucial in order to understand the following chapters. Chapter 4: Development and Application, explains the development of the damage detection and localization methodology, and presents unique case studies. These case studies thoroughly explained and the workflow of the developed methodology is given. The practical work lies within this chapter. Chapter 5: Results and Discussion, provides the efficiency of the developed methodology for the case studies given in the chapter before. The statistical background for the calculations and comparisons of success rates, and important metrics about ML are given. This chapter is visually heavy due to interpretations of the case study results. Chapter 6: Conclusion and Implications, presents the acknowledgments acquired from the study. The results of the study is processed and transmitted as several points of conclusions. Practical implications and insights are given, and suggestions for future work is provided. Chapter 7: References, includes all the citations used in the work in APA format. Chapter 8: Appendix, stores big graphs, figures and some interesting findings noticed during the work. Frequent visits to the appendix is expected, since the full sized summary tables from the literature review chapter is included here. Also, some part of the data used for ML can be found in this chapter.

Chapter 2

Literature Review

2.1 Structural Health Monitoring (SHM) Systems

2.1.1 Concept of Structural Health Monitoring

In the early days SHM has been developed for damage identification of aircraft in aerospace industry[25]. At the end of 1970s, it was implemented for offshore platforms[26]. Around 1990s, SHM started to get employed for civil engineering and infrastructure. Beck and Katafyglotis[27] designed a monitoring technique of a structure by detecting changes in its stiffness distribution. In 1999, Mita[28] discussed about the emerging need for SHM in Japan after 1995 Hyogo-Ken Nanbu Earthquake in which damages of beam-column joints in most of the buildings were noticed only after one-by-one inspection. In 2009, Semperlotti[29] stated: "Structural Health Monitoring (SHM) is a fairly new engineering field oriented to the development of damage detection systems able to facilitate the transition from scheduled maintenance to condition based maintenance." In the past decade, SHM grew rapidly parallel to the advancements on new sensing and control technologies[30, 31].

Speckmann and Henrich[1] present a great analogy in terms of understanding the SHM systems by comparing human body to airplanes, seen in Figure 2.1. Human body has nerves which transfers the signals to the brain. They work similar to sensors, if there is pain in any part of the body this signal is transferred to brain, and after evaluating the intensity of pain, brain decides to let it slip or go to a medical doctor. In an airplane, various sensors collect data from different points of the plane and collected at a computer. Just like the human brain, the computer evaluates the data and decides if a problem is present. Afterwards corrective actions might be taken.

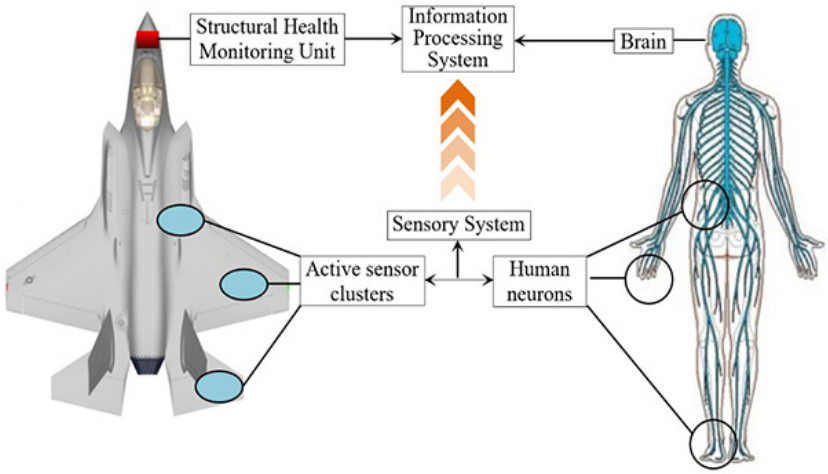

Figure 2.1: Speckmann and Henrich's Analogy[1]

2.1.2 Modal-driven and Data-driven SHM

Typically SHM applications are categorized into two types of approach: data-driven SHM and model-based SHM[32, 33]. These approaches differ significantly in technique, application, and required computational power.

Model-driven SHM relies on physical models or mathematical representations of the structures. These models are developed considering engineering principles, material properties, and boundary conditions. Frequently the finite element model (FEM) of the structure is used as a baseline in undamaged state. Model updating is performed in order to correct the initial results since models often produce different results than measured data[34]. This updated version of the model is identified as the reference model and damage is detected by considering the changes in new measurements. This approach has advantages such as lower data dependency, as limited sensor data is sufficient if the model is accurate, and the ability to forecast structural responses under hypothetical load scenarios and the downsides include a high computational cost due to the potential complexity of the structure and the accuracy of the results being dependent on the correctness of the modeling[35]. There are various studies employing model-driven method. Cao et al.[36] have developed a piezoelectric impedance measurement to detect damage by an inverse analysis. Another work is published by Moore et al.[37], where the model-driven method is utilized in order to identify cracks in a thin plate.

Data-driven SHM uses the information from the sensors directly to both understand the behavior of the structure and detect any possible damages. This method employs statistical pattern recognition (SPR), which is often done by machine learning (ML) algorithms. The careful selection of the model is crucial for this method since not every ML algorithm is fit to identify damage. The unique advantage of this method is the possibility to estimate the remaining life combined with damage detection[38]. Although

this is a unique feature, the black-box nature of some ML models must be considered. Furthermore, larger datasets are required compared to model-driven approach. Wang et al.[39] utilized a data-driven approach to identify and quantify the structural damages on Tianjin Yonghe Bridge located in Tianjin, China. Similarly, M. Döhler et al.[40] presented a vibration-based data-driven approach in order to detect small damages on the S101 Highway Bridge located in Austria. Another solution for SHM is hybrid methods, which combine model-driven and data-driven SHM techniques. This powerful approach involves developing baseline physics or mathematics-based models and simulating them to understand the structural responses. It is then combined with ML learning models enhanced with continuously updated real-time feedback. The hybrid approach is mostly used in SHM applications for aircraft and smart city infrastructures.

The decision between model-driven, data-driven, or hybrid approach, ultimately reduces to identifying the requirements, complexity of the physical structure, and the availability and quality of the existing data, which could serve the training of ML models. A comparison of model-driven and data-driven approaches is given in Table 2.1 to simplify the decision process.

Table 2.1: Comparison between Model-driven and Data-driven SHM Approaches

Property	**Model-driven SHM**	**Data-driven SHM**
Technique	Analytical models (physics or mathematics based)	Data-based, mostly relies on ML or Statistical Pattern Recognition (SPR)
Data Requirement	Less data required	Large datasets needed for ML training
Accuracy and Precision	High (if the model is correct)	High (if there is enough data)
Required Computation Power	Dependent on the model complexity	Often high (ML model training)
Interpretability	Easy (physics-based)	Hard (especially deep learning models)
Scalability	Limited (predefined structures)	High
Sensitivity to Environment	Low (predefined environmental effects)	High (real-time data)
Cost	Often high initial cost, but low maintenance cost	High (data collection and processing)

2.1.3 Various Applications of Structural Health Monitoring

The literature search for SHM reveals six commonly used structural assessment methods, namely, response-based techniques, reliability-based techniques, acoustic emission

(AE) method, feature extraction methods, computer vision, and machine learning(data-driven) methods. For simplicity and the frame of this study, only response-based techniques and relevant papers are reviewed in the following chapter. In SHM, response-based techniques assess the structural state by analyzing the system's natural operative responses. Controlled input forces or other forms of excitations are not required, and these techniques rely solely on measured responses, such as displacement, velocity, acceleration, strain etc.

2.1.3.1 Displacement-Based Approach

Displacement measurements provide valuable information about the state of the structure. Therefore it is common point of interest among researchers. An example of this work is presented by Xu, Song, and Masri[41]. This study used laser displacement sensors to identify damages at joint connections of structures. Measurement time series are utilized with the help of neural networks (NN) in order to find damage and asses the extent. The advantages of the proposed approach over the traditional methods are communicated, and the performance of the proposed approach is verified experimentally.

Huang et al.[42] provided displacement-based method utilizing accelerometers to compute mode-shapes, which are later associated with displacement of the nodes. This study presents the NODIS Method, an unique principle to identify damages with less sensors. The principle yields a coarse result but contributes to SHM by reducing the amount of sensors drastically(as less as 3). Another unique feature of this study is the precision. The approach takes the weight of the sensors into account. Ono, Ha and Fukada[43] utilized the influence lines in highway bridges, and by employing Displacement-Based Index (DBI) manage to sense the damages on a highway bridge. The study concluded that even far from the sensor damage could be detected if the parameters are set right.

Huseynov et al.[44] worked on bridges using inclinometers and presented that rotation is sensitive to damage. The study utilizes influence lines in order to differentiate healthy and damaged states.The study was able to identify damages as low as 7% change in stiffness over an extent of 2.5% bridge span on the experimental bridge included in the study.

Concluding the subsection, it is important to remark that displacement sensors are often difficult to install in operative conditions.

2.1.3.2 Strain-Based Approach

Strain is measured by utilizing strain gauges, Fiber Bragg grating (FBG) sensors, and piezoresistive sensor such as microelectromechanical systems (MEMS) [45, 46]. Strain is a localized property. Therefore a large number of strain gauges are often required.Although this sounds like a limitation, strain sensors are generally easy to

install. Jang, Sim and Spencer Jr.[47] presents the Strain Damage Locating Vectors (Strain DLV) method, focusing on the use of strain flexibility matrices. This study includes a numerical simulation of a 56-DOF planar truss model, and emphasizes the method's ability to locate damage using a smaller number of sensors. It is shown that better strain resolution results in improved performance in real-world applications.

Zhao et al.[48] utilized modal macro strain-based damage identification to detect damages on pipelines. Dynamic macro strain responses are gathered and modal macro strain (MMS) vectors are formed. Results show this method could reflect the damage and the extent.

Rageh, Linzell and Azam[49] monitors a bridge using strain gages and trains a artificial neural network (ANN) for damage detection.This study combines Proper Orthogonal Modes (POM) and ANN, and uses this methodology to assess stringer- floor beam connection state. This method is robust enough to predict the damage under high noise environments accurately. Glišic et al.[50] stress the significant improvement of fiber optic (FO) techniques for sensors, including strain gauges. This study utilizes Fiber Bragg-grating (FBG) sensors for strain measurement and presents long-gauge sensing principles based on the material properties at the macro level. This approach is validated by a large-scale application on Streicker Bridge in Princeton, New Jersey. The results show that FO sensing technologies, such as FBG sensors are successful in detecting and localizing the damage.

Tondreau and Deraemaeker[51] present two experimental applications of damage localization using dynamic strain measurements. A very large network of dynamic strain sensors is split into several independent local networks. This study uses modal filters to predict damage and is tested experimentally on two different structures.

2.1.3.3 Vibration-Based Approach

Damage alters the stiffness, mass, or energy dissipation properties of a structure. This alteration results in a change in the dynamic response of the structure compared to the undamaged state[52]. Therefore changes in vibration characteristics are an indicator of damage. For example, the location and the extent of damage could be identified by analyzing changes in the natural frequencies of that structure[53].

Vibration-based damage detection (VBDD) has been studied for the last 30 years[54], and vibration analysis (VA) has been applied to various areas such as power production[55], aerospace industry[56], civil construction industry[57, 58] for various reasons. Some applications of VA even include loose or foreign part detection, leak detection, etc[59]. The vibration-based approach consists of the natural frequency method, mode-shapes method, modal curvature method, modal strain energy method, damping method, Frequency response functions (FRFs), and matrix-based method. In the following, each method is briefly described and examples are provided for better understanding.

The presence of damage or deterioration in a structure results in changes in the

natural frequencies of the structure. Monitoring the changes in resonant frequencies is generally quick and often reliable. Therefore this method is a useful way to locate the damage or deterioration[60]. If the natural frequency of the structure is less than expected, a loss of stiffness is considered. Frequencies higher than expected indicate that the supports of the structure are stiffer than expected [61]. Generally, a change of about 5% in natural frequency is enough for damage detection with confidence[62]. This analysis is one of the earliest methods and countless work has been done on this topic[63]. For instance, Kim et al.[64] presented a comparison between frequency-based damage detection (FBDD) and mode-shape-based damage detection (MBDD), and concluded FBDD is better for damage detection, while MBDD is better for damage localization.

Mohan et al.[65] developed a correlation based algorithm to detect and localize the damage by analyzing experimental natural frequency change ratios and analytical natural frequency change ratios. Numerical models of cantilever beam with three different damage locations have been modelled and the methodology proved to be performing robustly when applied to a continuous system. For further information, Kannappan[66] provides a detailed review on damage detection in structures using natural frequency measurements.

Measuring mode shapes is a reliable approach for damage detection. However, measurement of the mode shapes is mostly labor intensive compared to natural frequencies, and a large number of sensors is required to identify a mode shape correctly[67]. This technique compares measured mode shapes and various features, such as curvature or modal strain energy to increase the sensitivity[68]. The basic principle of this method is detecting singularities in mode shapes since damage causes these singularities[69]. This approach requires data both from the undamaged and damaged state of the structure. Additionally, there are studies showing this approach is more effective for preliminary localization rather than point-blank localization[70].

The first employment of a mode shape information for detecting the location of a damage without the utilization of a finite element model (FEM) was presented by West in 1984[71, 72]. The test is done on an intact Space Shuttle Orbiter (SSO) body flap, and the mode shapes gathered while flap is subjected to acoustic loading. Then, the mode shapes partitioned and change in mechanical assurance criterion (MAC) was utilized to detect the structural damage location. MAC is a statistical indicator sensitive to differences in mode shapes, and it yields a good result comparing different mode shapes[73].

Chen and Buyukozturk[74], introduced a new feature for detecting damage in structures, the continuous symmetry measure, which evaluates the rotational, mirror, or translational symmetry in a mode shape of the structure. This method is based on mode shape analysis and proved its usefulness in the test cases of pipe cross section, NASA 8-bay model, and the IASC-ASCE benchmark structure.

Khoo, Mantena and Jadhav[75] presents another interesting study by employing

mode shapes and resonant pole shifts to detect damage in wooden wall structures. This study includes an experimental demonstration using an actual wooden wall, and proves SHM is able to monitor different materials. For further and updated information, An et al.[76] provide a review for various methods in SHM, including mode shape-based methods.

Another approach is mode shaped curvetures, which are more sensitive to the loss of stiffness than the mode shapes. Loss of a member generally causes a sudden change in mode shape's first and second derivative[77].

Roy[78] demonstrates this method and formulates the derivatives of mode shapes, and correlates them with damage location. This study includes an experimental case study of 6-story steel frame mounted on a shaker. The proposed approach is found to be competent enough for damage detection on various locations, even in the presence of noise. Shokrani et al.[79], present a novel approach based on principle component analysis (PCA), which can distinguish between variations due to damage and variation due to environmental factors. The approach indicates good performance on 2 numerical test cases for localization but severity is still a challenge.

Analyzing modal strain energies (MSE) is another approach to detect damage. Modal strain energy is calculated for each element on the structure. Then, it is compared with the undamaged state. The places with damages tend to have big differences in MSE compared to the undamaged state. Thanks to its extensive adaptability and effectiveness, MSE-based damage identification has been used widely for damage identification [80]. Shi, Law and Zhang[81] proposed the ratio of change in MSE for damage localization. This parameter is calculated by predicting the change in MSE in each element in a case of damage, and it is called modal strain energy change ratio (MSECR). The results of this study indicate that MSECR is effective and robust to locate damages in structures.

Nyugen et al.[82], discuss a recently developed forward method using the ratio of geometric modal strain energy to eigenvalue (GMSEE). Although this method is feasible, it relies on the assumption that the fractional modal strain energy is unchanged after damage. This assumption is acceptable for small size damages but large damages known to cause calculation errors[83]. Therefore an improved method which uses modal strain energy to eigenvalue (MSEE) instead of GMSEE is presented, and found out this method effectively identifies damage in truss structures.

Tan et al.[84] present a vibration-based technique, using only the first vibration mode, for predicting damage and its location. This study develops a procedure, namely the modal strain energy based damage index is first calculated using only the first bending mode. Then the ANN predicts the damage location and severity. The study concludes that this approach is efficient in the applications to steel beams, that are important structural components in buildings and bridges.

The damage in a structure generally cause an increase in damping within the struc-

ture. Mostly this characteristic is not sensitive enough to indicate damage. However there are some relevant work which managed to explore this method. Frizzarin et al.[85] developed a baseline-free, time-domain damage detection method for concrete structures. A strong correlation is observed between the increase in damping and decrease in structural stiffness due to seismic damages.

Montalvão, Ribeiro and Silva[86], developed a factor based on modal damping in order to identify delamination on composite materials such as carbon fiber reinforced plastics (CFRP). This study is applicable at low cost to structures that have not been instrumented before, and it provides a probability distribution of damage location. The study concludes that further research is required on the topic.

Another approach is the utilization of frequency response functions (FRFs). In the basis FRFs are derived from Fourier transform, and defined as a mathematical resprestenation between input and output of a system[87]. The utilization of the FRFs are convenient in the terms of data gathering since a small number of sensor are usually enough for real-time applications[88]. A minimum number of sensors located at critical points are able to measure the vibration response of the structures[89].

Hassani and Shadan[90], developed a new model updating-based method for damage identification based on incomplete FRFs. The study includes 2 numeric simulations such as, a 144-element, three-layer laminated composite plate and a 120-element, three-dimensional truss, as a test on bigger structures. This method managed to identify damages with closely-spaced frequencies. However, the authors also include that the study requires an experimental verification.

Bandara, Chan and Thambiratnam[91], combine FRFs with neural networks in order to develop a new method which reduces the dimension of the FRF data and transforms it to new damage indicators. This paper includes a case study, and the method is proven to be useful with a maximum error of 2%. Furthermore, the authors conclude that the neural networks are capable of recognizing nonlinear damages and their severities in structures. The last vibration-based method is matrix-based analysis. This technique involves changing the stiffness and flexibility matrices for the damaged case and comparing them with the undamaged case. Tomaszewska[92] utilized this approach for several test cases, including the Vistula Mounting Fortress in Gdańsk. The study found out that neglecting modal errors could result in distorted results, and the possibility to obtain the correct result is greater when flexibility and curvature indicators are employed together.

Wickramasinghe, Thambiratnam and Chan[93] developed new damage indices based on modal flexibility. The application results of these new indices based on only the first few modes confirm that he feasibility of the method is proven. This method is able to identify damages in single or combined states.

2.1.4 Summary of Relevant Work

Table 2.2 summarizes the key parameters used in previous studies in a simplified manner. It includes information such as the method used, the type of damage investigated, the system's capability in terms of localization and severity prediction, and whether the study includes experimental verification. For more details, a comprehensive version of this table is provided in Appendix A, which includes additional information on the sensor type used, sensor optimization availability, and the year of the studies. In the following table L2 means localization, L3 means severity prediction, and Exp. means experimental verification.

Table 2.2: Comparison of SHM Methods with Localization and Severity Detection Capabilities

Author	**Method**	**Damage Type**	**L2**	**L3**	**Exp.**
Xu, Song and Masri[41]	Displacement based	Joint connection damages	✓	✓	✓
Huang et al.[42]	Displacement based	Cracks	✓[1]	✗	✓
Ono, Ha and Fukada[43]	Displacement based	Unspecified[2]	✓	✗	✗
Huseynov et al.[44]	Displacement based	Unspecified[2]	✓	✗	✓
Jang, Sim and Spencer Jr.[47]	Strain based	Unspecified[2]	✓	✗	✓
Zhao et al.[48]	Strain based	Unspecified[2]	✓	✓	✗
Rageh, Linzell and Azam[49]	Strain based	Unspecified[2]	✓	✗	✓
Glišić et al.[50]	Strain based	Crack, ruptures	✓	✗	✓
Tondreau and Deraemaeker[51]	Strain based	Crack	✓	✗	✓
Kim et al.[64]	Natural frequency based	Crack	✓	✗	✗
Mohan et al.[65]	Natural frequency based	Material loss	✓	✗	✗

Author	Method	Damage Type	L2	L3	Exp.
Chen and Buyukozturk[74]	Mode-shape based	Corrosion, material loss	✓	✗	✓
Khoo, Mantena and Jadhav[75]	Mode-shape based	Material loss, termite degradation[3]	✓	✗	✓
Roy [78]	Mode-shape curvature based	Unspecified[2]	✓	✗	✓
Shokrani et al. [79]	Mode-shape curvature based	Unspecified[2]	✓	✓	✗
Zhang, Shi and Law [81]	Modal strain energies based	Unspecified[2]	✓	✗	✗
Nyugen et al. [82]	Modal strain energies based	Joint connection damages	✓	✓	✓
Tan et al.[84]	Modal strain energies based	Unspecified[2]	✓	✓	✓
Frizzarin et al.[85]	Damping analysis	Seismic damages	✓	✓	✓
Montalvão, Ribeiro and Silva[86]	Damping analysis	Delamination[4]	✓	✗	✗
Hassani and Shadan[90]	FRFs	Unspecified[2]	✓	✗	✗
Bandara, Chan, Thambiratnam[91]	FRFs	Unspecified[2]	✓	✓	✓
Tomaszewska[92]	Matrix-based	Unspecified[2]	✓	✓	✗
Wickramasinghe, Thambiratnam, Chan[93]	Matrix-based	Unspecified[2]	✓	✓	✗

1: Localization only on 2D. 2: Damage is modeled as stiffness reduction but type is not specified. 3: This damage is caused by termites.

4: This study works on composites.

2.2 Damage Detection with Machine Learning

As seen in the prior subsection, numerous methodologies have been developed with the aim of damage detection in civil, mechanical, and aerospace structures. In the past damage detection approaches was based on small sized data, mostly neglecting environmental effects, such as temperature, moisture etc. Today, with better technology, it is possible to acquire more complex, and much greater sized data. Although the data size is enormous, so told exponential development in the technology and computer science also provide valuable opportunities to address this issue, particularly through machine learning[94].

Machine learning (ML) is a branch of artificial intelligence (AI) field. The aim of ML is enabling the machines to learn from datasets on their own, without any pre-programming[95, 96]. During the learning process, the machine learning model creates associations and links between various pieces of data and forms a structure, which is able to make predictions given any data with the training format. This takes the burden of trying to make inferences from a huge dataset from the shoulders of the scientists and lands it on the shoulders of the machine. Another advantage is that mostly, with some computing power, machine learning models recognize some patterns that humans may not.

With the foretold emerging computing power in the last decade, machine learning (ML) models have become more feasible and extensively used in damage detection field, demonstrating high performance and rigorous accuracy[97].

2.2.1 Fundamentals of Damage Detection and Assessment

Dusseault and Gray[98] defined: "Mechanical damage is irreversible degradation of strength or stiffness, or alteration of flow properties, as a result of permanent changes in material fabric...". Detection and identification of damage is a crucial process for health monitoring for structural systems over their lifetime[99]. Damage detection, diagnosis, and prognosis are closely related to each other. Ryetter proposes a pioneering hierarchical structure in his PhD thesis[100] for the matter. The original four levels of damage identification according to Ryetter are:

1. Detection: this step outputs a qualitative indication of probable damage.
2. Localization: this step outputs a probable location of the damage.
3. Assessment: this step analyzes the extend of the damage.
4. Prediction: this step offers information about the structure, and estimates the residual life.

It is clear that this structure is sequential and for each level, information from the previous level is required. Worden and Dulieu-Barton[101] argues that there is one major exception in this structure, and it can be remedied by the introduction of a

"Classification" level. This level gives information about the type of damage, and finds place in-between level 2 and 3. This step is crucial for the next steps to achieve their goals because the extent of damage and especially the residual life is related to the damage progression, and different damage types have different progression mechanics. Without knowing the exact type of the damage, the residual life estimation is only an assumption. A brilliant example from their work illustrates this concept clearly:" For an aircraft in flight, for example, this is critical. If the diagnostic system signals serious damage but fails to indicate that there is time to land, the aircraft may be lost needlessly and at great expense when the crew bail out. Note that the primary concern is that the crew do bail out; issues of life safety far outweigh economic considerations." Therefore, the final form of damage identification structure includes 5 steps, which are represented in Figure 2.2. Further discussions on damage prognosis related to SHM could be found in the work of Farrar and Lieven[102].

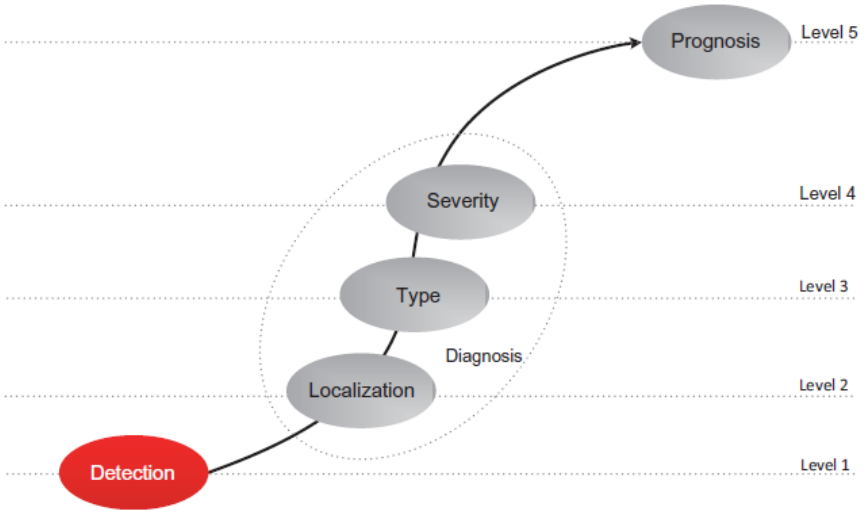

Figure 2.2: Hierarchical Structure of Damage Detection[2]

2.2.2 Supervised and Unsupervised Machine Learning

Machine learning (ML) techniques in SHM could be broadly classified into supervised and unsupervised learning. The main difference between these techniques is the labeled data. Supervised learning relies on labeled data to learn a function that maps the input to the output, while unsupervised learning tries to discover patterns in the data without labels[103]. Figure 2.3 explains the difference between supervised and unsupervised methods schemetically.

Supervised learning achieves high accuracy when labeled datasets are available. These labels are created by the human hand and pre-determined[104], meaning it require human intervention. This results in a unique advantage; all output created by the

ML model is meaningful to humans[105]. Although it is great to understand the results directly, human intervention creates the problem of human error, and the accuracy of the ML model is highly dependent on the correct labeling of the data. This imposes a disadvantage on the technique, especially if large datasets are used as it is costly to label large datasets correctly by human hand. Naturally, different supervised ML methods have varying properties. Caruana and Niculescu-Mizil[106], present a great comparison and overview of ten supervised learning methods including support vector machines (SVM), neural networks (NN), etc. S. B. Kotsiantis[107] explain various supervised classification methods, and provide an evaluation of these methods in terms of accuracy, learning speed, classification speed, tolerances etc.

Unsupervised learning produces the output from the knowledge gathered from the data. Contrary to supervised learning, it is up to the system to produce the output without human involvement[108]. These methods are better at identifying hidden patterns that may be overlooked by humans while labeling. This results in the correct detection of complex damage patterns. However, this technique falls behind supervised learning in terms of detecting the type of damage[109]. Similar to the studies on supervised learning, Naeem et al.[110] provide a deep insight about unsupervised machine learning, including step-by-step application of various algorithms. Usama et al.[111] present another comprehensive study about unsupervised machine learning on the subject of networking. This study also includes various applications.

Figure 2.3: Comparison of Supervised and Unsupervised Machine Learning[3, 4]

Regarding the SHM, a supervised classification algorithm could be developed if both the damaged and undamaged data are available. This requires either extensive data collected through time or model-driven approaches to create these datasets. Most of the time this data is limited or even unavailable. Therefore instead of supervised, mostly unsupervised learning is employed, which trains on the available data without the feedback, and detects the outliers[112]. From this aspect, unsupervised learning has a clear

advantage over supervised learning as it doesn't require undamaged state information. However, as told before, unsupervised learning is far weaker compared to supervised learning in terms of predicting location. Furthermore, most of the ML applications do not consider environmental factors, which could produce significant changes in dynamic responses rather than damage[113]. These effects have been studied by different researchers[114, 115, 116, 117] and the impact found out to be significant. Therefore an unsupervised approach is not optimal when utilized alone[118]. A combination of supervised and unsupervised techniques is required to achieve better performance on SHM applications.

2.2.3 Applications of Machine Learning in Damage Detection

Damage detection identifies changes in structural responses to external loads, and indicates the presence of damage[119]. Most common and easiest way for damage detection is visual inspections. However, this approach is highly subjective in finding different damage modes, sometimes completely internal, and requires great experience for precise identifications. Furthermore, some of these techniques are destructive for the material[120]. Non-destructive evaluation (NDE) is a good alternative for better damage identification, providing less subjectivity. Currently, numerous NDE methods are available, and most of them perform very-well in damage detection and localization. However, often these methods require special equipment, which may be expensive to buy and maintain. Most importantly, these techniques are not developed and therefore not suitable for live-monitoring. On the other hand, data-driven methods in SHM is gaining popularity due to the advancements in sensor technology, high-speed internet, and cloud based systems[121]. Extensive research has been conducted in this topic and the following part reviews some of the efforts in damage detection with machine learning.

Bayane et al.[122] present a real-time application of damage detection with machine learning. A steel railway bridge instrumented with 16 strain gauges, 5 piezoelectric uniaxial accelerometers, and 1 inclinometer captured an anomaly in March 2023. After careful inspection the reason of the anomaly is detected as a crack in the steel structure. On the basis of this data, new data is synthesized and used for ML. Anomaly detection models such as isolation forest (IF), robust random cut forest (RRCF), one-class support vector machine (OCSVM), local outlier factor (LOF), Mahalanobis distance (MD) are utilized in this study. The training process is unsupervised, since anomaly detection algorithms are used. In the training data environmental effects are also included, by contacting the local weather station. It has been observed that during an anomaly event such as crack formation, all five models managed to succesfully identified the anomaly. Although, the accelerometers did not experience significant change during the anomaly, strain gauges detected the anomaly instantly. The study concludes that such methodlogies are consistent and provide reliable results for damage detection.

Park et al.[123] describe a sequential damage detection approach for beams by us-

ing time-modal features. Artifical neural networks (ANNs) are employed as machine learning models. The study develops a ensemble method where two different machine learning models are operating linked to each other. From the acceleration data time-domain features are extracted and fed into the first phase neural networks which is specialized on predicting only damage occurence. If first phase neural networks predict the presence of damage within the beam, second phase neural network is activated. This phase is fed with frequency-domain features, again extracted from accelerations, and the location and severity prediction is obtained. Both of the neural networks are trained with simulated data from finite element analysis (FEA). The training is supervised. The proposed technique is tested with various load cases, and proven feasible. The study concludes that further studies focusing on sensor placement, optimization, and tests with environmental conditions can be performed.

Yeung and Smith[124] present a methodology where vibration data is used for damage detection. Neural networks are employed as machine learning models, and a comparison between two model are given. The study focuses on riveted connection damages located on various places in main girders on Clifton Suspension Bridge located in Bristol, UK. Singular and multiple damage modes are tested. Both the training and the test data is obtained through simulation environment with (FEM). Traffic induced vibration is simulated with addition of noise in order to conform the real-world applications. Fast Fourier Transform (FFT) is used to obtain the response spectra and feature vectors are derived. Two unsupervised ML models are selected and comparison in terms of sensitivity, advantages and limitations, and sensitivity to noise are provided. The study concludes that a reliable damage identification can be achieved even in noisy environments, if the neural networks are optimized.

Parisi et al.[125] describe a new method of damage detection and localization in steel truss railway bridges through ML tools. ML algorithms are trained with raw strain time series data obtained from FEA. Although the data is simulated the FE model is based on Quisi Bridge located in Valencia, Spain. Various damage conditions and locations are considered and the data is automatically created through simulation. Generated data is fed into a k-Nearest Neighbors (kNN) model to select the most informative features, and then these features are used in the training of a convolutional neural network (CNN). Damage location is set as a classification problem, and training has been carried out with supervised approach. The CNN models train on predicting both the damage location and the severity. However, their succes in predicting the severity is relatively low compared to their succes in damage localisation. The study concludes that it is possible to employ raw strain sensor signals, without any pre-processing, in order to predict the location and the severity of damage.

Bigoni and Hesthaven[126] propose a simulation based, data-driven damage detection approach. Synthetic datasets of complex structures are created and the damage is simulated. Time series signal from pre-selected sensor locations are extracted an used as features after selection. One-class Support Vector Machines (SVM) are used as machine

learning models with the aim of anomaly detection. The study follows a semi-supervised approach, also called one-class classification, where labeled data from undamaged state is used for training, and unlabeled data from both damaged and undamaged states are used for testing. Machine learning model is working in two-steps. First a binary (damaged or undamaged) prediction is made, and then outputs of multiple classifiers are exploited for the outlying data in order to obtain information about the location and severity of the damage. The proposed methodology shows succes in both 2D and 3D application. Hovewer, it is yet to be experimentally verified.

Kim and Philen[127] present a machine learning study about detecting cracks and corrosion on metallic materials. Most appopriate excitation signal is determined in the study. Various time-frequency method comparison are also included. The training data is syntetically generated through Abaqus® software. AdaBoost machine learning model is employed for classification on 2D plates. Simulated tests are verified with a real-life test conducted on a beam with corrosion and crack damage intentionally induced. The study employs GML AdaBoost MATLAB Toolbox for machine learning application and therefore follows a supervised approach. It has been found out that the correct classification and confidence levels depend upon mostly on the training sample properties, number of training samples, and number of iterations. Four different signal processing methods, short time Fourier transform, Wigner-Ville distribution, wavelet transform, and matching pursuit are examined, and short time Fourier transform is chosen. Damage classification is performed with the spectogram and AdaBoost. The study concludes that classification between different damage modes are possible using AdaBoost.

Ying et al.[128] propose a new data-driven framework for robust damage detection based on machine learning. This paper focuses on steel pipes and demonstrates the effectiveness of the proposed framework. Damage is simulated by mass scatterer grease-coupled to the pipe surface. Ultrasonic waves are measured with piezoelectric wafers, and various features are extracted from a variety of signal-processing techniques. This study extracts 365 features for machine learning, since a high number of feeatures are not computationally efficient, feature selection is performed. For feature selection adaptive boosting (AdaBoost) is used and the selected features are verified with the same model again. Five different classifiers are formulated including only AdaBoost, support vector machines (SVMs), and various combinations of these models. During testing, all of the trained models achieve good performance for damage detection, and the study concludes that machine learning based damage detection frameworks show promising results in pipe monitoring. This study only focus on damage detection, not localization or severity.

Nick et al.[129] present a comparisonal study where couple of machine learning models are used in damage detection. The study follows a two-step approach. First stage ML model is responsible of identifying the presence of the damage and localizing, while second stage predicts the type of the damage and its severity. First stage is trained

unsupervised, and the second stage is trained supervised. For the first stage the ML models k-means with different k values, and self-organizing maps (SOM) with different number of output neurons are considered. For the second stage support vector machines (SVMs), naïve Bayes classifiers, and feed-forward neural networks (FNN) are employed. Excluding SOM, each model is tested with and without principal component analysis (PCA) which reduces the dimension of the data. Both the training and the test dataset are composed of 30 samples. The study concludes, for damage type classification and severity prediction, SVM models are the most accurate(in the range 77-90%) and the use of PCA reduces the accuracy of the SVM models around 10% in general. Naïve Bayes classifiers perform noticeably worse than SVMs (73%) and perform worse with PCA (60%) applied. FNN models are ranked last with a the accuracy around 60% with or without PCA performed. The accuracy results for damage detection and localization are not given since this process was handled unsupervised. The study concludes that, the obtained results are encouraging for developing multiagent systems as they allow the discovery of significant differences between different ML models.

Gui et al.[130] present a comparison of three optimization based machine learning methods. Grid-search (GS), particle swarm optimization (PSO), and genetic algorithm (GA) are employed to optimize the penalty coefficient and kernel function parameter for SVMs. Autoregressive (AR) model and residual errors (RE) are considered as damage feature extractors and detected damages in a 3-story steel frame structure. Support vector machines (SVMs) are trained with the features extracted from AR model and REs with foretold different optimization methods. Comparison of these three cases are provided. Optimization based SVMs exhibited high accuracy results for damage detection, while RE features based SVM performing significantly better than AR feature based. In all cases RE based features confirmed to be more sensitive to presence of damage. Among the optimization methods GS provided best accuracy, however this method found out to be more costly in terms of computation power compared with others. The comparison between GA and PSO yielded nearly same results for best accuracy, but GA required less amount of samples in each subset decreasing the data size. Therefore, the genetic algorithm (GA) is identified as a robust and suitable optimization method for damage detection SVMs. The study concludes that SVMs can successfully distinguish between undamaged and damaged cases, even with interferences present such as operational and environmental conditions.

2.2.4 Summary of Relevant Work

The summary of the reviewed relevant work on machine learning approaches for damage detection is provided in Table 2.3. This table summarizes some key parameters of the studies in a simple manner, such as the data source for machine learning (ML), used ML model, the method's capability in terms of localization and severity prediction, and whether the study is experimentally verified. A more detailed version of this table can be found in Appendix B. Detailed version also includes the structure which the

method is applied to, is the training process supervised or unsupervised, and the year of the studies.

In the following table L2 means localization, L3 means severity prediction, and Exp. means the experimental verification. In need of any extra information, one can refer to the detailed version.

Table 2.3: Comparison of Studies on Machine Learning Approaches for Damage Detection

Author	**Method**	**Damage Type**	**L2**	**L3**	**Exp.**
Bayane et al.[122]	Strain, acceleration measurements	Anomaly detection algorithms[1]	✗	✗	✓
Park et al.[123][2]	Acceleration measurements	Artificial neural network (ANN)	✓	✓	✓
Yeung and Smith[124]	Vibration data	Probabilistic resource allocation network(PRAN) and DIGNET network	✗	✗	✗
Parisi et al.[125]	Strain gauges	k-nearest neighbors and convolutional neural network (CNN)	✓	✓	✗
Bigoni et al.[126][3]	Guided waves	Support vector machine (SVM)	✓	✓	✗
Kim and Philen[127]	Various time-frequency measurements	AdaBoost	✓	✗	✓
Ying et al.[128]	Ultrasonic measurements	Support vector machines (SVM) and AdaBoost	✗	✗	✓
Smarsly et al.[131][4]	Acceleration measurements	Artificial neural network (ANN)	✗	✗	✓

Author	Data	Machine Learning Model	L2	L3	Exp.
Nick et al.[129][5]	Acoustic emission (AE)	Support vector machine (SVM), naïve Bayes classifiers, and feed-forward neural network (FNN), k-means, and self-organizing maps (SOMs)	✓	✓	✗
Gui et al.[130]	Acceleration measurements	Support vector machines (SVMS) with different optimization methods	✓	✗	✓

1: Isolation forest, one-class support vector machine, local outlier factor, and Mahalanobis distance. 2: Requires training with real data. 3: States undamaged state is labeled, and the rest unlabeled. 4: Focuses on sensor problems and miscalibrations. 5: Damage presence and localization results are not given as accuracy, but as time metrics.

2.3 Laminated Composite Structures

Composite materials are created by combination of two or more materials having different mechanical properties. This yields a new material with enhanced characteristics. Typically one material, called matrix, serves as a medium and links the constituents. The resulting properties are dependent on the matrix and the constituents. Composite materials are mostly heterogeneous and often anisotropic in nature[132].

Traditionally composites have different types. As instance, fiber-reinforced composites materials utilize slender fibers in order to increase the strength and stiffness along their axis, while the matrix shields them from any environmental corrosive. A common approach is the employment of laminated composite structures. These structures are created by thin layers, named lamina, adhered together. Laminated structures offer the optimization of mechanical properties by changing fibre orientation angles and stacking sequences[133]. Additionally fiber volume fraction, number of layers, and thickness of the layers are considered as effective design parameters influencing the behavior of the laminate. Although the possibilities are basically infinite, fibre orientation angles mostly vary between four values namely 0°, 45°, -45°, 90°, for practical applications[134].

2.3.1 Defects and Damage Modes in Laminate Structures

Damages can occur on all known materials, whether it is a manufacturing error, or beacause of a problem arised during working conditions. Some of these damages are ma-

trix cracking, fiber-breakage, delamination, transverse cracking, fiber-matrix debonding, matrix degregation and blistering[135]. As seen in their names, these damages are particular to composite materials and each have different damage mechanisms.

Ranging from microscopic defects to large impact damages, Heslehurst[10] suggests there are 52 defect types that are separatable from each other. These defects are listed on the following table.

Table 2.4: Defects and Damage Types in Composite Materials[10]

Defects			
Bearing surface damage	Blistering	Contamination	Corner crack
Corner/edge splitting	Corner radius delaminations	Cracks	Creep
Crushing	Cuts and scratches	Damaged filaments	Delaminations
Dents	Edge damage	Erosion	Excessive ply overlap
Fastener holes	Fiber distribution variance	Fiber faults	Fiber kinks
Fiber/matrix debonds	Fiber misalignment	Fracture	Holes and penetration
Impact damage	Marcelled fibers	Matrix cracking	Matrix crazing
Miscollination	Mismatched parts	Missing plies	Moisture pickup
Non-uniform agglomeration of hardener agents	Over-aged prepreg	Over/under cured	Pills or fuzz balls
Ply underlap or gap	Porosity	Prepreg variability	Reworked areas
Surface damage	Surface oxidation	Surface swelling	Thermal stresses
Translaminar cracks	Unbond or debond	Variation in density	Variation in fiber-volume ratio
Variation in thickness	Voids	Warping	Wrong materials

Focusing on this studies subject, all of these unique defect and damage modes can not be explained in this study. Therefore this study focuses on only the most common and critical defect and damages. The following damage modes are selected as the focus point of this subsection: delamination, matrix cracking, fiber breakage or pull-out, porosity(voids), and fiber/matrix debonding. Since they are recognized as the most often occuring damage modes in composite laminates.

The reason, possible extent and the related work regarding to these damage types are provided in the next subsection. For further reading on the different defect and damage modes of laminate composite structures, relevant references can be employed.

2.3.2 Common Defects and Damage Detection

2.3.2.1 Delamination

Composite laminates are made up by stacking individual plies. The matrix material (usually a resin) bonds the plies together. The loss of adhesive force results in delamination. The plies no longer act together and behave as individual, compromising the structural integrity of the laminate. Delamination is one of the most common failure modes seen in composite structures[136]. Therefore significant amount of work has been published in this topic.

Delamination should not be misinterpreted as debonding. Although, both of the damage modes result in similar stiffness reducing effects. The term debonding is mostly used for the defect introduced while manufacturing, due to a region not bonding properly. Both damage modes are seen in the Figure 2.4.

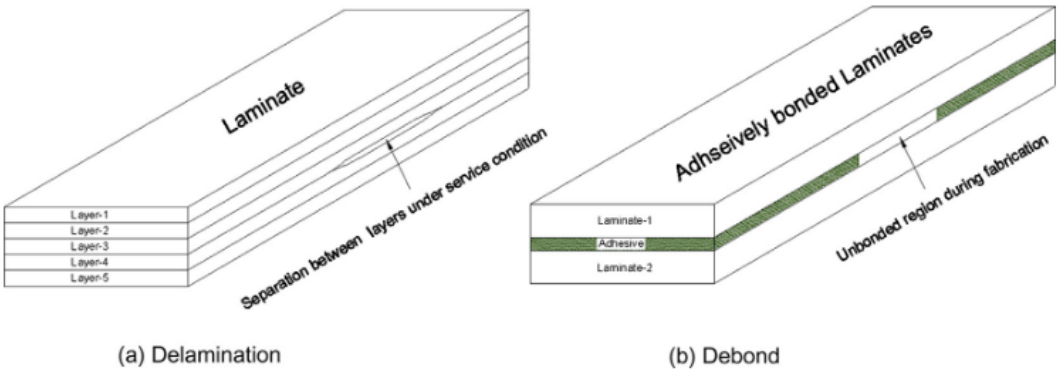

Figure 2.4: Delamination and Debonding[5]

Delamination affects the stiffness of the laminate structure and may lead to early failures. Also, delamination may result in local stress concentrations and local instabilities causing the further growth of the defect, concluding in total failure of the part.

Another dangerous aspect of delamination is the difficulty to spot it. Delamination is mostly internal and invisible from the surface, and leads to catasthropic failure in time if not detected. It is known as one of the most life-limiting damages[137].

Delamination may occur because of remaining interlaminar stresses, by impacts, eccentricities in the load paths and from discontinuities(cracks) in the structure[138].Also, mechanical processes such as drilling, layer defects, insufficient resin, air bubbles and residual lubricant may catalize the formation of a delamination[139, 140, 141].

In real world, delamination and debond damage modes typically involve a mixed mode failure phenomena[5]. Since delaminations are mostly internal and invisible to eye, real-time monitoring is critical to detect the defect before the damage accumulates and leads to a failure. There are numerous work related to detecting the delaminations in a composite laminate. Most applications use either strain measurements or, non-destructive evaluation (NDE).

Chai et al.[142] studied on unidirectional carbon/epoxy prepeg with the aim of inspecting the growth of delamination. The damage is created by an low-velocity impact and the resulting deformation is mapped with two high-speed cameras. This study found out that the growth behaviour of delamination during the rapid-growth phase is consistent, as observed in repeated tests. This finding is useful for developing a model for delamination growth. Although this study is not about delamination detection, it provides base insight about the propagation of the damage.

Kim et al.[143] employed strain gauges to localize the damage in a unidirectional graphite/epoxy prepreg laminate. Delamination is created by a indentor pressing onto the composite material under controlled conditions. Later, some of the materials are scanned with C-scan in order to verify the presence of the delamination, and also to determine the size of it. By using embedded and surface mounted strain gauges, the localization of the delamination is achieved under some limitations. The study concluded that the strain gauges must be located on-top or near the delamination location in order to detect it succesfully. The results indicate that a large number of sensors are needed to cover a large structure, but some selected, critical areas can be monitored with the technique.

Saravanos et al.[144] used piezoelectric sensors on a unidirectional graphite/epoxy laminate with the aim of detecting the presence of delamination. Piezoelectric sensors are either bonded or embedded into the laminate and the structure is subjected to vibration. In the case of continuous piezoelectric layers bonded to upper and lower surface, it was possible to detect the presence of delamination. Furthermore, it has been found out that the voltage differences between upper and lower terminals are feasible to detect the location of the delamination. It should be noted that this study does not explain how delamination is created, and the basis of the proposed technique is classical laminate theory (CLT).

Muc and Stawiarski[145] intoduced computational procedures to characterize the

dynamic behavior of beams and cylindirical panels. Structures with piezoelectric sensors are developed and the vawe propagation is employed in order to identify delaminations. The placement of the piezoelectric sensor and the geometrical structure of the part are identified as limitations which affects the success of this technique.

Aggelis et al.[146] used acoustic emission (AE) sensors in order to detect the presence of delamination and matrix cracking in a unidirectional glass fibre/epoxy resin. The damage is introduced as small inclusions to the surface of the laminate for both damage modes. The study concluded that the increase in wave transmission is correlated with damage accumulation. The study does not include the damage localization.

A more recent study by Gherlone and Roy[147], employs fiber optic strain gauges distributed along the surface of a CFRP laminate. This study is done numerically and delamination is modeled as separate top and bottom meshes at the location of delamination. Then, a damage index is computed and the location of the delamination is predicted. There are numerical case studies included within the study and the robustness of the method is tested with noisy data. The unique feature of this study is the utilization of iFEM, which is independent of the structure's material properties. This improves the practicality of the technique significantly. The key limitation of this study is that the strain sensors must be placed near to the damage location in order to ensure accurate predictions.

2.3.2.2 Matrix Cracking

Matrix cracking is a common damage mode in laminated composite structures. It is also known as intralaminar cracking[148], or transverse cracking (in case the layers oriented perpendicular to the load) It is defined as formation of micro or macro-scale cracks within the resin matrix, which binds the reinforcing fibers. In a composite lamina, the matrix maintaines the fiber alignment, transfers the stress between fibers and provides shear and transverse load resistance. A crack formation in this phase compromises the strength and the stiffness of the lamina. Significant amount of work has been published about the matrix cracking[149, 150, 151].

Once occured, matrix cracking reduces the stiffness of the compromised lamina, and causes stress redistribution over the whole laminate. It modifies the thermal expansion properties of the laminate, causing unintentional expansion and more crack formations. Matrix cracking may also lead to delamination between plies, and most importantly this failure mode allows fluid infiltration into the resin matrix, which causes different detrimental effects[152].

Crack formation is mostly encouraged by transverse tensile stresses, out-of-plane shear stress, mismatching thermal expansion properties between layers, and monotonic fatigue loads. Matrix cracking is often the first damage mode occuring in laminates having 90°plies[153]. The study of Parvizi et al.[154] show that the formation of cracks have a relation with the thickness of the 90°lamina. As the thickness of the 90°lamina

decreases below the thickness of 0°lamina the microcrack initiation increases.

Matrix cracking is a dangerous damage mode because it can couple with other damage modes and produce catastropic results. A matrix crack coupled with delamination is given in the Figure 2.5.

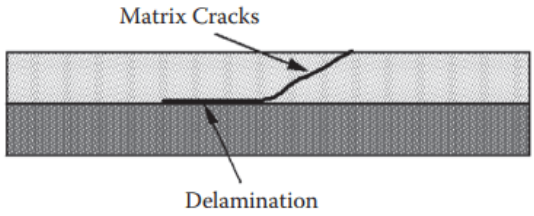

Figure 2.5: Matrix Crack and Delamination Coupled[6]

Various studies aiming to detect matrix cracking is present in the literature. Some of them given below.

Prashant et al.[155] developed a genetic fuzzy system in order to localize the matrix cracking in glass/epoxy laminates. The study uses frequency measurements as data, and is able to localize the cracking. The system shows great success but it is not experimentally verified, and all of the process is handled on simulation environment, requiring experimental verification. It must be noted that the developed system is able to predict the severity of the crack, which is rare to come by.

Todoroki et al.[156] utilized electrical probes mounted on tank structures made from CFRP to detect matrix cracking. Since, in the operating condition the tank structures are filled with various fluids, e.g. fuel, chemicals, water etc., the probes can only be mounted at the outer surface of the tank. Although this study does not localize the matrix cracking, it has found out that electrical resistance is increasing linearly with increasing density of matric cracks. This study is experimentally verified by performing cracks under tensile tests, and measuring the electrical resistance changes of the specimens.

Mardanshahi et al.[157] used guided wave propagation and artificial intelligence approaches in order to detect the presence of the matrix cracking. Glass/epoxy laminates are used in this study. Various specimens are prepared with different matrix cracking intensity and excited with actuator. The data is collected with a digital oscilloscope and standard procedures, such as feature selection, is carried out for the application of machine learning. The study trained 3 different models to predict the presence and severity of matrix cracking. The trained models show success in detecting the presence and severity of matrix cracking. Hovewer, this study does not focus on localization.

Prosser et al.[158] describe an advanced, waveform-based acoustic emission (AE) system used to detect matrix cracking in graphite/epoxy laminates. This study shows exact one-to-one correlation between AE crack signals and observed cracks. It is high-

lighted that the localization accuracy of the AE data is excellent, and only shows an average absolute difference of 3.2 mm compared to microscopy measurements. The matrix cracking is initiated by tensile loadings and sensor number is discussed. However, the severity of the cracking is not focused on.

Liu et al.[159] present a Lamb waves-based automated method for early detection an accurate evaluation oof matrix cracking in laminates. A quantification as "anomaly indices" are developed in order to asses the severity of the matrix cracking. This study is experimentally verified. The specimen exposed to tensile cycling loadin in order to encourage the occurence of matrix cracking and the wave propagation is monitored with two piezoelectric sensors. Recursive quantitative analysis (RQA) features of Lamb wave signals are used. It has found out that the RQA features can succesfully characterize matrix cracking in laminates, independent of geometry and damage mechanics. This system is proven to be effective at detecting early stage matrix cracking, and the proposed "anomaly indices" are shown as a effective index for predicting the severity of the cracking.

2.3.2.3 Fiber Breakage

Fiber breakage is another common damage mode seen in laminated composite structures. It is defined as the rupture of the fibers within the laminate, and may have different reasons. Fiber breakage can occur in the presence of high stresses and indentation effects[160]. Since most of the load on the laminated structure is carried by the fibers, a fiber failure can decrease the mechanical performance of the laminated material[161].

Fiber breakage is also often associated with impact damages. The shape of the impacting object is also important. It has been observed that the impact of an ogival shaped object introduces more fiber breakage, while the impact of a spherical shape introduces more delamination[162]. Fortunately, the fiber breakage caused from impact is generally limited to the a small area near impact zone and it is constrained by object size and impact energy[163].

Fiber breakage is a progressive damage mode. A high amount of the mechanical properties of a laminate composite is determined by the strength of reinforcing fibers[164], while resin contribution is relatively small. Inherently, most of the individual fibers have varying strength, because of weak points randomly located on their length. When the applied load surpasses the mechanical strength of a weak point, that fiber breaks, and the load carried by it gets transferred to other fibers. This increases the carried stress of other fibers. Then another neighboring fiber breaks, and the cycle goes on. This creates a cluster of broken fibers, that further overloads the neighboring fibers into creating more defects[165]. Fiber breakage and this process is seen in Figure 2.6.

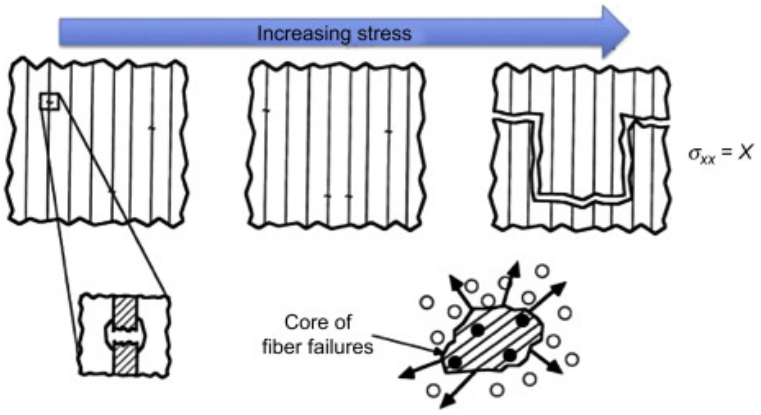

Figure 2.6: Fiber Breakage and Progressive Damage[7]

There is numerous work related to detection of fiber breakage within composite laminates. The following part overviews some of them.

Ativitavas et al.[166] describe a new lo-amplitude filtering technique for identifying fiber breakge in Fiber reinforces plastics (FRPs) from acoustic emission (AE) data. This study highlights the association of fiber breakage with high-amplitude AE signal hits and high signal strength. There are two experimental case studies included within this work. In the first scenario the specimens undergo a tensile loading scheme, while in the second case the specimens are subjected to bending by a four-point bending test. This study concludes that fiber breakage can be differentiated by low-amplitude filtering technique than other damage modes, since fiber breakage produces high-amplitude and high signal strength AE hits.

Malik et al.[167] present a unique way to study the fracture of individual fibers in real-time. Custom made small-diameter optical fibers (SDOF) are used in the study. The experimental study includes a light source illuminating the laminated structure parallel to the fibers from one side, and a high-speed camera tracking the light intensity from the opposite side. The camera is activated by the AE sensors located on the specimen. After tensile loading, the collected light intensity with the camera is transferred to Matlab for processing and it can be seen that the fractured fibers no longer transmitting light, therefore looking dimmer or completely black. This way the very fractured fiber can be detected immediately as the fracture happens.

Kidangan et al.[168] introduce a novel approach by localizing the fiber breakage in CFRP materials by employing thermograph. While the specimens are prepared, a small inclusion is performed in order to simulate the fiber breakage. The test setup includes a induction coil, the damaged laminate and a thermal camera. The coil is used to induct current in the carbon fibers, strating from a 0°orientation respect to the axis normal to laminate. Then it is rotated in order to understand the orientation of fiber breakage. When a breakage is present on the current orientation the resistance

increases due to decreased fiber cross-section, or matrix material. Therefore more heat is produced at the breakage location resulting in higher temperature compared with the cold state. This study is unique in the way that it can both localize the fiber breakage and determine the orientation.

Pasadas et al.[169] highlight that ultrasonic guided waves testing (GWT) offers a promising alternative for damage detection in composite structures. The study focuses on a two-step process to locate and evaluate fiber breakage in CFPR specimens, using guided wave testing (GWT) and eddy current testing (ECT). After the careful selection of frequency, incident angle,and the excitation source, the specimen is excited with a pulser and the resultant signal is gathered via receiver. Then the results are post-processed in order to detect any anomalies. The study concludes that this two-step process is succesful in detecting and characterizing fiber breakage in the laminate. Possible future work is given as characterizing different defect types, since guided waves are also sensitive to other types of damages occuring in composite materials.

2.3.2.4 Porosity

Porosity, also knows as voids, is one of the most common damage types seen in composite laminates. It refers to the presence of voids, air pockets, or simply unfilled volumes in the matrix or between the fiber and the matrix. When the voids increase in size, it is not possible to adress them in continuum level but as a different discrete object[170]. It is nearly impossible to produce a composite laminate without porosity, the only question is the balance between void sources and void sinks, and a good strategy will be designing the composite in a way that void sinks overcome the void sources[171].

Porosity form in composite laminates mostly because of the presence of air bubbles and volatile substances liberated during curing phase[172]. Various chemical composition, mixing, mechanical treatment, thickness of the laminate, vacuum pressure are also effective in the formation of porosity. Therefore the formation and density of the porosity is a difficult phenomena, controlled by numerous factors.

High levels of porosity is recognized as a serious problem for composite laminate, since the compressive and interlaminar shear strength depends heavily on thematrix properties, which are naturally reduced in the presence of porosity[173]. Contrarily, the tensile strength of the laminate composite is relatively unaffacted by the porosity, since reinforcing fibers are the dominant load carrying structure under tensile loads[174].

It is important to quantify the amount of porosity in order to ensure the quality of the composite material. Ultrasonic testing, optical microscopy, x-ray tomography are commonly utilized for porosity quantization. Metallographic image of a specimen showing different type of porosities are given in Figure 2.7.

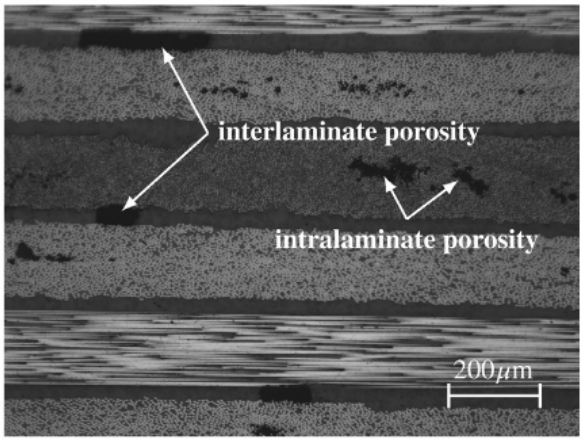

Figure 2.7: Different Type of Porosities[8]

There are different techniques studied in the literature for detecting porosity. Some are given below.

Lu et al.[175] employ terahertz (THz) spectroscopy measurements in a glass-fiber reinforced plastic (GFRP) material in order to predict the density of porosity. The obtained data from various specimens are fed to a support vector regression (SVR) machine learning model. Then an ensemble model is created, which outperforms every single machine learning model. A summary of different ensemble models are given and a optimized solution is presented. The study manages to develop a highly succesfull machine learning model, which can predict the porosity of GFRP materials in a range.

Bayat et al.[176] present temporal enhanced ultrasound (TeUS) in order to predict the porosity density of laminate composite structures. The offered technique provides an alternative for traditional non-destructive evaluation (NDE) methods. It is stated that TeUS can capture the porosity in a more realiable manner compared with other conventional methods, since it is based on multiple readings from one specimen. At the same time, it has been noticed that this technique is quite robust, even detecting small changes in porosity density.

Ajith and Gopalakrishnan[177] developed a wave-based method to quantify the porosity density. Wave propogation is modeled using spectral finite element method (SFEM), which is also based on the modified version of rule of mixtures rule. This study also present that the same methodology is also able to localize the highly porous regions on the laminate.

Hudson et al.[178] developed a in-situ technique to detect the porosity in CFRP materials during elevated-temperature autoclave cure. The system is based on a ultrasonic inspection system, which is cooled during the autoclave process. The porpsity is monitored via the reflections of ultrasonic waves. This technique is able to detect and localize the porosities as soon as they occur during the autoclave process. The localization of the porosities are verified through microscopy. Other than detection and

localization of the porosities, this tecnique provides a localized cure monitoring over the laminate in real-time.

2.3.2.5 Fiber-Matrix Debonding

Fiber-matrix debonding is another common damage mode occuring in composite laminates. The fiber-matrix interface is generally considered a weak spot, especially exposed to off-axial loads[179]. This damage refers to the complete separation of the matrix from the surface of the reinforcing fiber, or simply a loss of adhesion force between them. Since this interface is responsible for transferring the load from matrix to fiber and vica versa, it is a critical damage mode for the laminate.

Debonding generally initiates a relatively low stress at the interface between matrix and the fiber. This defect occurs because of excessive shear-transfer stresses, especially in the presence of short fibers, and may be referred as matrix cracking at the microscopic level[10] .

Debonding generally results in loss of shear transfer and overall strength degregation of the laminate. It is a dangerous damage mode because of its progressive nature, similar to fiber breakage. Interface debonding increases the stress distribution in the neighboring fiber-matrix interfaces, initiating further debonding. It is also associated with the initiation of secondary damage, such as matrix cracking and delamination.

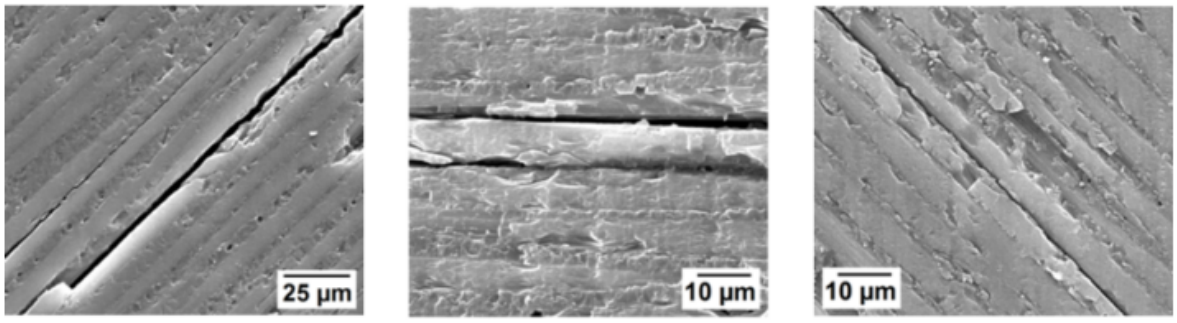

Figure 2.8: Fiber-Matrix Debonding in Different Orientations[9]

Detecting fiber-matrix debonding with direct observation is difficult since it occurs at the microscale level. It can be detected with scanning electron microscopy (SEM), where high-reolution images of interface surfaces can be observed. Other detection methods are acoustic emission (AE) and ultrasonic testing. Multiple fiber-matrix debonding is given in Figure 2.8, observed with SEM.

There are numerous work related to detection of fiber-matrix debonding in the literature. For instance, Li et al.[180] present a novel idea of using fiber optic Doppler (FOD) sensors to detect the presence of debonding at lap joints. The study explains the working principle of FOD sensors and utilizes this sensors to capture guided wave

signals. The delay in the arrival is used to detect the debonding. The study do not focus on localizing the damage, since the lap joints are already small areas by definition. It is highlighted that FOD sensors can self-calibrate meaning, contrary to other guided-wave-based damage detection systems, the damage detection do not rely on potentially unreliable reference measurements. The study is experimentally verified and succesfully demonstrates debonding detection with FOD sensors.

Ahmet et al.[181] state that the current optical pulsed thermography non-destructive testing (OPTNDT) techniques are not efficient to detect damages at the influence of noisy environments. Therefore, this paper presents the sparse emsemble matrix factorization approach in order to eliminate the noise and enhance the resolution of damage detection. The so told methodology is experimentally tested on 6 different damaged specimens and the results are presented. Compared with other methods the the results of damage detection is highly noise free, and the resolution is enhanced. The study indicates that the proposed algorithm is able to quantify subsurface debonds in CFRP materials. It should be noted that this study focuses on generally on debonding, not only fiber-matrix debonding.

Hamam et al.[182] utilize acoustic emission (AE) in order to detect fiber-matrix debonding in laminate structures. The study discusses the challanges in establishing a direct link between various damage modes and AE signals, such as material properties and sensor effects. Numerical modeling and simulation are presented as a novel approach in terms of overcoming the foretold challanges. In order to verify the simulated results, a tensile test is performed both in real-life and simulation-environment, and the results are found out to be aligned well. Then, couple of other simulated analysis is done, testing the ability of AE for detecting fiber-matrix debonding. It is shown that the fiber-matrix debonding produces generally lower amplitude AE signals compared to fiber breakage. However, the ability to detect and differentiate different damages is limited by the sensor proximity to the defect location. The study concludes that different damage modes may be differentiated with well sensor placement.

Uddin et al.[183] utilize a dual-vision image-base approach in order to study the mechanics of fiber-matrix debonding. This study presents a full-field distribution of out-of-plane displacements. Then, a 3D finite element (FE) model is used to identify the resultant properties of fiber-matrix debonding. The simulated models are compared with experimental results and verified. Various images are supplied in order to explain the progression of damage modes, and quantification of fiber-matrix debonding propagation along the fiber length is described. Significant work is presented on in-plane and out-of-plane debonding mechanism. The study concludes that dual-vision approach is effective in terms of characterizing fiber-matrix debonding and initiation. Although this study do not focus on detection and localization, it provides highly valuable insight about fiber-matrix debonding, including the explanation of initiation and propagation mechanism.

2.3.3 Summary of the Relevant Work

The summary of the reviewed work on damage detection in composite laminates are provided in Table 2.5. The table summarizes some key parameters in a simple manner, such as method used, the type of damage investigated, the system's capability in terms of localization and severity prediction, and whether the study includes experimental verification. Detailed version of this table also includes how the damage is created, which type of sensors are used, the material used, information about sensor number optimization, and the year of studies. This detailed version can be found in Appendix C.

In the following table L2 means localization, L3 means severity prediction, and Exp. means the experimental verification. Please refer to detailed version in need of any extra information.

Table 2.5: Comparison of Various Studies on Damage Detection in Composite Structures

Author	**Damage Type**	**Material**	**L2**	**L3**	**Exp.**
Chai et al.[142][1]	Delamination	Unidirectional carbon/epoxy prepeg	✗	✗	✓
Kim et al.[143]	Delamination	Unidirectional carbon/epoxy prepeg	✓	✗	✓
Saravanos et al.[144][2]	Delamination	T300/934	✓	✗	✓
Muc and Stawiarski.[145][3]	Delamination	Unspecified[4]	✓	✗	✓
Aggelis et al.[146]	Delamination, matrix cracking	Unidirectional glass/epoxy	✗	✗	✓
Gherlone and Roy.[147]	Delamination	CFRP	✓	✗	✗
Prashant et al.[155]	Matrix cracking	Glass/epoxy	✓	✓	✗
Todoroki et al.[156]	Matrix cracking	CFRP	✗	✗	✓
Mardanshahi[157]	Matrix cracking	Glass/epoxy	✗	✓	✓
Prosser et al.[158]	Matrix cracking	CFRP	✓	✗	✓
Liu et al.[159]	Matrix cracking	CFRP	✗	✓	✓

Author	Damage Type	Material	L2	L3	Exp.
Ativitavas et al.[166][5]	Fiber breakage	FRP-vinly ester resin reinforced with glass fibers	✗	✗	✓
Malik et al.[167]	Fiber breakage	Epoxy/amine with custom fibers	✓[6]	✗	✓
Kidangan et al.[168]	Fiber breakage	CFRP	✓	✗	✓
Pasadas et al.[169]	Fiber breakage	CFRP	✓	✗	✓
Lu et al.[175]	Porosity[7]	GFRP	✓	✗	✓
Bayat et al.[176]	Porosity[8]	AS4/8552	✓	✗	✓
Ajith and Gopalakrishnan.[177]	Porosity	CFRP	✓	✗	✓
Hudson et al.[178]	Porosity	CFRP	✓	✗	✓
Li et al.[180]	Fiber-matrix debonding[9]	CFRP	✗	✗	✓
Ahmed et al.[181]	Debonding[10]	CFRP	✓	✗	✓
Hamam et al.[182][11]	Fiber-matrix debonding, fiber breakage	Epoxy/amine matrix with long carbon fibers	✗	✗	✓
Uddin et al.[183][12]	Fiber-matrix debonding	GFRP	✗	✗	✓

1: Focuses on damage growth, not detection. 2: Based on CLT. 3: Uses only one sensor. 4: Properties given in text. 5: Does not focus on localization. 6: Detects the broken fiber, not location. 7: Predicts porosity density. 8: Predicts porosity density. 9: Only focuses on lap joints. 10: Focuses on multiple subsurface defects, not only fiber-matrix debonding. 11: Optimizes sensor location, not number. 12: Does not focus on localization.

Relevant work shows that numerous methodologies are developed with the aim of damage detection in composite structures. Most of the studies focus on only one damage mode at the time. Also, it is noticible that most of these methodologies are not applied in-situ and not applicable in real-time. Development of a multi-damage mode detecting methodology and new methodologies which may operate during the parts working cycle, in real-time, would surely be contributing to the field.

Chapter 3

Theoretical Background and Methodology

3.1 Displacement, Strain, and Stress Fields

This study relies on a methodology based on strain, stress, and displacement fields. For any given material with same geometric properties, undamaged and damaged states differentiate numerically in these properties. Therefore, short descriptions of these properties are provided in the following subsections.

3.1.1 Displacement Field

Before defining any of the foretold mechanical properties, some assumptions regarding to continuum mechanics are required. Continumm mechanics describes the macro-scale behavior of matter that is under mechanical loading. It is a combination of mathematical and physical laws. Continuum mechanics employ The Newtonian reference frame, where the world is assumed as a three dimensional Euclidean space, where each point is defined by coordinates (x_1, x_2, x_3). This vector space contains all real numbers and all possible coordinates. Vectors can be disassembled to components of perpendicular unit vectors $\{e_1, e_2, e_3\}$. Newton's law are assumed to hold in this space.

Matter is treated as continuum, it can be divided indefinitely and it is locally homogeneous. This means any small part of the material has the exact same physical properties (e.g., density), regardless of scale. The matter is defined as a collection of infinite connected particles.

In order to describe motion, reference and deformed configuration of a solid body must be defined. A configuration of a solid refers to the specific region in space it occupies. To analyze motion or deformation, typically an appropriate reference configuration must be given. This is commonly the initial, undeformed state of the solid body, though it could be any reasonable shape the solid might take. When external

loads act on the body, deformation occur and solid body moves to a new configuration. This configuration is commonly referred as deformed or current configuration of the solid.

In certain problems such as fluid flow or materials with growth or changing microstructures, a fixed initial reference configuration is not feasible. In these cases a deformed configuration may be used instead as a reference.

Mathematically, deformation is modeled as 1:1 mapping from points in the reference configuration to the corresponding points in the deformed configuration. Let's assume ε_i is the corresponding coordinates of a point(Cartesian coordinate system, polar coordinate sytem does not matter) in the initial, undeformed solid body. As the external force acts the solid will start to deform, and the values represented by ε_i will start to change due to deformation. This is deformation mapping, and can be expressed as Equation 3.1, where ε_k is the deformation at point k, and t is time.

$$\eta_i = (\varepsilon_k, t) \tag{3.1}$$

There are conditions for a deformation to be physically admissible. The coordinates must specify a unique position in Newtonian reference frame. This means, a coordinate transformation $x_i(\varepsilon_k)$ must exist, such that x_i are components in an orthogonal basis, which is assumed to be stationary in Newtonian dynamics. The mapping fucntion $f_i(\varepsilon_k)$ must be injective on the full set real numbers, and it must be invertible. The function f_i must be continuous and contentiously differentiable. The Jacobian determinant of the transformation must be positive ensuring no folding or overlapping occurs in space, this is given in Equation 3.2.

$$det(\partial\eta_i/\partial\varepsilon_k) > 0 \tag{3.2}$$

The positions of particles in both undeformed and deformed configurations are expressed using a Cartesian inertial reference frame. The undeformed position is denoted as x_i, while the deformed position after the motion is denoted as $y_i(x_k)$.

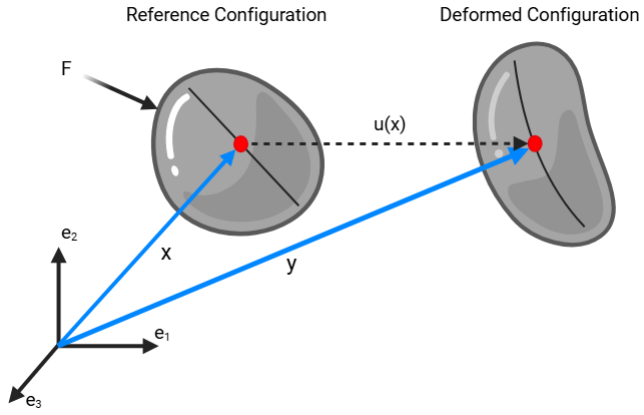

Figure 3.1: Initial and Deformed Configurations

In Figure 3.1, $u(x,t)$ is called the displacement vector and describes the motion of each point in the solid body. As seen, a point at position x has moved to a new point y at time t. Therefore the relative displacement vector can be defined as Equation 3.3.

$$\mathbf{y} = \mathbf{x} + \mathbf{u}(\mathbf{x}, t) \tag{3.3}$$

Considering the coordinate system as Cartesian, and the reference configuration to be current state, following equation is obtained.

$$\mathbf{u}(\mathbf{x}, t) = \begin{pmatrix} u_1(\mathbf{x}, t) \\ u_2(\mathbf{x}, t) \\ u_3(\mathbf{x}, t) \end{pmatrix} \tag{3.4}$$

This is called the displacement field of a solid body, given in Equation 3.4, which describes the motion of a deformable body. It is the basis for computing strain and stress.

3.1.2 Strain Field

Strain is a core principle in both continuum and structural mechanics. It is a dimensionless measure of the deformation. Any material subjected to external forces experiences strain as a response. It is defined as relative displacement and represents the relative displacement between particles in a solid body.

The following part describes the derivation of the strain field following the guidance of the published work by Wierzbicki[184]. Most of the explanation is an adaptation of the original work.

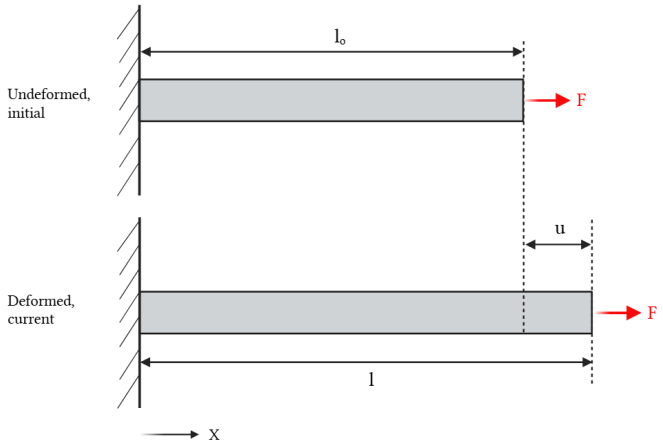

Figure 3.2: Simple Beam in Unidirectional Loading

Let's consider a one-dimensional beam fixed at one and subjected to a tensile load at the other end. As explained, the external load causes elongation on the loading direction. Initial length of the beam is denoted as l_o, and the current, deformed length is denoted by l, seen in Figure 3.2. Note that the investigation is one-dimensional, only on X axis. The strain is assumed to be homogeneous in current case, meaning local and the average strains are the same. Therefore, strain can be defined by considering the total length of the beam. Displacement at the fixed end of the beam ($x = 0$) is zero($u(x = 0) = 0$). At the free-end($x = l$) displacement is calculated as Equation 3.6.

$$u(x = l) = l - l_o \tag{3.5}$$

At the risk of repeating, strain is defined as relative displacement. Considering different reference points, there are different definitions for strain. Following equations represent various approaches of strain measurement.

$$\varepsilon = \frac{l - l_o}{l_o} \quad \text{Engineering strain} \tag{3.6}$$

$$\varepsilon = \frac{1}{2}\frac{l^2 - l_o^2}{l^2} \quad \text{Cauchy strain} \tag{3.7}$$

$$\varepsilon = \ln \frac{l}{l_o} \quad \text{Logarithmic strain} \tag{3.8}$$

Each of the equations stated above are valid definitions of strain. Unsurprisingly, only the engineering strain is relevant for most of the studies in the literature, since it provides a straightforward and practical approach for evaluating material deformation. Also, considering a small strain ($l_o + l \approx 2l_o$ and $l - l_o \approx 0$), both of the other definitions basically reduces to engineering strain.

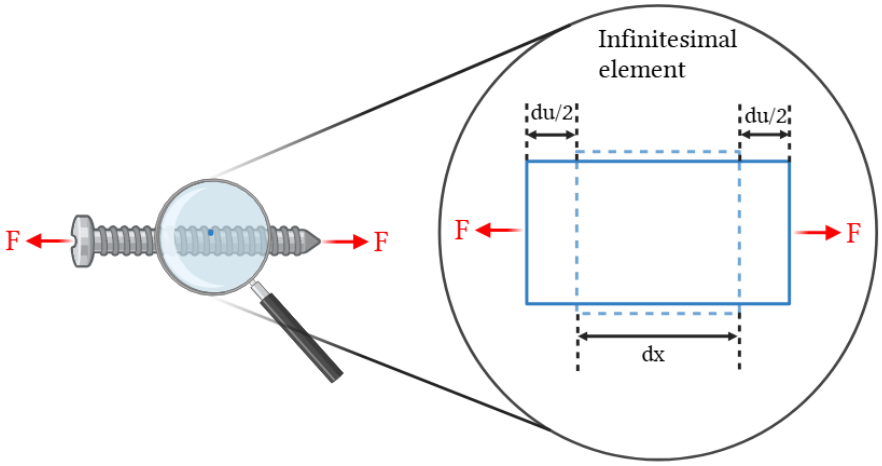

Figure 3.3: Strain on a Infinitesimal Element

Let's imagine the strain as inhomogenous. In this case strain must be defined locally, not for the entire part. In Figure 3.3, an infinitely small element with length dx under a tensile load is considered. Exposed to the load, a change in length du is observed in the infinitesimal element. New (deformed) length of the element becomes $dx + du$. Remembering the definition engineering strain from Equation 3.7, engineering strain of the infinitesimal element is given in Equation 3.10.

$$\varepsilon_{\text{eng}} = \frac{(\mathrm{d}x + \mathrm{d}u) - \mathrm{d}x}{\mathrm{d}x} = \frac{\mathrm{d}u}{\mathrm{d}x} \tag{3.9}$$

It should be noted that the spatial derivative of the displacement field (Equation 3.4) is the displacement gradient given as:

$$D = \frac{\mathrm{d}u}{\mathrm{d}x} \tag{3.10}$$

Inspecting Equation 3.10 and 3.11, it may appear that the engineering strain and the displacement gradient is the same, but this is only true for uniaxial scenarios. For the uniaxial state, strain is the simply the displacement gradient. However, this is not valid for the three-dimensional (3D) application.

To extend this concept into the three-dimensional space, Equation 3.10 is re-written as follows.

$$\mathrm{d}u = \varepsilon \mathrm{d}x \tag{3.11}$$

Considering an Euclidian space an arbitrary point in a solid body is represented as the vector $x = \{x_1, x_2, x_3\}$ or alternatively x_i, where i indicates the directions $i = 1, 2, 3$.

The displacement of this arbitrary point is also a vector with direction components $u = \{u_1, u_2, u_3\}$. Summing the components in each direction, and substituting in Equation 3.12 displacement increment vector is obtained.

$$\mathrm{d}u_1(x_1, x_2, x_3) = \frac{\partial u_1}{\partial x_1}\mathrm{d}x_1 + \frac{\partial u_1}{\partial x_2}\mathrm{d}x_2 + \frac{\partial u_1}{\partial x_3}\mathrm{d}x_3 \tag{3.12}$$

Employing the subscripts i and j, where j is the "dummy" index, the following equation is obtained.

$$\mathrm{d}u_i(x_i) = \frac{\partial u_i}{\partial x_1}\mathrm{d}x_1 + \frac{\partial u_i}{\partial x_2}\mathrm{d}x_2 + \frac{\partial u_i}{\partial x_3}\mathrm{d}x_3 = \sum_{j=1}^{3} \frac{\partial u_i}{\partial x_j}\mathrm{d}x_j \tag{3.13}$$

Then the displacement gradient becomes:

$$D = \frac{\partial u_i}{\partial x_j} \tag{3.14}$$

The displacement gradient is not a symetric tensor, it includes the rigid body motion terms. Re-writing the expression in Equation 3.15 in an equivalent form the asymmetry is visible.

$$D = \frac{\partial u_i}{\partial x_j} = \frac{1}{2}\left(\frac{\partial u_i}{\partial x_j} + \frac{\partial u_j}{\partial x_i}\right) + \frac{1}{2}\left(\frac{\partial u_i}{\partial x_j} - \frac{\partial u_j}{\partial x_i}\right) \tag{3.15}$$

The strain tensor ε_{ij} is defined as the symmetric term of the displacement gradient in the equivalent form. This is the first term of Equation 3.16.

$$\varepsilon_{ij} = \frac{1}{2}\left(\frac{\partial u_i}{\partial x_j} + \frac{\partial u_j}{\partial x_i}\right) \tag{3.16}$$

By transposing the indices i and j:

$$\epsilon_{ji} = \frac{1}{2}\left(\frac{\partial u_j}{\partial x_i} + \frac{\partial u_i}{\partial x_j}\right) \tag{3.17}$$

Now, the first term of Equation 3.18 is the second term of Equation 3.17, and the second term of Equation 3.18 is the first term of Equation 3.17. This signifies that the strain tensor is symmetric.

$$\varepsilon_{ij} = \varepsilon_{ji} \tag{3.18}$$

The second term of the Equation 3.16 is called the spin tensor ω_{ij}.

$$\omega_{ij} = \frac{1}{2}\left(\frac{\partial u_i}{\partial x_j} - \frac{\partial u_j}{\partial x_i}\right) \tag{3.19}$$

It is easy to see that after the transpose of the subscripts, the spin tensor shows asymmetry because of the negative sign of the second term.

$$w_{ij} = -w_{ji} \tag{3.20}$$

The diagonal terms of the spin tensor $(\omega_{11}, \omega_{22}, \omega_{33})$ are equal to zero from the definition. Therefore the components of the strain tensor are as follows:

$$i = 1,\ j = 1 \quad \varepsilon_{11} = \frac{1}{2}\left(\frac{\partial u_1}{\partial x_1} + \frac{\partial u_1}{\partial x_1}\right) = \frac{\partial u_1}{\partial x_1} \tag{3.21}$$

$$i = 2,\ j = 2 \quad \varepsilon_{22} = \frac{\partial u_2}{\partial x_2} \tag{3.22}$$

$$i = 3,\ j = 3 \quad \varepsilon_{33} = \frac{\partial u_3}{\partial x_3} \tag{3.23}$$

$$i = 1,\ j = 2 \quad \varepsilon_{12} = \varepsilon_{21} = \frac{1}{2}\left(\frac{\partial u_1}{\partial x_2} + \frac{\partial u_2}{\partial x_1}\right) \tag{3.24}$$

$$i = 2,\ j = 3 \quad \varepsilon_{23} = \varepsilon_{32} = \frac{1}{2}\left(\frac{\partial u_2}{\partial x_3} + \frac{\partial u_3}{\partial x_2}\right) \tag{3.25}$$

$$i = 3,\ j = 1 \quad \varepsilon_{31} = \varepsilon_{13} = \frac{1}{2}\left(\frac{\partial u_3}{\partial x_1} + \frac{\partial u_1}{\partial x_3}\right) \tag{3.26}$$

Constructing the strain tensor:

$$\varepsilon_{ij} = \begin{bmatrix} \varepsilon_{11} & \varepsilon_{12} & \varepsilon_{13} \\ \varepsilon_{21} & \varepsilon_{22} & \varepsilon_{23} \\ \varepsilon_{31} & \varepsilon_{32} & \varepsilon_{33} \end{bmatrix} \tag{3.27}$$

Substituting the components in Equation 3.28, the strain tensor is obtained.

$$\varepsilon_{ij} = \begin{bmatrix} \frac{\partial u_1}{\partial x_1} & \frac{1}{2}\left(\frac{\partial u_1}{\partial x_2} + \frac{\partial u_2}{\partial x_1}\right) & \frac{1}{2}\left(\frac{\partial u_1}{\partial x_3} + \frac{\partial u_3}{\partial x_1}\right) \\ \frac{1}{2}\left(\frac{\partial u_2}{\partial x_1} + \frac{\partial u_1}{\partial x_2}\right) & \frac{\partial u_2}{\partial x_2} & \frac{1}{2}\left(\frac{\partial u_2}{\partial x_3} + \frac{\partial u_3}{\partial x_2}\right) \\ \frac{1}{2}\left(\frac{\partial u_3}{\partial x_1} + \frac{\partial u_1}{\partial x_3}\right) & \frac{1}{2}\left(\frac{\partial u_3}{\partial x_2} + \frac{\partial u_2}{\partial x_3}\right) & \frac{\partial u_3}{\partial x_3} \end{bmatrix} \tag{3.28}$$

Strain field and strain tensor are not the same things. Strain tensor is the local representation of the strain field at a given point. Strain field is a function of strain tensors, defined at every point of the structure.

Although, there are new developing methodologies providing better resolution in strain measurement such as light microscopy[185], traditional strain gauges based on electrical principals are commonly used.

Strain is important since it describes how the material deforms under applied load. A thorough understanding of the strain behavior of any material is a key point for designing long-lasting structures, as it helps to predict the response of the material under any given load.

Furthermore, as in our study, strain analysis plays a critical role in ensuring structural integrity and safety of engineering structures. In civil engineering, monitoring strain in bridges or buildings helps to detect overloading before failure occurs, various work on this topic are included in the literature review. In aerospace and automative industries, strain measurements are used for lightweigh design without compromising strength, resulting in efficiency increase. It is even studied on biological materials for medical device developments.

3.1.3 Stress Field

The stress field refers to the distribution of internal stresses throughout a material or structure subjected to external forces. Since external loading can cause deformation or changes in the material, stress fields are crucial for understanding the behavior of the material under load. Understanding the stress field in a material or structure is essential for predicting failure, analyzing how loads distribute within complex geometries, and designing safe structures. Furthermore, stress field provides insights about how the solid body experience internal forces, especially near discontinuities, boundaries, and most importantly defects. Stress is closely related to strain, remembering the Hooke's law given in equation below, where E is the Young's modulus, and ε is the strain.

$$\sigma = E\varepsilon \tag{3.29}$$

The following section follows the work of David Dye[186], and defines the stress field. Most of the explanation and the figures are adapted from the original work.

Let's start with a two-dimensional (2D) element in a material, with dx as the length and dy is the height. The element is infinitely small and there are forces acting on the element on each side. The forces are denoted as A, B, C, D seen in Figure 3.4.

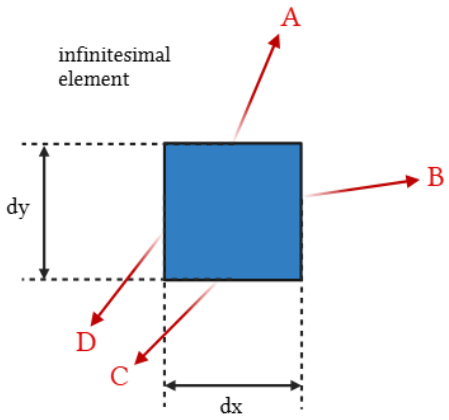

Figure 3.4: Forces on a 2D Infinitesimall Element

Resolving these forces in their respective x and y coordinates, the following distribution is obtained in Figure 3.5.

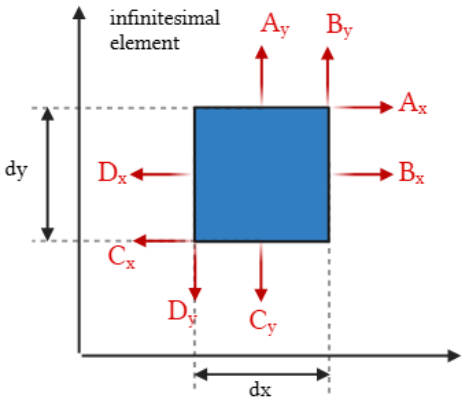

Figure 3.5: Forces Resolved into Components

These forces can be converted into stresses, considering the length dx and the height dy of the element. It should be noted that the resultant of the forces and moments must be zero, if the element is in equilibrium. In the following figure, the first subscript denotes the normal plane and the second subscript indicates the direction. For equilibrium condition to be met, the following must be true $\tau_{xy} = \tau_{yx}$, otherwise the element will spin. Therefore, only three stresses are enough to construct stress tensor.

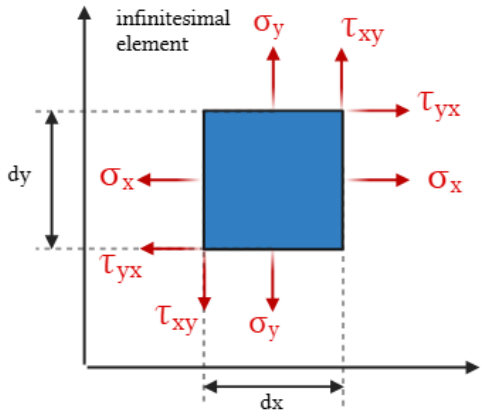

Figure 3.6: Stresses in 2D Element

Moving onto the three-dimensional space, stress can be written as a second rank tensor. Therefore it is a 3x3 matrix, where i is the direction of the stress, and j is the direction of the plane normal to loading face. The normal stresses are denoted with the subscript ii, and the shear stresses are denoted with subscript ij or ji with the condition $i \neq j$. The visualization of these components are given in Figure 3.7.

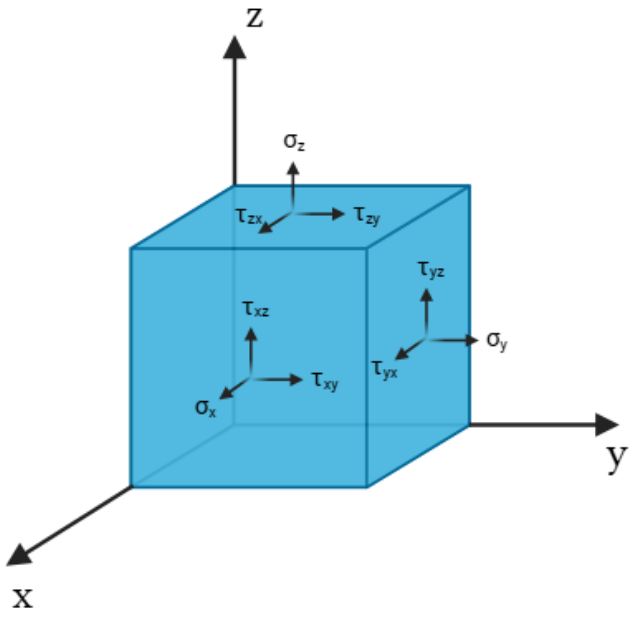

Figure 3.7: Stresses on a Infitesimal Element

The general stress tensor in three-dimensions ia written as :

$$\sigma_{ij} = \begin{pmatrix} \sigma_x & \sigma_{xy} & \sigma_{xz} \\ \sigma_{xy} & \sigma_y & \sigma_{yz} \\ \sigma_{xz} & \sigma_{yz} & \sigma_z \end{pmatrix} \tag{3.30}$$

where $\sigma_x = \sigma_{xx}$, $\sigma_{yx} = \sigma_{yy}$, and $\sigma_z = \sigma_{zz}$.

The condition for the equilibrium can be seen as $\sigma_{ij} = \sigma_{ji}$, which reduces the 9 independent components to 6 independent component. It is seen that the stress tensor is a symmetric tensor. It should be noted that the stress field and the strain tensor are not the same things, though they are related. Strain tensor describes the stresses in a single point, while stress field describes the stresses in the whole structure. Simply, stress field contains all of the stress tensor in a structure, and maps a tensor to every single point.

3.2 Ensemble Methods in Machine Learning

In machine learning applications, ensemble methods utilize multiple machine learning algorithms to obtain a better prediction than the prediction obtained by any constituent model alone[187].Frequently, evaluation with multiple different models exceeds the performance of only one model, and provides a more generic model. Ensemble machine learning models are specifically better at balancing low variance and low bias, and therefore they align well with real-world applications and produce significantly better results. The main techniques for ensemble machine learning applications are bagging, boosting, and stacking. The ensemble methods will be described in detail in the next section.

Bagging (Bootstrap Aggregating), combines especially high-variance machine learning models and their variations and produces a more stable and better performing model. This technique divides the dataset into multiple random subsets and feeds them into different models. Each model outputs a prediction and the final predictions done by voting, with or without weights, for classification problems, and with mathematical average for regression problems. Random forest algorithm is the most typical example of this technique. In a random forest model, multiple decision trees work simultaneously in order to produce a final prediction.

Boosting techniques combines multiple weak machine learning algorithms and trains them consecutively, while feeding the next model with the residual error obtained by the prior model. Every new model attempts to correctly predict which was not correctly predicted by the prior model. These models generally include less bias, but care should be given in the training process, since they are susceptible to overfitting. AdaBoost, Gradient Boosting, XGBoost and LightGBM are the most popular models based on boosting. Although, boosting models show impressing overall performance, the required

computation power is costlier than bagging techniques and it is more sensitive to the hyper-parameter tuning.

Stacking, also called as Stacked Generalization, is an ensemble method where various different machine learning models are brought together. It is a more flexible technique compared to others, since it allows different machine learning models working together, such as neural networks, decision trees, support vector machines, etc. These models are trained with the same data, and generate different outputs. Then, as a second step, these outputs are used as features for a "meta model". Meta model trains on the outputs of the other models and creates the final output. The strengths of each machine learning model are combined together in the meta model. However, stacking is a highly complex method, particularly when a diverse pool of models are employed. Therefore, it requires careful data preparation and mostly cross-validation after training.

The working principle of Bagging is explained in its dedicated section, and it is visualized in Figure 3.11. Similarly, the structure of Boosting is found in its section, and in Figure 3.12. Since stacking is not employed in this study, it does not have a dedicated section, but the working principle of stacking can be seen in Figure 3.8.

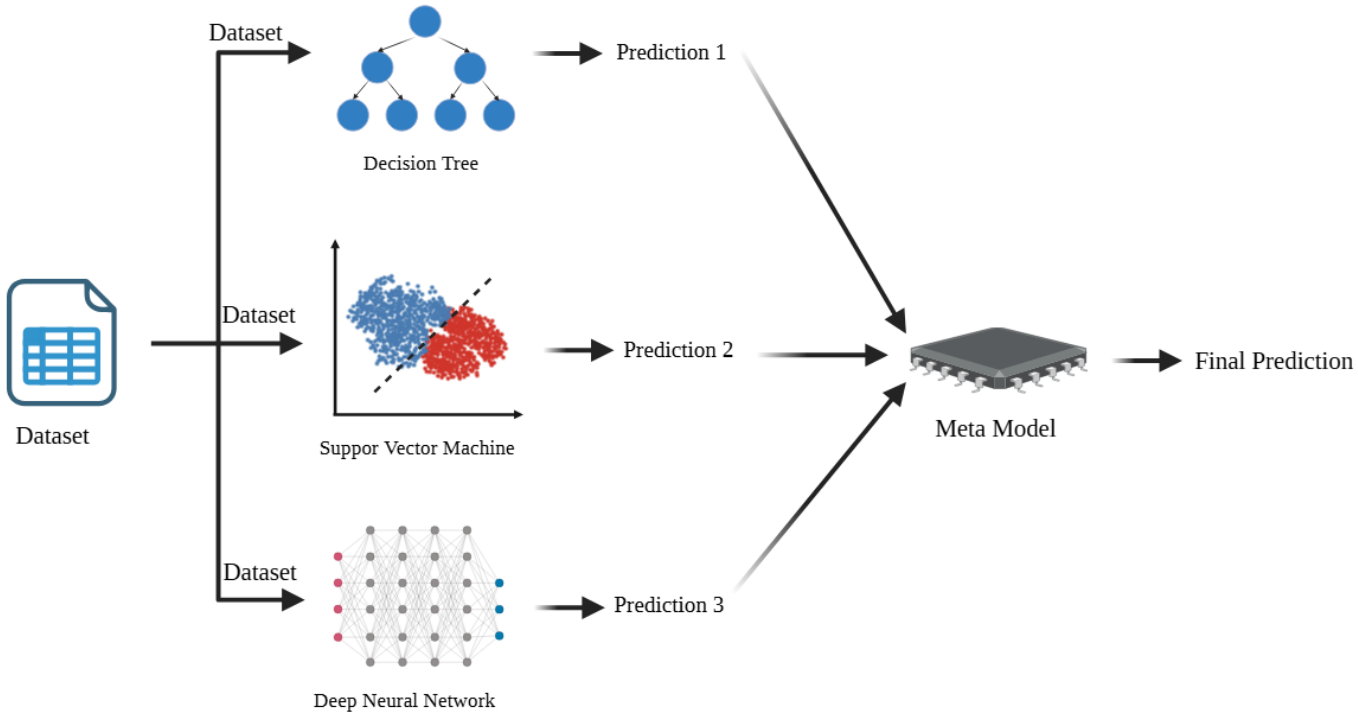

Figure 3.8: Working Principle of Stacking Technique

As explained, ensemble methods perform well where individual models make mistakes. Along these advantage, there are disadvantages such as high computation cost, low interpretability, and high complexity data preparation process. Especially for big

datasets, selecting the right ensemble strategy is crucial. A well prepared ensemble method produces significantly better results compared to other individual machine learning models.

3.3 Structure of Selected Machine Learning Models

The applications, given in Chapter 4, employ three machine learning algorithms for damage detection and localization, namely neural networks (NN), random forest (RF), and Extreme Gradient Boosting (XGBoost). The following section is dedicated to explain the working principles of these ML models.

3.3.1 Neural Networks

Neural networks (NNs), or also known as artificial neural networks (ANNs), are a computational model inspired from the very neurons and their connections in the human brain, and they have long been employed for modeling decision-making systems[188]. Neural networks use interconnected nodes (neurons) to process data and learn complex patterns. The connections resemble the synapses in the brain. Each of the nodes, or neurons, receives signals from the connected nodes at the prior layer and processes the data before sending the output to other connected nodes at the superior layer. The received signals are real numbers, computated according to a non-linear function, called the activation function. This function takes the sum of all gathered signals and produces an output, which will be sent to the connected nodes at superior layer. The strength of the signal at different connections are determined by its weight, which is adjusted during the learning step.

The layered structure consist of three type of layers. First layer is the input layer, and it receives the raw input features (e.g., color of a pixel, sensor readings, etc.). Number of the neurons on this layer is equal to number of input features. There is exactly one neuron per feature. The layers located between input and the output are called hidden layers. Each hidden layer applies non-linear transformations with the activation function, and transfers the information to the next layer. A NN model might have one or more hidden layers. If there are at least two hidden layers, the network is typically called a deep neural network[189]. The output layer is the last layer of any NN model. This layer produces the final output of the network. The number of neurons are dependen on the task. For instance, binary classification use just one neuron but multi-class classifiers use neuron numbers equal to output classes. The graphical representation of a neural network is given in Figure 3.9.

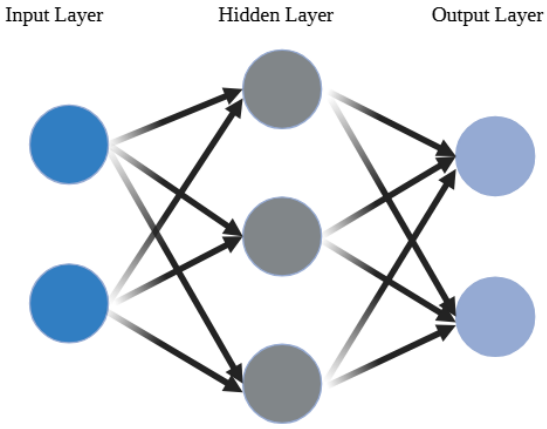

Figure 3.9: A Simple Neural Network

Each of the nodes, or neurons, follow a mathematical process for determining its output. Suppose that a neuron with label j receives inputs $x_1, x_2, ..., x_n$, each coming from a single neuron. The propagation function computes the total input p_j to the neuron, given in Equation 3.31.

$$p_j = \sum_{i=1}^{n} w_{ij} x_i \tag{3.31}$$

Here, x_i is the input coming from the neuron i, ω_{ij} is the weight of the connection between the neurons i and j. A bias term b_j can be added to the value as well.

$$p_j = \sum_{i=1}^{n} w_{ij} x_i + b_j \tag{3.32}$$

The value of p_j is called the pre-activation value. Then, an activation function (ϕ) is applied in order to compute the actual activation value ($\phi(p_j)$) of the neuron. Finally, this value is sent to all of the connected neurons. Figure 3.10 explains the workflow visually.

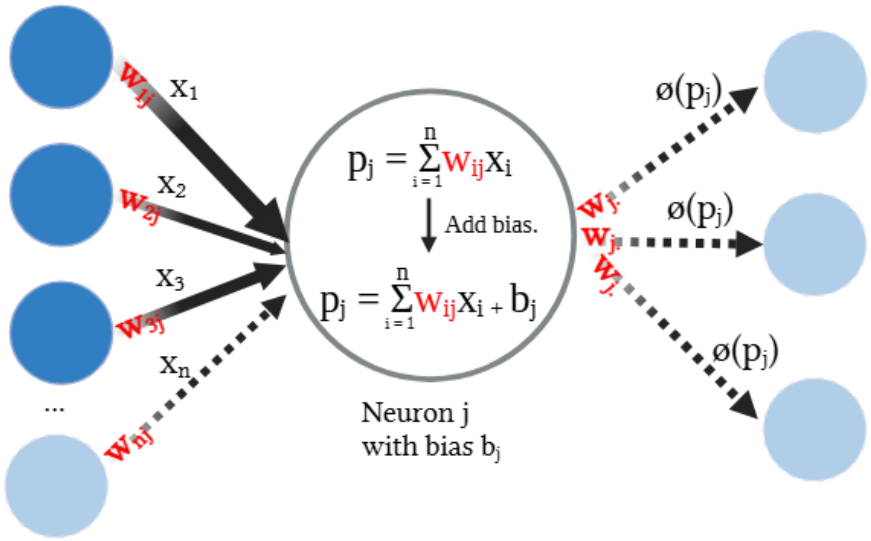

Figure 3.10: Simplified Mathematical Background of a Neuron

Here, ω_{ij} or $\omega_{j.}$ represents the weight of the connections, which is also visualized with line thickness. The activation function ϕ might differ regarding to the study, since each of them provide unique strength and weaknesses. The most common activation functions are given in the following equations.

$$\text{Sigmoid:} \quad \phi(p_j) = \frac{1}{1 + e^{-p_j}} \tag{3.33}$$

$$\text{ReLU:} \quad \phi(p_j) = \max(0, p_j) \tag{3.34}$$

$$\text{Tanh:} \quad \phi(p_j) = \tanh(p_j) \tag{3.35}$$

3.3.2 Random Forest

Random forest, or also called as random decision forest, is a machine learning algorithm for classfication, regression, and other tasks. It consists of the combination of multiple decision trees. Each of the decision trees are trained with different random subset of the dataset. This improves the accuracy of the model and reduces the risk of overfitting. Random forest is an inherently ensemble method, meaning the final prediction includes the contribution of each three. Simply put, each independent tree votes on the result.

For classification, majority voting is employed while for regression problems average of all predictions is used. Working principle for classification is given in Figure 3.11. It can be seen that each decision tree takes a random subset of the data, this is called

bootstrap sampling. Furthermore, each branch randomly selects the features for training. Therefore, the similarity between trees are minimized and each prediction gets calculated uniquely.

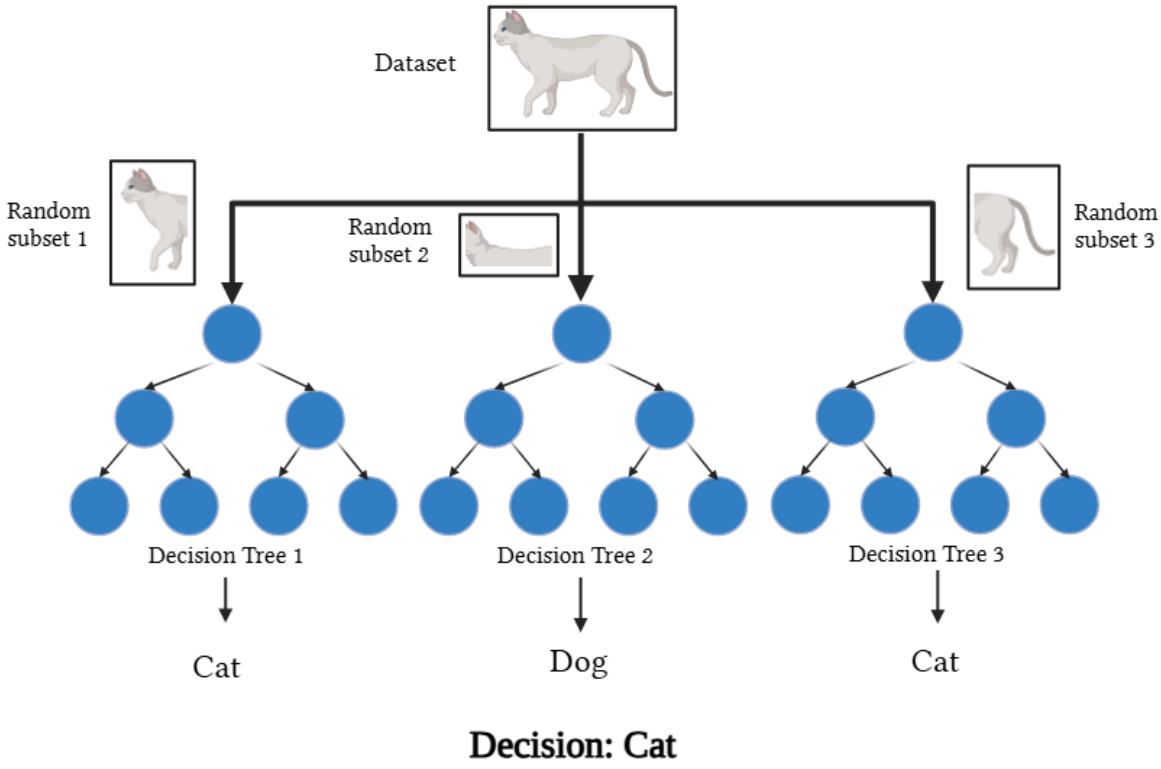

Figure 3.11: Working Principle of Classification Random Forest

The mathematical structure behind random forest relies on Bagging (Bootstrap Aggregation), and random feature selection. It is important to understand the mathematics behind the random forest algorithms in order to better optimize the model for applications. Let's suppose D is the total dataset, and N decision trees are to be created.

$$D = \{(x_1, y_1), (x_2, y_2), ..., (x_n, y_n)\} \tag{3.36}$$

where $D_1 = (x_1, y_1)$, $D_2 = (x_2, y_2)$, $D_n = (x_n, y_n)$, and $\vee D_i \subset D$. Here, each D_i represents a random subset used for the corresponding decision tree. This process is called Bootstrap Aggregation or Bagging. The decision process starts with the first node, and at each split random features (k) are selected as training features from all of the present features (f). Considering Figure 3.11, this can be visualized as one split

takes the outline of the cat and the average color of the subset as features, and another split takes number of total colors, and the standard deviation of the color distribution as features. Following equations are commonly used in random feature selection, where d is the total available features, and k is the selected features.

$$\text{Classification:} \quad k = \sqrt{d} \tag{3.37}$$

$$\text{Regression:} \quad k = d/3 \tag{3.38}$$

For classification applications, the split quality is measures with the metric Gini Impurity:

$$G(t) = 1 - \sum_{i=1}^{C} p_i^2 \tag{3.39}$$

where p_i is the number of sample belonging to the class i, while C represents number of classes. Alternatively, entropy (information gain) can be used as a measure for split quality, given in Equation 3.40.

$$H(t) = -\sum_{i=1}^{C} p_i \log(p_i) \tag{3.40}$$

Regarding these metrics, the more homogeneous the subset, better the split quality. For classification, each decision tree outputs a decision with their internal function $h_i(x)$, where x is the input features. The final prediction (y) is determined with the decision of all trees.

$$y = \text{mode}\left(h_1(x), h_2(x), \ldots, h_n(x)\right) \tag{3.41}$$

For regression applications, final prediction is the statistical average of the tree outputs, given in Equation 3.42.

$$y = \frac{1}{N} \sum_{i=1}^{N} h_i(x) \tag{3.42}$$

Random forest algorithm is particularly favored in situations where model interpretability, robustness to noise, and resistance to overfitting is important. Due to its ensemble nature, combining predictions of multiple models, random forest performs well on complex and high-dimensional datasets, and is capable of capturing non-linear realtionships among the features.

3.3.3 Extreme Gradient Boosting (XGBoost)

XGBoost, also known as Extreme Gradient Boosting, is a machine learning model based on decision trees. The core part of the model is an ensemble method called boosting. This method trains multiple relatively weak machine learning models consecutively, which ends up as a strong model. There are various optimization techniques employed, in order to make the training process faster, more accurate and more stable. Each decision tree, tries to reduce the error caused by the prior trees. Therefore, the error gets minimized through each step.

The training process is carried out according to an objective function. This function not only minimizes the error, but penalizes the complexity formed by the model, preventing overfitting. XGBoost is a strong model for both classification and regression problems, but the application area of XGBoost is not limited to these. With XGBoost, ranking, anomaly detection, and time series forecasting can be performed with high speed and accuracy.

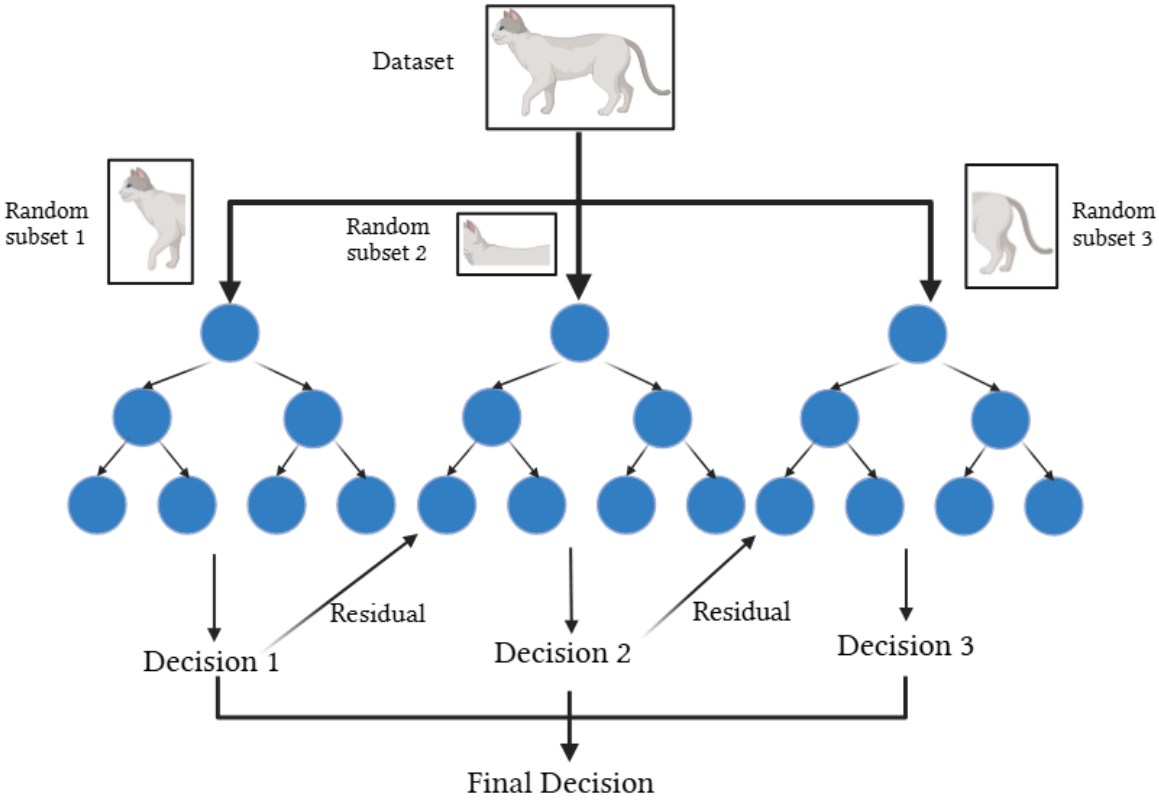

Figure 3.12: Working Principle of XGBoosting

The working principle of the XGBoost model is provided in Figure 3.12. The most important features which differentiate XGBoost from other gradient boosting algo-

rithms are penalization of trees, extra randomization parameter, and automatic feature selection.

The mathematical procedure in the background for XGBoost starts with an initial prediction $y_{pred}^{(t-1)}$ from the first decision tree. It is important to not confuse this with the final prediction. This initial prediction is fed to the next tree with the residual prediction, and the cycle goes on. Equation 3.43 shows the process.

$$y_{pred}^{(t)} = y_{pred}^{(t-1)} + \eta \cdot f_t(x) \tag{3.43}$$

Where η is the learning rate, $f_t(x)$ is the residual, and $y_{pred}^{(t)}$ is the prediction of current tree, which is the t-th tree.

The objective function is the base mathematical structure that determines what is to be optimized in the training process of XGBoost. A good objective function provides better predictions. The objective function is given in Equation 3.44.

$$OF = \sum_{i=1}^{n} l(y_i, \hat{y}_i) + \sum_{t=1}^{T} \Omega(h_t) \tag{3.44}$$

This equation consists of two terms. The first term is called the loss function given in Equation 3.45.

$$\sum_{i=1}^{n} l(y_i, \hat{y}_i) \tag{3.45}$$

Where y_i is the real value, and $\hat{y}_i$ is the prediction of the model. Function l compares these two values and generates an error. For regression mean squared error (MSE),and for classification log loss or cross entropy are commonly employed. The model attempts to minimize these errors. The second term is the regularization, given in Equation 3.46.

$$\sum_{t=1}^{T} \Omega(h_t) \tag{3.46}$$

Here, h_t is the learning function in the t-th tree, and Ω is the penalization function for complexity. This term tries to reduce the error without adding complexity to the model. This function is where XGBoost makes a difference. The internal structure of the function is given below.

$$\Omega(h_t) = \gamma J + \frac{1}{2}\lambda \sum_{j=1}^{J} w_j^2 \tag{3.47}$$

Where j is the leaf number in a decision tree, ω_j is the weight of j-th leaf, and γ, λ are the hyper-parameters for model tuning.

Chapter 4

Development and Application

4.1 Test Case

Two different models are considered for the numerical work. First model is a composite plate with one edge clamped,and the other edge is free. The free edge is loaded with two 50N forces. This configuration is commonly used to study bending and deformation behavior under static loading. The height of the plate is 400 mm, while the length is 2000 mm. Nastran/Patran is used for modeling and mechanical analysis. The first model, also called Model 1, is given in Figure 4.1.

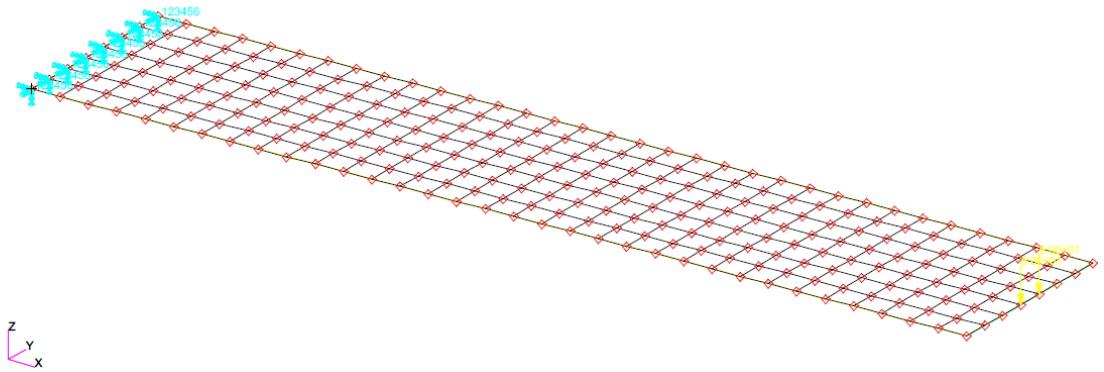

Figure 4.1: Isometric Projection of Model 1

The model is meshed using quadratic element for finite element analysis (FEM). There are 231 elements in the mesh, seen in Figure 4.2. The mesh has been kept coarse, considering both the computation power limitations, and the scope of the study aiming to verify the methodology rather than providing a robust application.

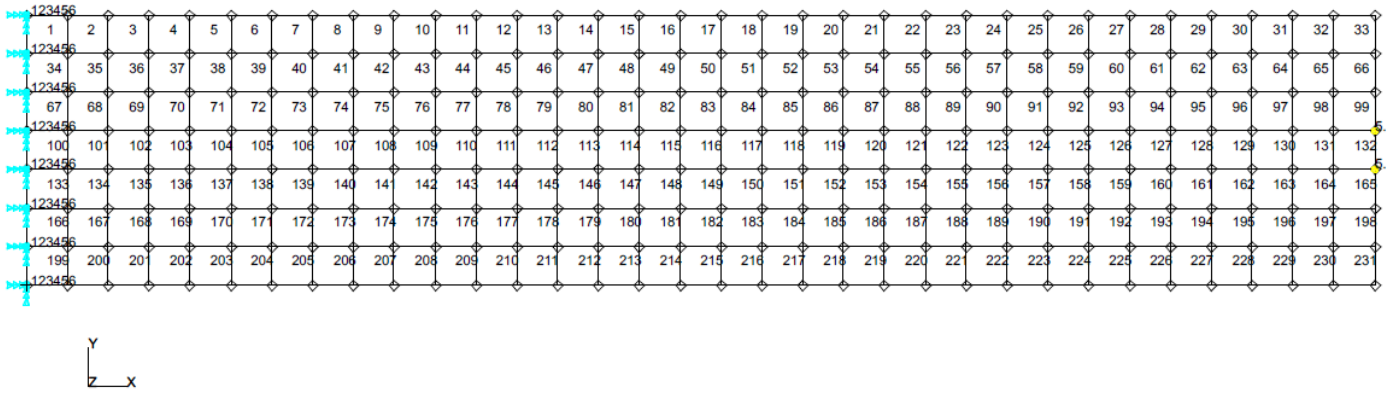

Figure 4.2: Top View of Model 1 Including Mesh Numbers

The fixed support can be seen on the left end, while two application points of the forces can bee seen on right. This configuration of supports and loads are shared in both models.

Second model, also called Model 2, shares the same length and height with Model 1. As a variation, this model has two stiffeners built into the composite structure. The material of the stiffeners is the same with the structure and the width of each stiffeners is 10 mm. Model 2 is given in Figure 4.3

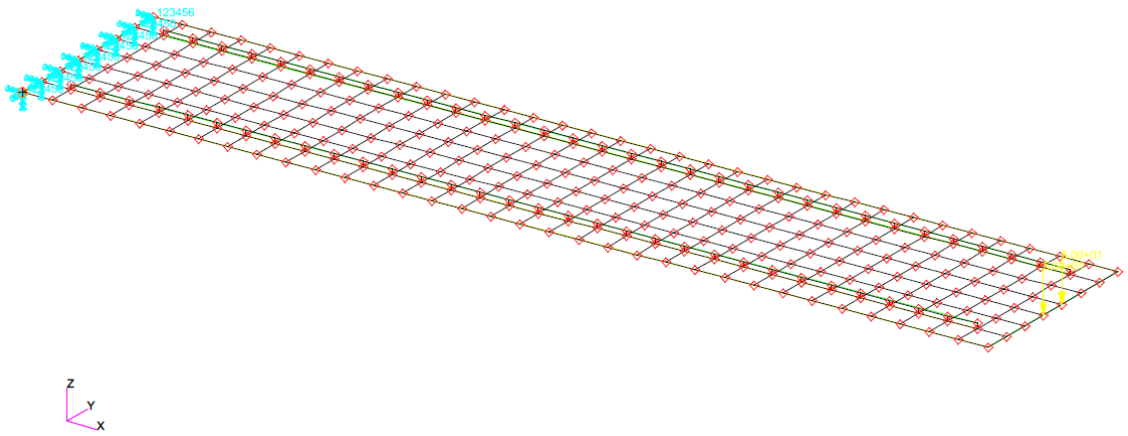

Figure 4.3: Isometric Projection of Model 2

Stiffeners are added to the structure to challenge the system more further. The presence of stiffeners makes the strain, stress, and displacement fields more complex, resulting in harder patterns for machine learning algorithms. Meshed version of the

model has 293 elements in total, given in Figure 4.4. Material properties are the same in both models.

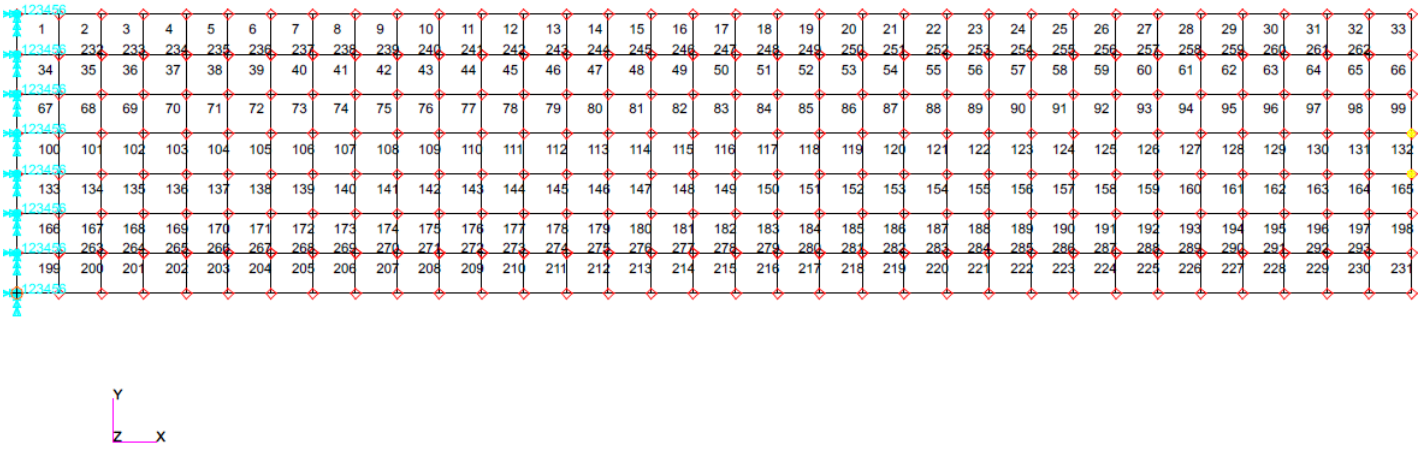

Figure 4.4: Top View of Model 2 Including Mesh Numbers

The composite laminate consists of 3 plies, each 0.5 mm thick, with fiber orientations $[0°/90°/+45°]$. The material is specified to be CFRP, and the properties are given in Table 4.1.

Table 4.1: Material Properties of CFRP

Property	**Value**	**Unit**
Elastic Modulus, E_1	135	GPa
Elastic Modulus, E_2	10	GPa
Poisson's Ratio, ν_{12}	0.3	-
Shear Modulus, G_{12}	5	GPa
Shear Modulus, G_{23}	5	GPa
Shear Modulus, G_{13}	5	GPa
Density	1.6	g/cm^3

The given material properties are shared for both models, including the stiffeners in Model 2.

4.2 Data Generation

Required data for training the machine learning models has been gathered through structural analysis in Nastran/Patran. Undamaged version of both models are modeled, and strain, stress, and displacement fields are collected from the first ply. Afterwards, different elements are considered to be defected and the stiffness of those elements has been halved[190], reflecting damage. No geometric changes are introduced in the mesh; the defect is purely modeled through material property degradation. Then, these damaged cases are simulated and again strain, stress, and displacement fields are collected. One defected element per analysis has been considered.

Figure 4.5: Selected Elements for Defects

The selected elements for damage simulation are $SelectedElements = \{3, 6, 9, 12, 15, 18, 21, 24, 27, 30, 33, 102, 105, 108, 111, 114, 117, 120, 123, 126, 129, 132, 201, 204, 207, 210, 213, 216, 219, 222, 225, 228, 231\}$. Since the distribution of the training data is important, these elements are highlighted with red in Figure 4.5. An even distribution, including each section of the composite plane has been aimed, in order to have a more general training dataset.

This process has been followed for each ply. First, the damage is assumed to be on the top (1st) ply and all 33 selected elements have been considered damaged in single cases. Then, the damage is assumed to be in mid (2nd) ply and again all elements have been considered damaged in single cases. Finally, the same procedure is applied assuming the damage is located at bottom (3rd) ply. Therefore, a total of 99 simulations has been performed to acquire the initial training dataset, with each 33 of the entries belonging to damage cases on a different ply.

Considering the required number of analyses are high, automation is adopted with Python, which made handling the damage modeling and structural analysis workflow much easier and time-efficient. The initial dataset is available in Appendix D.

4.3 Numerical Case 1

This numerical case employs Model 1 as base model and neural networks as the machine learning approach. As a reminder of the model, the undamaged condition of Model 1 is given in Figure 4.6.

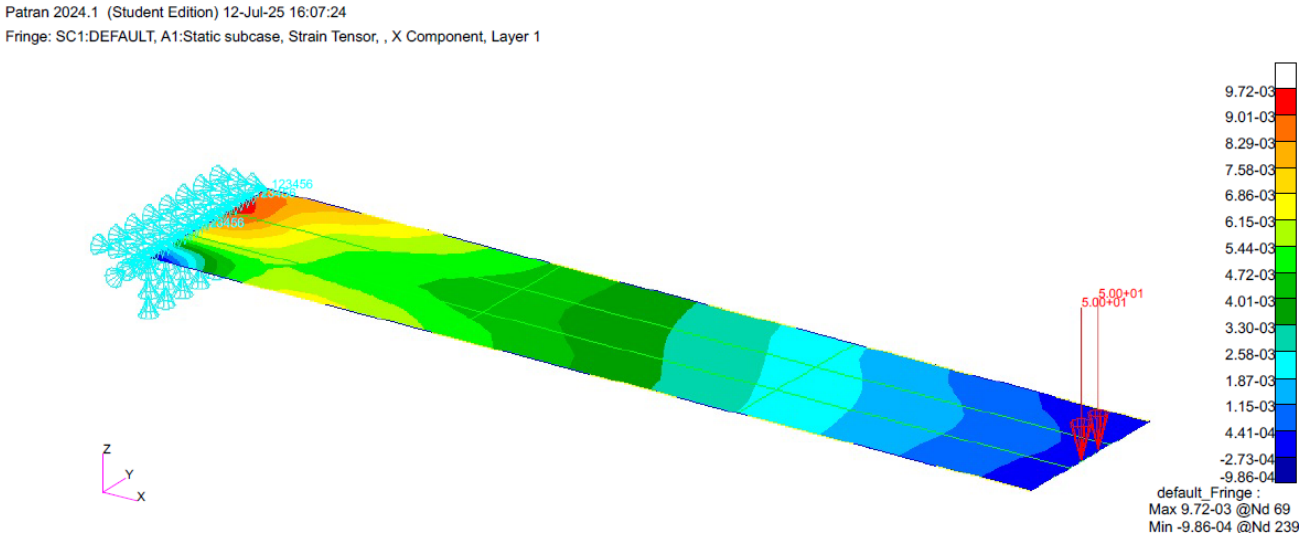

Figure 4.6: X Component of Strain in Undamaged Condition of Model 1

4.3.1 Feature Engineering and Data Preparation

The machine learning model is selected as Graph Neural Network (GNN). The advantage of the GNN is that the structure of the neural network is similar compared to a dicretized domain with nodes and elements. Therefore, it can represent associations between different elements with higher accuracy compared to other machine learning model. The initial data obtained from the analyses was 22.869 by 12 in size. The row number is equal to element number multiplied by damage scenarios ($231x99$), while the columns store the features. Initial dataset included the following features: *"Element ID", "X Coordinate", "Y Coordinate", "Strain in X Axis", "Strain in Y Axis", "Stress in X Axis", "Stress in Y Axis", "Stress in Z Axis", "Displacement in X Axis", "Displacement in Y Axis", "Displacement in Z Axis"*. Each element has been treated as individual, and the association between the elements are modeled considering 8 neighbors. GNN considers these "neighborships" and combines the information from the original element and the neighbor elements while training. Visual explanation given in Figure 4.7.

During data extraction from raw analysis files, additional 2 columns are produced storing the damage presence(0:undamaged, 1:damaged), and damaged ply(0:no damage, 1:damage on ply 1, 2:damage on ply 2, 3:damage on ply 3). The data shaped so, because the detection and localization can be treated differently in case of any need.

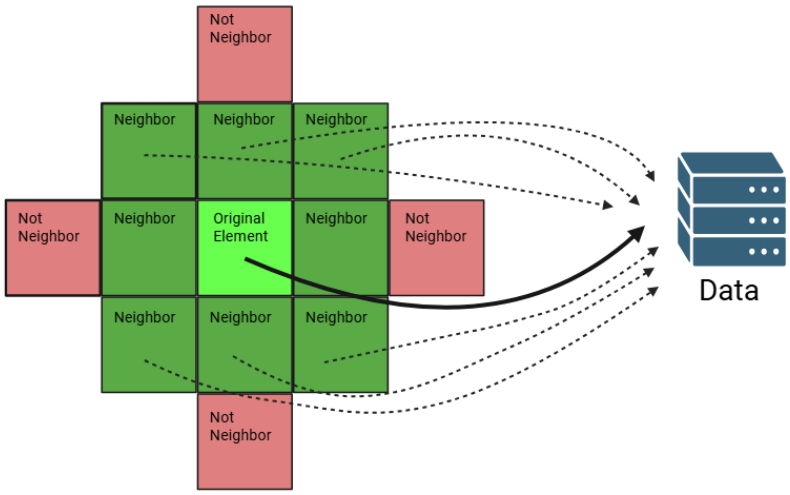

Figure 4.7: GNN Neighborhood Structure with 8 Neighbors

During feature engineering, additional features were derived from the raw data. The generation of new features, in this test case and in others, are conducted according to the learning capacity of the ML model. The undamaged condition of the plate was taken as a reference, denoted by the subscript i. The absolute differences between the current and reference values of strain in the x-direction (Equation 4.1), stress in the x-direction (Equation 4.2), and strain in the y-direction were calculated and used as new features.

$$\varepsilon_{x_diff} = |\varepsilon_{x_i} - \varepsilon_x| \tag{4.1}$$

$$\sigma_{diff} = |\sigma_{x_i} - \sigma_x| \tag{4.2}$$

$$\varepsilon_{y_{diff}} = |\varepsilon_{y_i} - \varepsilon_y| \tag{4.3}$$

Additionally, another feature called "strain difference magnitude" is derived from the derived values, given in Equation 4.4.

$$\varepsilon_{diff} = \sqrt[2]{\varepsilon^2_{x_{diff}} + \varepsilon^2_{y_{diff}}} \tag{4.4}$$

Since only one damaged element has been considered per analysis, the dataset was unbalanced. It was including undamaged elements more than the damaged elements, which may affect the performance of the machine learning model. Most machine learning models tend to neglect or overlook the under-represented samples in the unbalanced

learning datasets. Therefore, Synthetic Minority Oversampling Technique (SMOTE) has been employed to deal with the unbalance of the training dataset, and more samples are generated synthetically for under-represented samples.

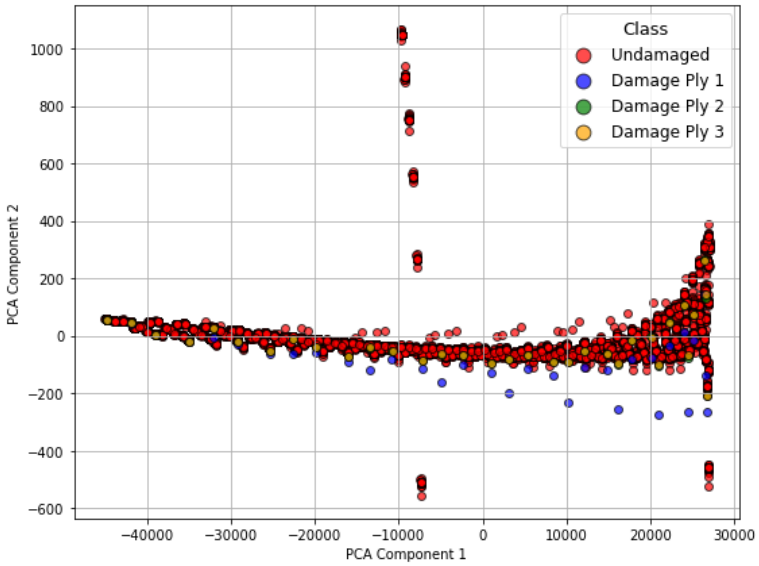

Figure 4.8: PCA Projection of the Initial Data

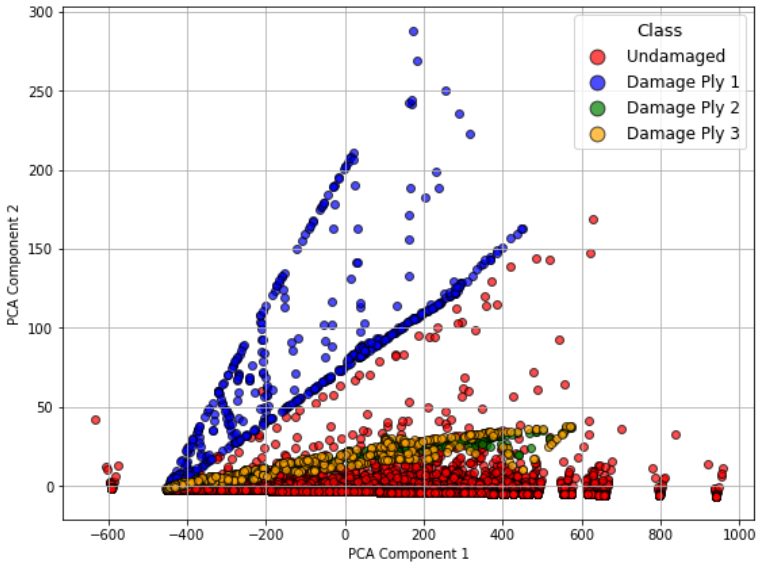

Figure 4.9: PCA Projection after Feature Engineering and SMOTE

Since the data is of high dimensions, Principal Component Analysis (PCA) has been utilized to visualize the data, and understand the effect of feature engineering. It is important to remark that PCA only captures linear correlations in the data and does not

account for non-linear relationships between features. Figure 4.8 show the distribution of the initial dataset, and the Figure 4.9 shows the distribution of the dataset after feature engineering and SMOTE application. It is noticeable that the initial data is completely overlapping, this signifies the linear distinction between the undamaged and damaged cases is low. After the application of feature engineering, a better partition is obtained. However, the damages on ply 2 and ply 3 are still hard to differentiate linearly, regarding the figure.

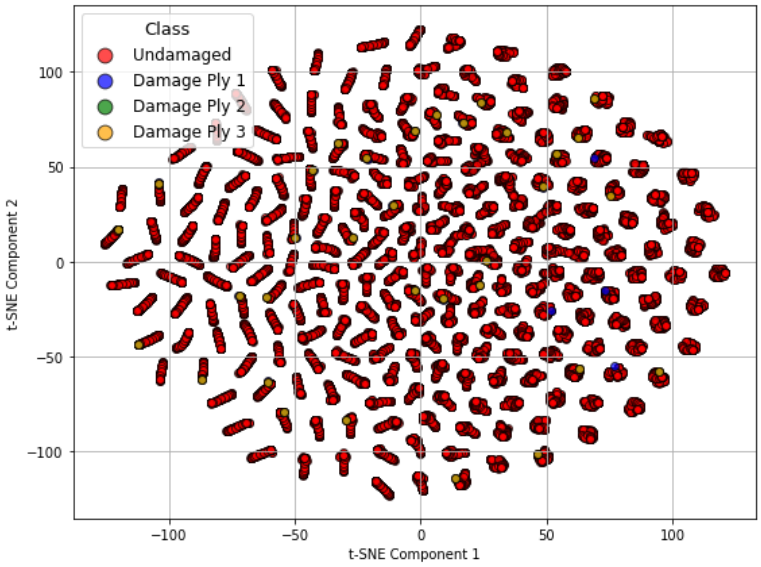

Figure 4.10: t-SNE Projection of the Initial Data

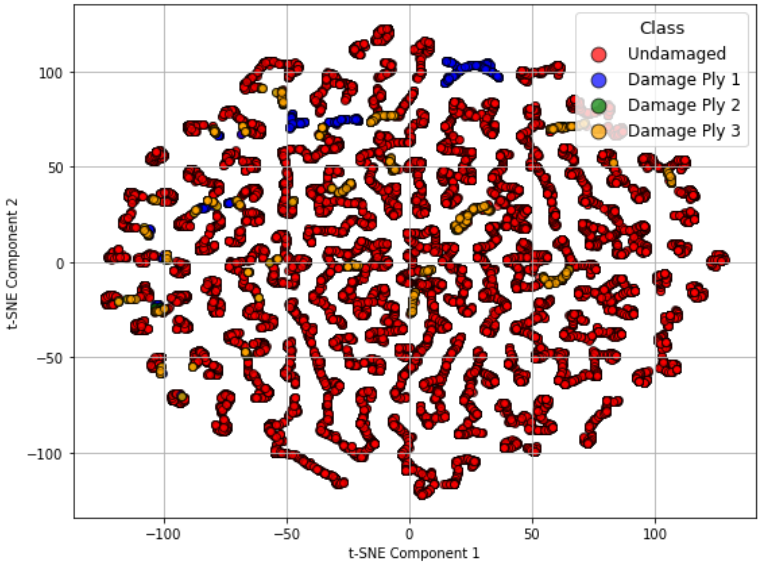

Figure 4.11: t-SNE Projection after Feature Engineering and SMOTE

Although the data does not exhibit clear separation in the principal components, this suggests that more complex, non-linear relationships may exist. In such cases, non-linear dimensionality reduction techniques such as t-Distributed Stochastic Neighbor Embedding (t-SNE) or Uniform Manifold Approximation and Projection (UMAP) can provide additional insights into the structure of the data and potential separability.

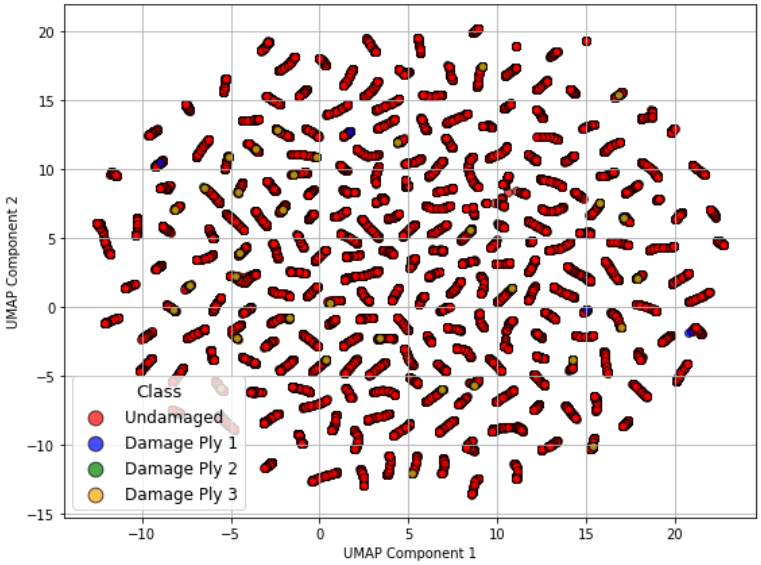

Figure 4.12: UMAP Projection of the Initial Data

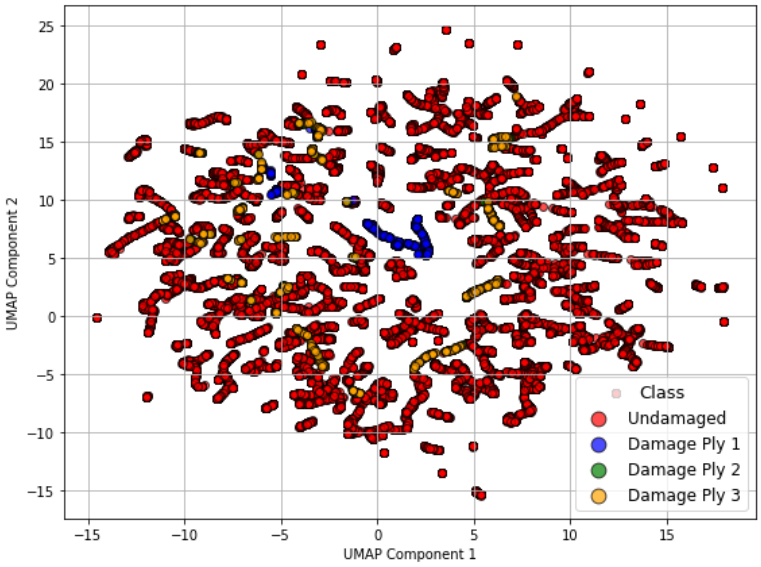

Figure 4.13: UMAP Projection after Feature Engineering and SMOTE

t-SNE projections of the initial data and the processed data are given in Figure 4.10

and 4.11, while UMAP projections are given in Figure 4.12 and 4.13. These figures signify that the non-linear separation shows similar characteristics to linear separation made by PCA. Damages on plies 1 and 3 are relatively separable from the undamaged case, but damages on ply 2 are still overlapping. Although not certain, it is highly probable that the machine learning model will face difficulties in distinguishing ply 2 damages due to the lack of clear separation in the feature space.

4.3.2 Modeling and Training Process

Stated previously, a GNN model is developed for the application. The model has been trained with the dataset explained in the previous section. Four potential outputs(0:no damage, 1:damage on ply 1, 2:damage on ply 2, 3:damage on ply 3) are specified. The model trained and evaluated the test data independently, without any ensemble.

The model is composed of two stacked Graph Attention Network (GAT) layers designed to process node-level features in a graph structure. It takes 9-dimensional input features for each node and outputs a 4-class classification. On the first layer the input dimension is 9, number of attention heads are 4, and the output dimension per head is 32. Since concatenation is enabled, the outputs of the heads are concatenated, resulting in a combined output of 128 features per node. Activation function is Exponential Linear Unit (ELU). This layer enhances the feature representation by learning multiple attention-based projections.

Second layer has the input dimension 128, 4 attention heads. Concatenation is not enabled in this layer, which means the output of the attention heads are just averaged, but not concatenated. So, the final output dimension per node is 4, which corresponds with the classification categories. This layer compresses the features into a class score vector per node.

Each node in the graph receives a 4-dimensional output vector, which is passed through a cross-entropy loss to compute the training loss. Final prediction is made by taking the index of the maximum value stored in the vector, per node. Information on both layers is given in Table 4.2. Other training parameters are provided in Table 4.3.

Table 4.2: Layer Properties

Layer	**Input Dim.**	**#Heads**	**Output Dim.**	**Activation Function**
GATConv1	9	4	$32 \times 4 = 128$	ELU
GATConv2	128	4	4	None

Table 4.3: Training Parameters and Details

Parameter	**Value**
Loss Function	Cross-Entropy Loss
Optimizer	Adam (Learning Rate = 0.001)
Early Stopping Patience	50 epochs
Max Epochs	1000 (early stopping applied)
SMOTE	Applied for class balancing
Output Classes	4 (Undamaged, Damage Ply 1, Damage Ply 2, Damage Ply 3)
Device	CPU

4.4 Numerical Case 2

For this numerical case Model 1 is considered as the base model and random forest machine learning models is selected for damage localization. Unlike the previous model, which relied solely on a single graph neural network algorithm, this version utilizes an ensemble of multiple models to improve the accuracy. Figure 4.14 is given as a reminder of the model.

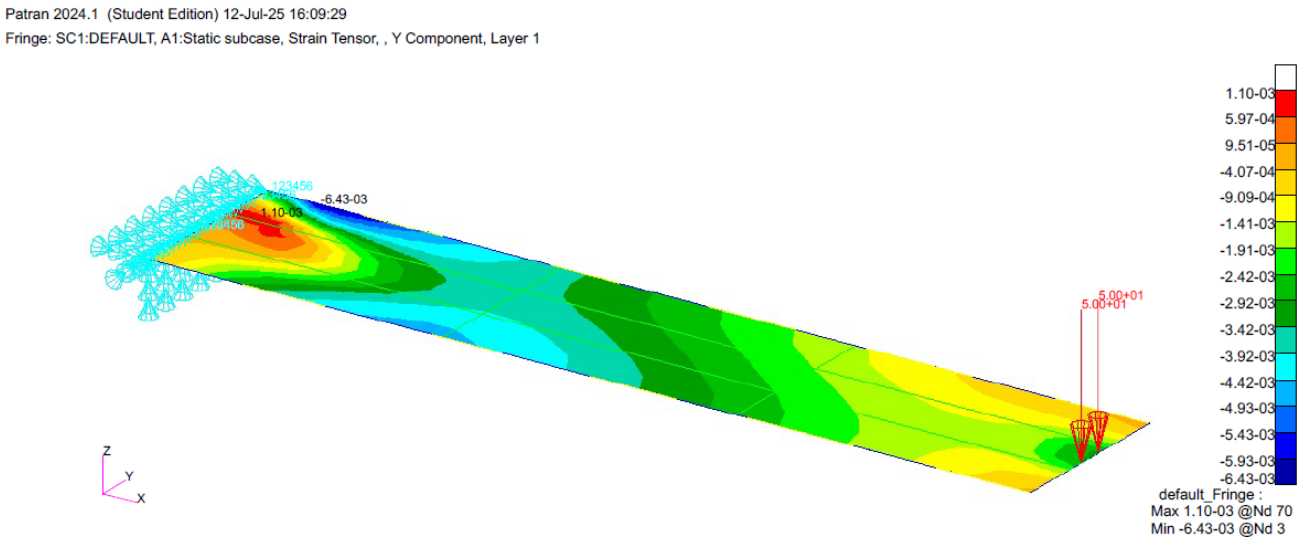

Figure 4.14: Y Component of Strain in Undamaged Condition of Model 1

4.4.1 Feature Engineering and Data Preparation

The initial data gathered from the model is the same with the previous numerical study, but contrarily the approach is quite different. The processed data is fed to 4 different ML model to determine the location of the damage. Each of these models are trained on different datasets, which makes them specialized in detecting damages on different plies. A voting system is used for the final prediction. Afterwards, the same data is again processed and fed to another ML model for specifying the damaged ply. Table 4.4 contains the brief explanation of the ML models, and the next section explains the developed structure clearly. Since data preparation procedure for each model is same, only one data preparation process, for L1Spc, is given.

Table 4.4: Employed Machine Learning Models

Name	**ML Model**	**Training Data**
L1Spc	Random Forest	Damage only on Ply 1
L2Spc	Random Forest	Damage only on Ply 2
L3Spc	Random Forest	Damage only on Ply 3
L123Spc	Random Forest	All damage cases
PlyDetector	XGBoost	All damage cases

As stated, the initial data is the same as the previous study. The size of the data is 22.869 by 12 in size. Each one third of this dataset corresponds to damage on a specific ply. The raw data included the columns *"Element ID", "X Coordinate", "Y Coordinate", "Strain in X Axis", "Strain in Y Axis", "Stress in X Axis", "Stress in Y Axis", "Stress in Z Axis", "Displacement in X Axis", "Displacement in Y Axis", "Displacement in Z Axis"*. Considering the model L1Spc, the training data must contain only the damage cases of the first ply. Therefore, the required data is extracted from the main dataset. After the extraction size, of the dataset was 7.623 by 12. Afterwards, the differences compared to the reference state is computed.

Unlike the NN in the previous study, this model and the other models are trained to predict only the presence of the damage primarily, not the damaged ply specifically. Therefore, only two outputs are possible, damaged or undamaged. A feature significance study has been conducted by training a preliminary random forest model to select the best features for the training. The result is given in Figure 4.15, where Y axis shows the importance of the feature on a percentage basis. The top six most important features identified by the machine learning model include the differences in Y-direction stress, X-direction strain, X-direction stress, and Y-direction strain compared to the undamaged reference case, as well as the absolute values of stress and strain in the X-direction.

Once again the data is found out to be unbalanced, including only 33 damage labels compared to 7.590 undamaged labels since the elements are treated individually. Therefore, SMOTE is employed to balance the learning dataset.

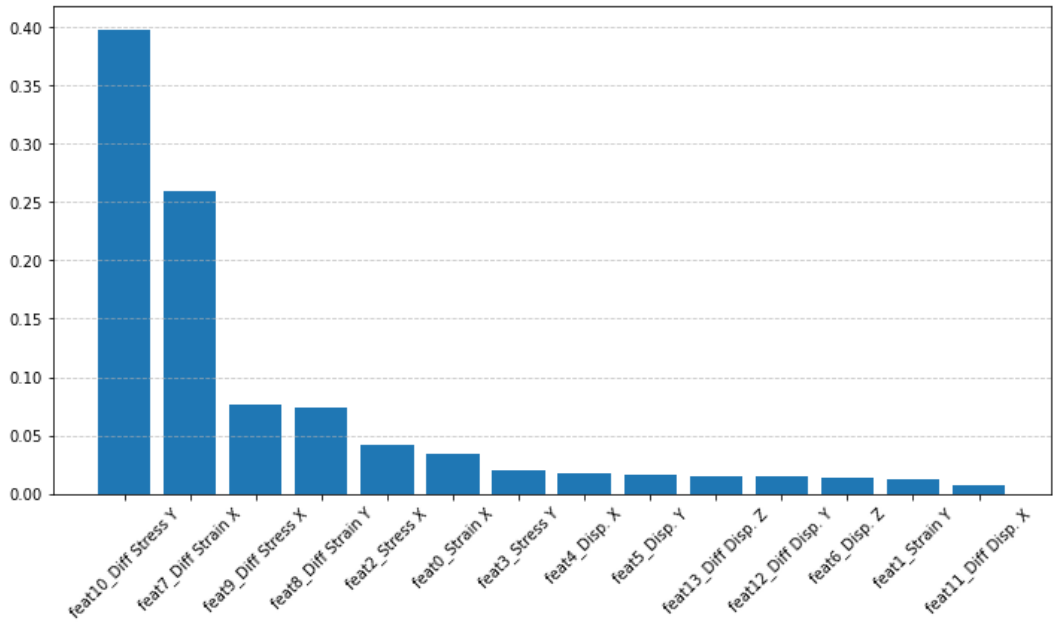

Figure 4.15: Feature Importance for L1Spc

Additionally, 3 extra features have been derived in order to have better separability. The first derived feature is the strain ratio, calculated as in Equation 4.5. Secondly, the same ratio is derived for x-direction stresses, given in Equation 4.6. Finally, the magnitude of strain differences in both x and y-directions is employed, featured in Equation 4.7.

$$\varepsilon_{x_{ratio}} = \frac{|\varepsilon_{x_i} - \varepsilon_x|}{\varepsilon_x} \tag{4.5}$$

$$\sigma_{x_{ratio}} = \frac{|\sigma_{x_i} - \sigma_x|}{\sigma_x} \tag{4.6}$$

$$\varepsilon_{diff} = \sqrt[2]{\varepsilon^2_{x_{diff}} + \varepsilon^2_{y_{diff}}} \tag{4.7}$$

The most affecting 6 features are selected from the feature significance study. A dataset containing these features and the derived features is created. To visualize the learning dataset PCA, t-SNE, and UMAP are employed. It is important to remark that

these models only differentiate between damaged and undamaged conditions. Before and after PCA results are given in Figure 4.16 and 4.17, t-SNE result are given in 4.18 and 4.19, and UMAP results are given in 4.20 and 4.21.

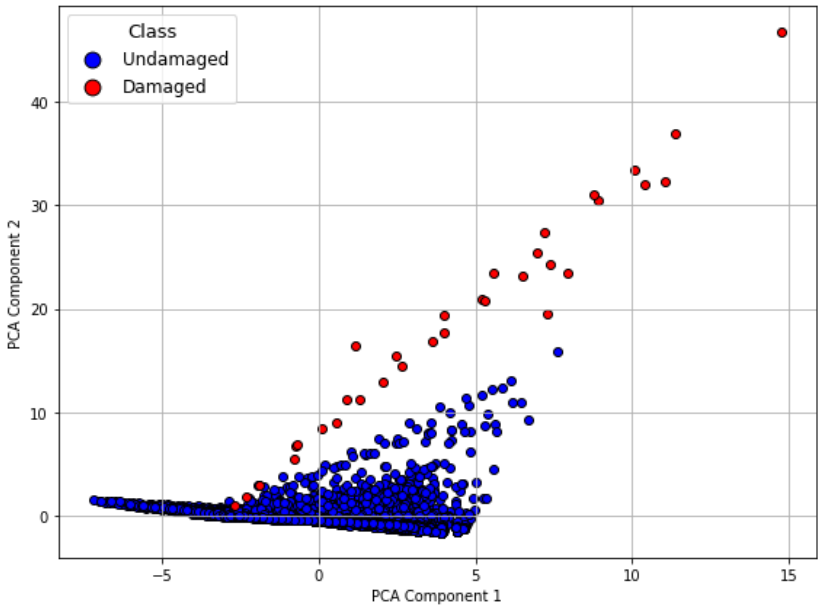

Figure 4.16: PCA Projection of the Initial Data

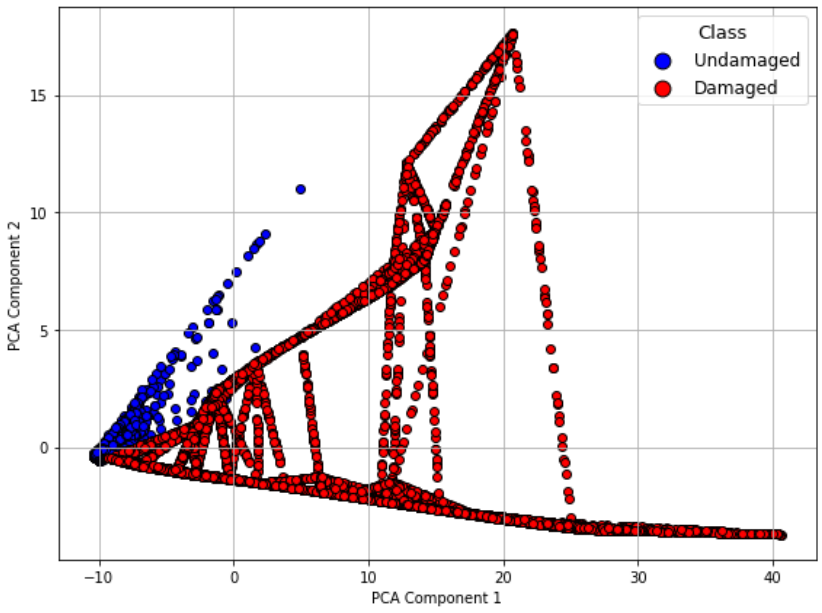

Figure 4.17: PCA Projection after Feature Engineering and SMOTE

It is easy to notice that even the initial data has a linear separation, with each labels

overlapping only on a small area. After the SMOTE application the separation is not disturbed, meaning the dataset has a good teaching potential. Regardless, t-SNE and UMAP projections are still examined to see any non-linear associations.

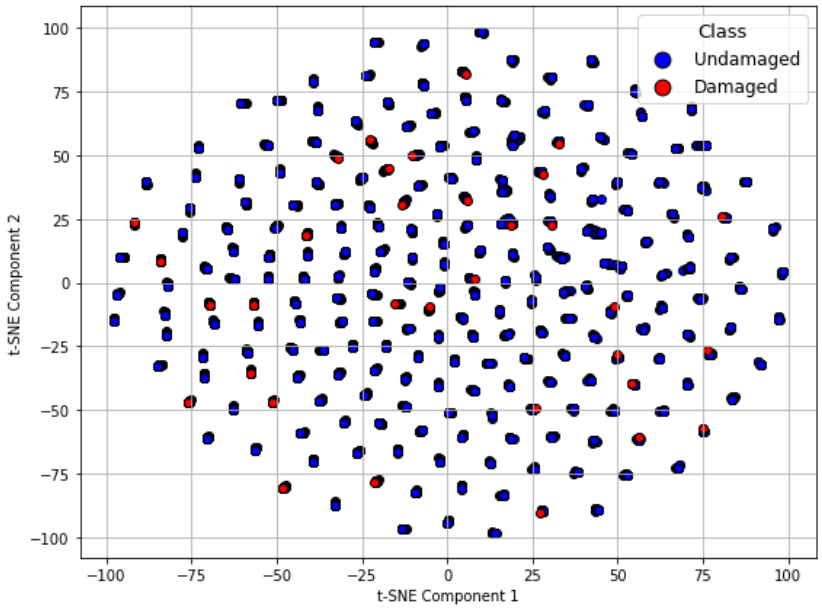

Figure 4.18: t-SNE Projection of the Initial Data

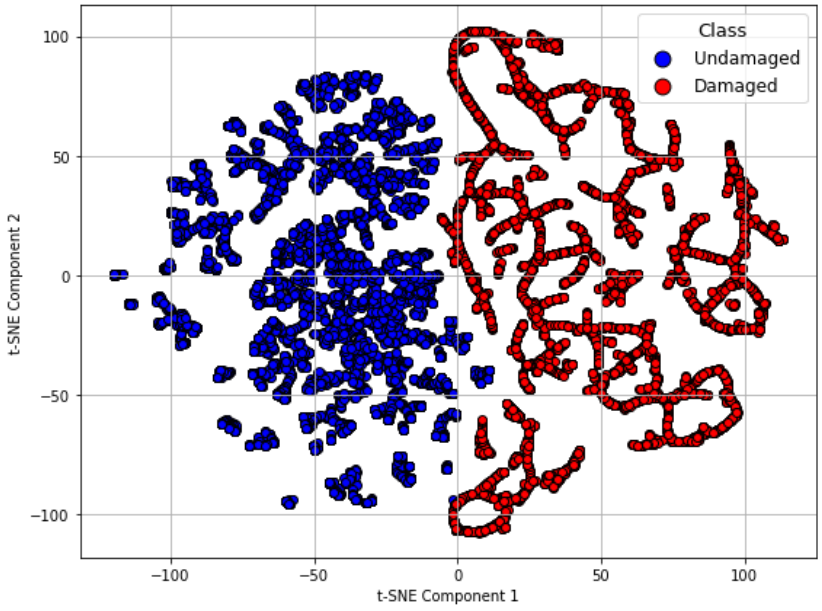

Figure 4.19: t-SNE Projection after Feature Engineering and SMOTE

In the inital t-SNE projection, it is noticed that there are some overlapping. This

means the data has non-linear relationships. After feature engineering, and SMOTE, nearly all overlapping is resolved and the data is distributed separately.

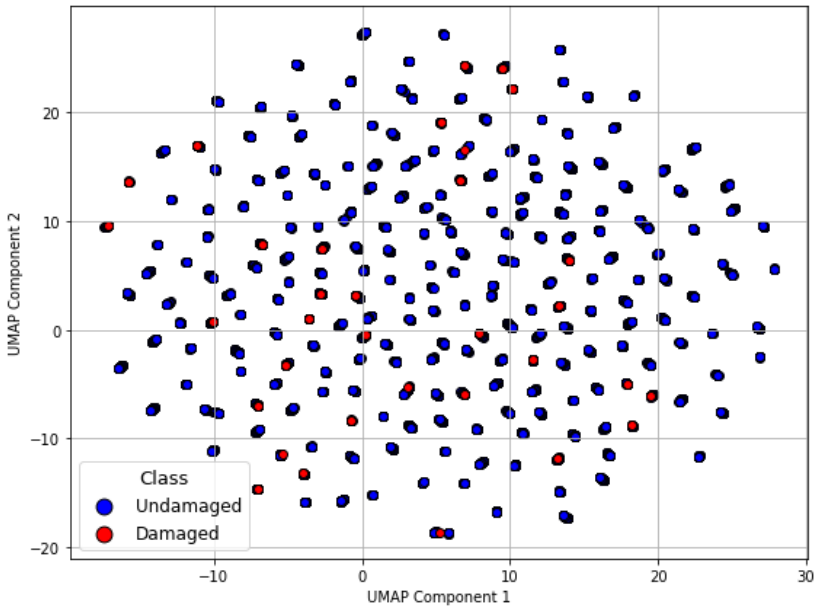

Figure 4.20: UMAP Projection of the Initial Data

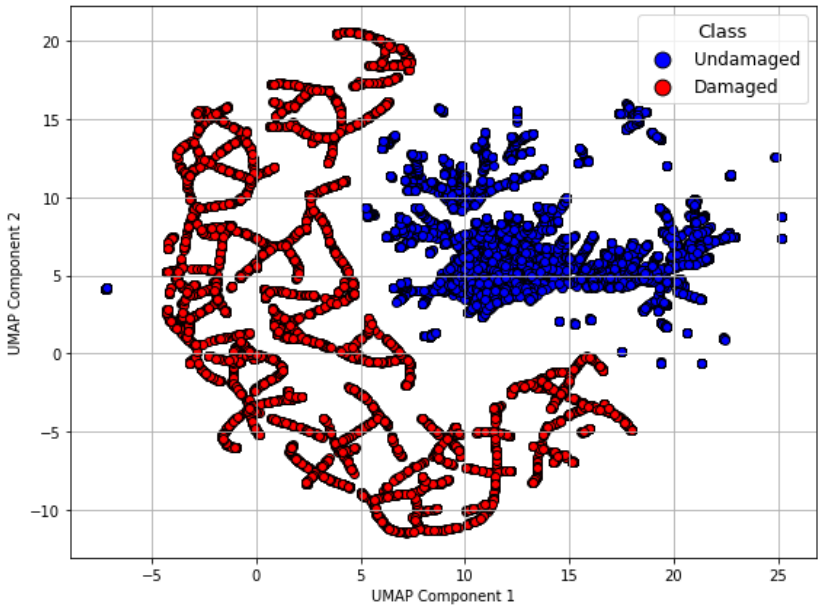

Figure 4.21: UMAP Projection after Feature Selection and SMOTE

The UMAP projection of the data simply verifies the inferences obtained from the

t-SNE application. There are overlapping data points in the initial data, which are resolved after feature engineering and SMOTE.

4.4.2 Modeling and Training Process

The structure of the developed ensemble system is briefly described in the first paragraph of the previous section. The ensemble method contains a total of five ML model, four for general damage localization, one for ply-level specification. Therefore, the ensemble system consists of two layers, given in Figure 4.22. One can refer to Table 4.2 for information about the presented ML models.

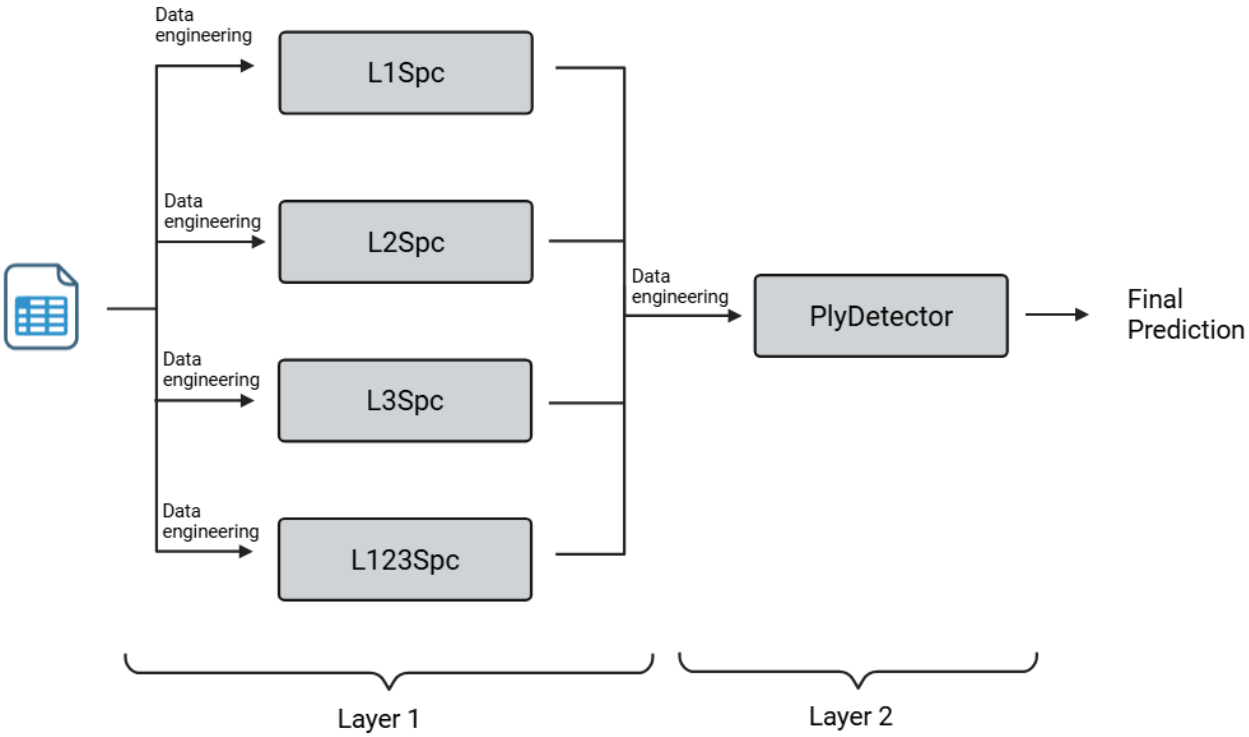

Figure 4.22: Developed Ensemble Structure

Each of the ML models located on "Layer 1" is trained on a different dataset with the aim of specializing on a ply. Model L1Spc is only trained on damage cases for the top ply. Model L2Spc is trained only on damage cases of middle ply, and model L3Spc is trained only on damage cases for the bottom ply. Model L123Spc is trained on all the damage cases and provides a general prediction. The models are awaited to exhibit high sensitivity to damage occurring within the specific layer it was trained on. Each model outputs a value between 0 and 1 for each element in the structure indicating the probability of that element being damaged. To obtain the final prediction of damaged elements, a weighted voting scheme is employed across the individual models. The final damage probability prediction for each element is calculated as:

$$DamageProbability_i = 0,2P_{L1Spc} + 0,2P_{L2Spc} + 0,2P_{L3Spc} + 0,4P_{L123Spc} \quad (4.8)$$

where i denotes the element, and P reflects the probability output for element i from the specified ML model. If the probability is over 50%, the element is considered damaged.

One can notice the weight of model L123Spc is twice the others. This is intentionally selected since the model is more general than the other models and provides a supervision on them. The training parameters of the models on "Layer 1" is given in Table 4.5.

Table 4.5: Hyperparameter Settings Used for Each Random Forest Model

Model	**Number of Trees**	**Splitting Criterion**	**Max. Depth**	**No. of Features**
L1Spc	100	Gini	Not Specified	Square Root (sqrt)
L2Spc	100	Gini	Not Specified	Square Root (sqrt)
L3Spc	100	Gini	Not Specified	Square Root (sqrt)
L123Spc	100	Gini	30	Square Root (sqrt)

In the table, the "No. of Features" column specifies the number of considered features, and "Max. Depth" defines the maximum growth of the decision trees. If not specified the decision trees grow until they converge, if specified the growth of the tree is limited. The growth of the model L123Spc is limited to prevent the model learning too much of the damage cases of a singular ply.

"Layer 2" includes a single machine learning model, implemented as an XGBoost model. XGBoost selected because of it's resilience to noise, which is found out to be highly disruptive for ply-level specification. This model predicts the specific ply where the damage is located. It uses both raw data and data from the previous layer. After processing the data with the presented procedure, the model outputs a prediction, identifying the damaged ply. By combining this prediction with the prediction from the previous layer, the final prediction is obtained.

Table 4.6: Important Hyperparameters of the PlyDetector

Model	**Learning Rate**	**Max Depth**	**No. Estimators**	**Gamma**	**Subsample**
PlyDetector	0.02	3	500	2	0.7

4.5 Numerical Case 3

For this numerical case Model 2 is considered as the base model and XGBoost machine learning models are selected for damage localization. This numerical case utilizes the same ensemble structure as the previous numerical case, but the ML models are different. The presence of stiffeners in Model 2 generates a more complex distribution of strains, stresses and displacements on the structure, which is a big challenge for the proposed system. Figure 4.23 is given as a remainder of the Model 2.

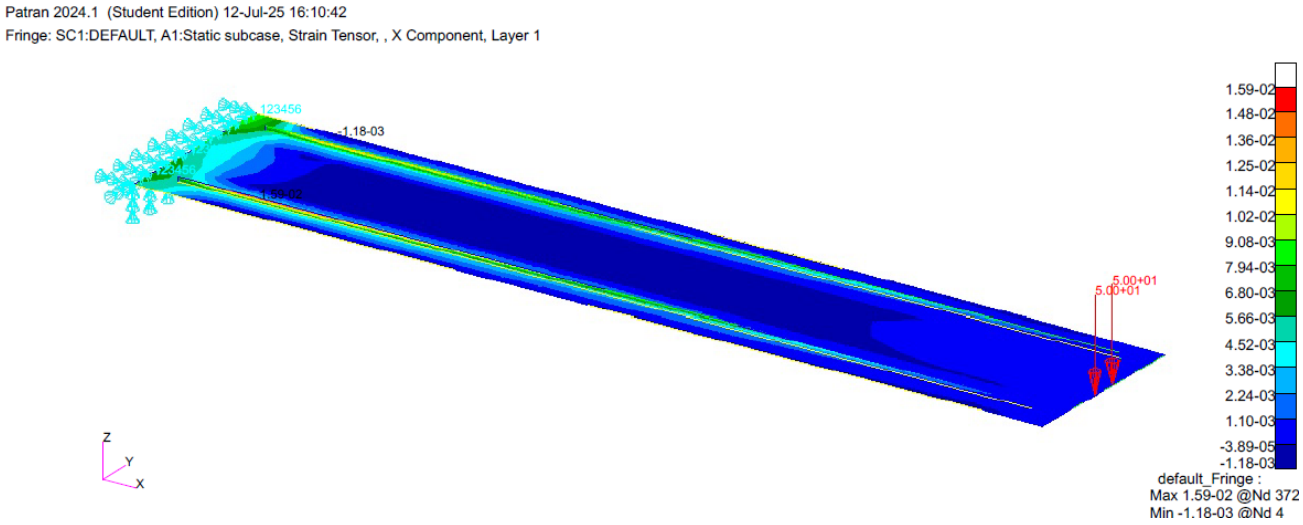

Figure 4.23: X Component of Strain in Undamaged Condition of Model 2

4.5.1 Feature Engineering and Data Preparation

The initial data gathered from the model is different than the last two numerical studies, since the structural model is changed. However, the approach for both the feature engineering, data preparation, and the ensemble structure is the same as the previous case study. The ensemble system includes five machine learning models, with four dedicated to element-level detection and one to ply-level classification. Similar to the previous case study, only one data preparation process is provided, this time for L2Spc, as the data preparation procedure is identical.

The data is different from the previous numerical studies, but the data size is the same considering the same number of elements in the structure. The size of the data is 22.869 by 14. Each one third of this dataset corresponds to damage on a specific ply. The raw data included the columns *"Element ID", "X Coordinate", "Y Coordinate", "Strain in X Axis", "Strain in Y Axis", "Stress in X Axis", "Stress in Y Axis", "Stress in Z Axis", "Displacement in X Axis", "Displacement in Y Axis", "Displacement in Z Axis"," In-plane Shear Strain"," In-plane Shear Stress"*. Unlike the previous this dataset included shear strain and shear stresses. Considering the model L2Spc, the training data must contain only the damage cases of the middle ply. Therefore, the

training data is extracted from the main dataset. After the extraction, size of the dataset was 7.623 by 14.

The differences compared to the reference state is computed. Similar to the previous study, a feature importance study is conducted given in Figure 4.24. The top six most important features are found out to be differences in strain in X-direction, stress in X-direction, shear stress, shear strain strain in Y-direction compared to reference undamaged case, and the displacement in Z-direction.

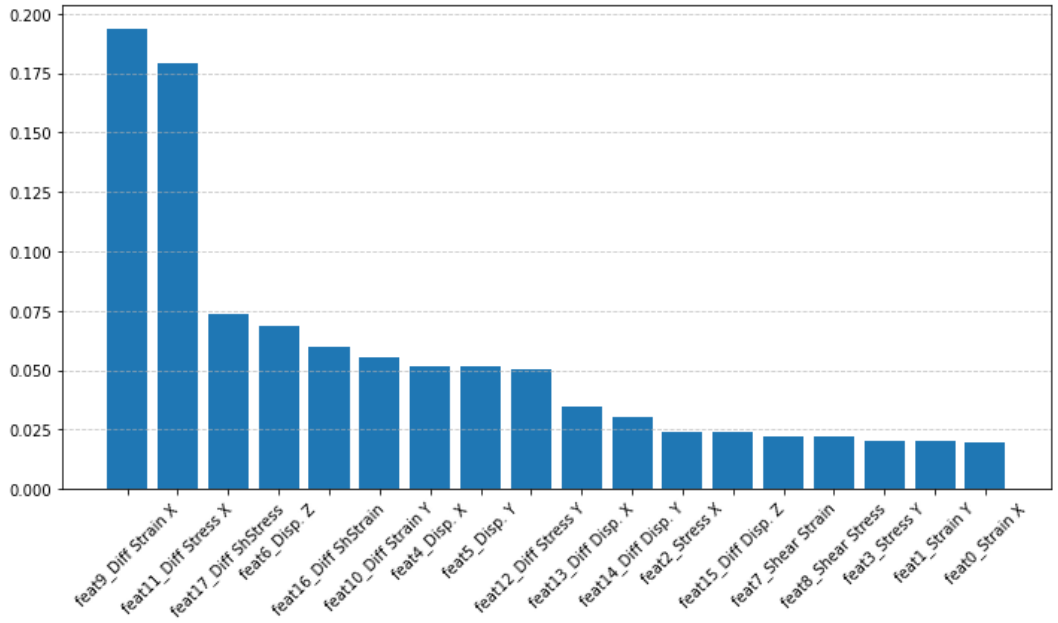

Figure 4.24: Feature Importance for L2Spc

Again, the dataset was unbalanced. There was only 33 damaged cases, compared to 7.590 undamaged cases, since the elements are treated individually. Therefore SMOTE is applied in order to balance the dataset.

Additional two features are derived from the top six most important features. The first derived feature is the absolute difference change of strain in X-direction, and the second feature is the absolute difference change of stress in X-direction. The calculation of the first derived term is given in Equation 4.9, where $\varepsilon_{x_{avg}}$ is the average value calculated with the prior and superior neighbors.

$$\Delta\varepsilon_{diff_x} = \frac{\varepsilon_x - \varepsilon_{x_{avg}}}{\varepsilon_{x_{avg}}} \tag{4.9}$$

The formula of the second derived term is given in Equation 4.10, where $\sigma_{x_{avg}}$ is the average calculated with the prior and superior neighbors.

$$\Delta\sigma_{diff_x} = \frac{\sigma_x - \sigma_{x_{avg}}}{\sigma_{x_{avg}}} \tag{4.10}$$

The two derived features are added to the most important six features to obtain the learning dataset for L2Spc. PCA projection of the initial data and the processed data are given in Figure 4.25 and 4.26

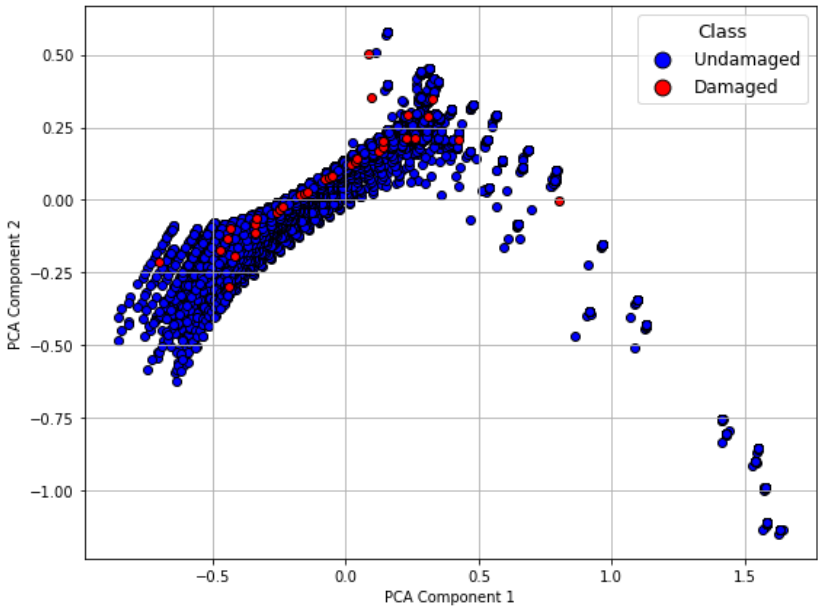

Figure 4.25: PCA Projection of the Initial Data

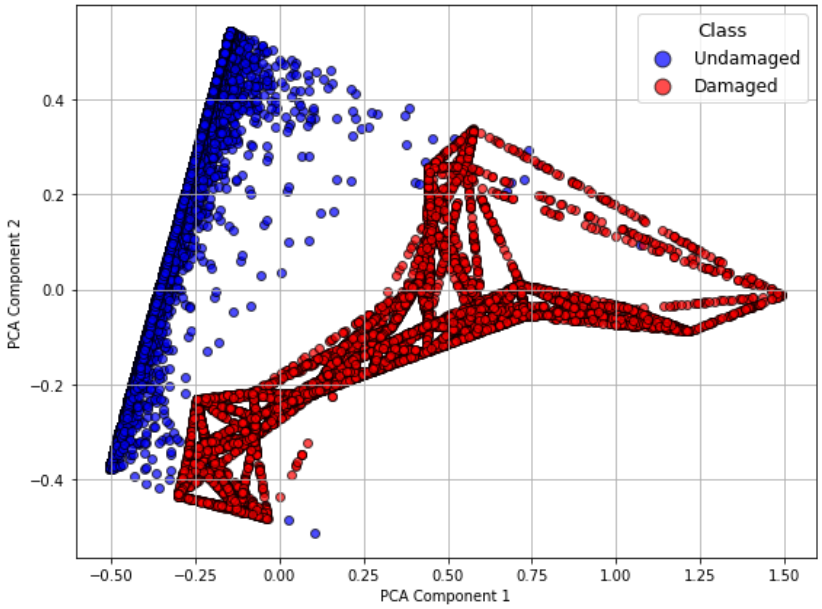

Figure 4.26: PCA Projection after Feature Engineering and SMOTE

The PCA projection of the processed data reveal a clear linear separation. Although, this is probably enough for the ML models to classify the data, t-SNE and the UMAP projections are also helpful to understand the relationship in data. t-SNE projections are given in Figure 4.27 and 4.28.

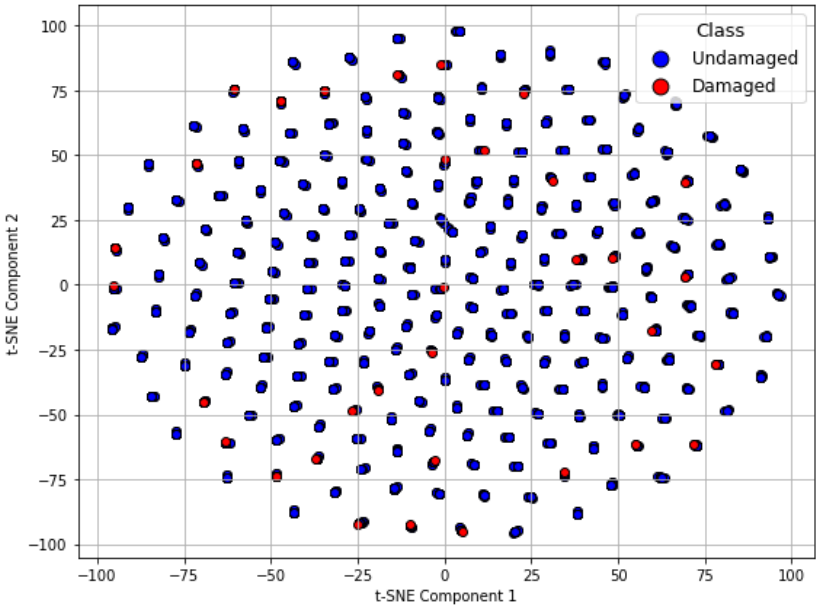

Figure 4.27: t-SNE Projection of the Initial Data

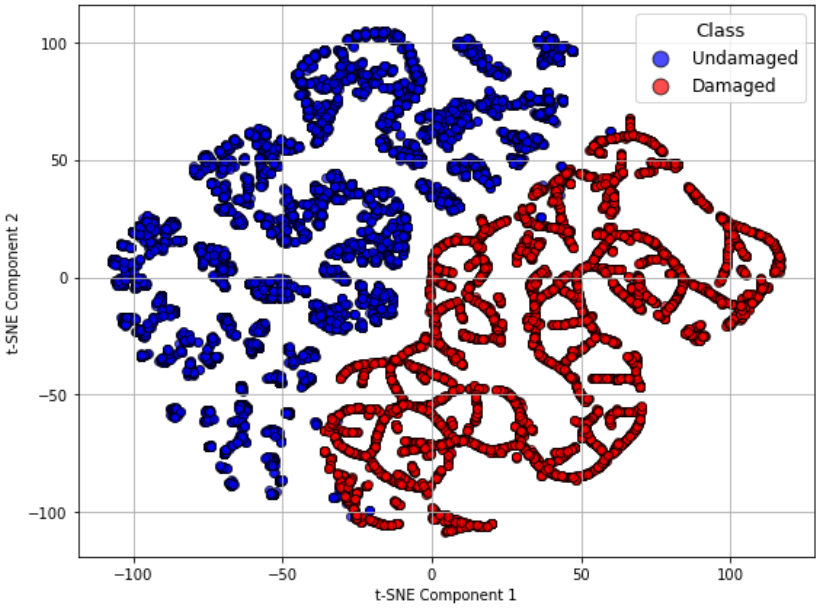

Figure 4.28: t-SNE Projection after Feature Engineering and SMOTE

The UMAP projections are given in Figure 4.29 and 4.30.

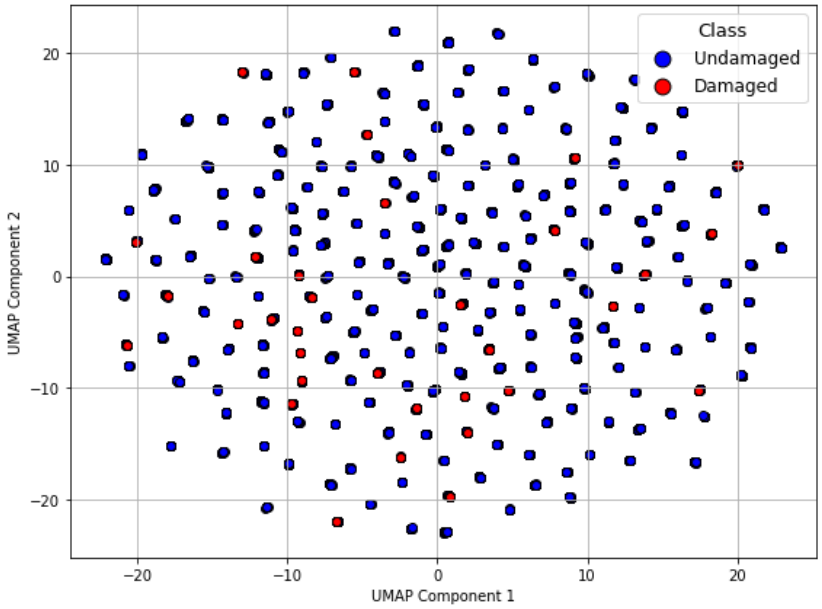

Figure 4.29: UMAP Projection of the Initial Data

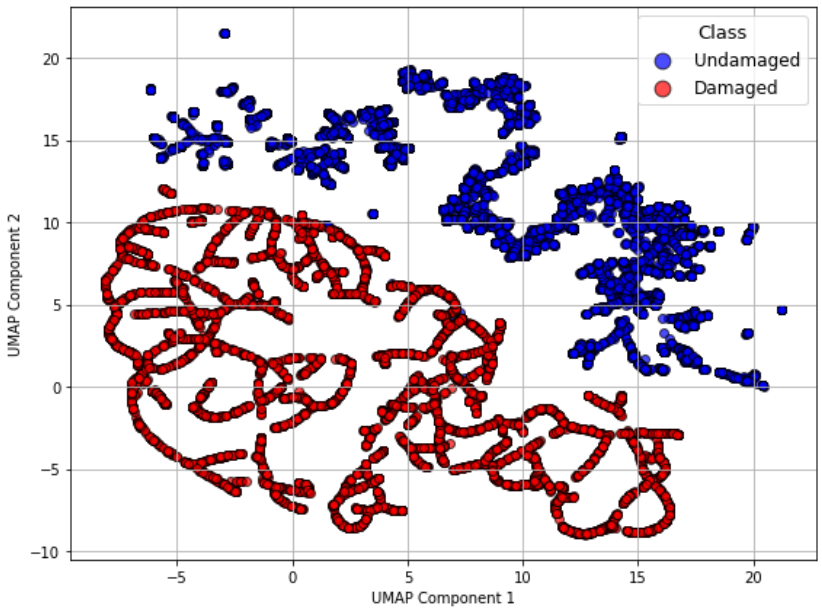

Figure 4.30: UMAP Projection after Feature Engineering and SMOTE

Considering the data distribution on PCA, t-SNE, and UMAP projections, the processed data is highly separable, showing small overlaps.

4.5.2 Modeling and Training Process

The structure of the ensemble system is the same as the previous ensemble system. There are five ML models, four for damage localization, and one for ply-level specification. Damage localization ML models are located in the first layer, while the ply-level specification model is located on the second layer. Unlike the previous application, all of the machine learning models are selected as XGBoost. This selection is done due to the high robustness of XGBoost model, taking the complexity of Model 2 into account. A brief explanation of the ML models are given in Table 4.7.

Table 4.7: Employed Machine Learning Models for Numerical Case 3

Name	**ML Model**	**Training Data**
L1Spc	XGBoost	Damage only on Ply 1
L2Spc	XGBoost	Damage only on Ply 2
L3Spc	XGBoost	Damage only on Ply 3
L123Spc	XGBoost	All damage cases
PlyDetector	XGBoost	All damage cases

The hierarchical structure of the ML models is identical to the previous numerical case, given in Figure 4.22. The calculation of the final prediction is also identical to the previous case, given in Equation 4.8. It should be noted that adjustments in the behavior of the system is possible by changing weights.

Important parameters used in the training of the ML models in this numerical case is given in Table 4.8.

Table 4.8: Important Hyperparameters of the ML Models

Model	**Learning Rate**	**Max Depth**	**No Estimators**	**Gamma**	**Subsample**
L1Spc	0.1	5	200	0	1
L2Spc	0.1	5	200	0	1
L3Spc	0.1	5	200	0	1
L123Spc	0.1	5	200	0	1
PlyDetector	0.01	7	1500	1	0.8

Chapter 5

Results and Discussion

5.1 Custom Scoring Function

In damage localization tasks, especially in structural health monitoring (SHM) applications involving spatially distributed systems such as finite element meshes, traditional evaluation metrics (accuracy, precision, or recall) may not sufficiently reflect the performance of the developed system. For instance, in structural health monitoring, the accurate detection of damaged elements (true positives) is significantly more critical than identifying undamaged ones (true negatives), as the former has direct implications for safety.

To adress this limitation, a custom neighbor-based scoring function is developed. This method is referred as Neigborhood-Constrained Scoring Strategy, and only rewards predictions that are both correct in terms of class and spatially constrained. This means no false positives are allowed outside the neighbor elements of the true damage location. Specifically, for each element where the true label is positive, a score is awarded only if the predicted label for that element is also positive and the model does not predict damage elsewhere except potentially within its defined neighborhood. The neighbors of an element is defined as the elements which are in contact with the base element, given in Figure 5.1.

This strict criterion ensures that the scoring favors not just the detection, but accurate and focused localization, which is critical for SHM applications where false alarms outside the affected zone could lead to unnecessary inspections or misinformed maintenance decisions, resulting in economic loss. The proposed metric captures the success of the localization better considering realistic scenarios.

It should be noted that the developed scoring function only assesses the performance of the localization, not the ply-level specification. For ply-level specification a more simple scoring function has been defined. The model is awarded a full point in case of correct prediction. If the predicted element is correct but the ply is wrong, half point

is awarded. In case of wrong prediction except the neighbors, a deduction equal to the full point is applied.

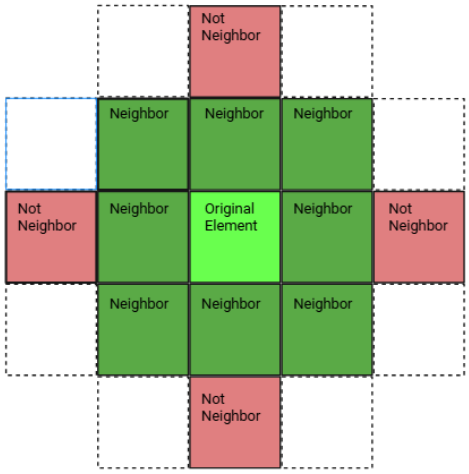

Figure 5.1: Definition of Neighborhood on FEM

The following examples are provided to provide a better explanation of the scoring functions, both for localization and ply-level identification. The threshold for

The damage is on Element 70. The model predicts the damage location correctly, thus earns 1 point. This damage case is represented in Figure 5.2.

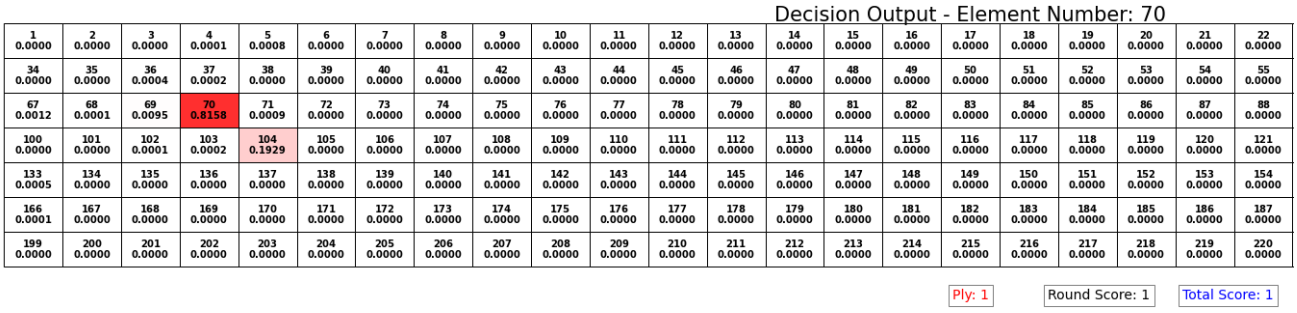

1 0.0000	2 0.0000	3 0.0000	4 0.0001	5 0.0008	6 0.0000	7 0.0000	8 0.0000	9 0.0000	10 0.0000	11 0.0000	12 0.0000	13 0.0000	14 0.0000	15 0.0000	16 0.0000	17 0.0000	18 0.0000	19 0.0000	20 0.0000	21 0.0000	22 0.0000
34 0.0000	35 0.0000	36 0.0004	37 0.0002	38 0.0000	39 0.0000	40 0.0000	41 0.0000	42 0.0000	43 0.0000	44 0.0000	45 0.0000	46 0.0000	47 0.0000	48 0.0000	49 0.0000	50 0.0000	51 0.0000	52 0.0000	53 0.0000	54 0.0000	55 0.0000
67 0.0012	68 0.0001	69 0.0095	70 0.8158	71 0.0009	72 0.0000	73 0.0000	74 0.0000	75 0.0000	76 0.0000	77 0.0000	78 0.0000	79 0.0000	80 0.0000	81 0.0000	82 0.0000	83 0.0000	84 0.0000	85 0.0000	86 0.0000	87 0.0000	88 0.0000
100 0.0000	101 0.0000	102 0.0001	103 0.0002	104 0.1929	105 0.0000	106 0.0000	107 0.0000	108 0.0000	109 0.0000	110 0.0000	111 0.0000	112 0.0000	113 0.0000	114 0.0000	115 0.0000	116 0.0000	117 0.0000	118 0.0000	119 0.0000	120 0.0000	121 0.0000
133 0.0005	134 0.0000	135 0.0000	136 0.0000	137 0.0000	138 0.0000	139 0.0000	140 0.0000	141 0.0000	142 0.0000	143 0.0000	144 0.0000	145 0.0000	146 0.0000	147 0.0000	148 0.0000	149 0.0000	150 0.0000	151 0.0000	152 0.0000	153 0.0000	154 0.0000
166 0.0001	167 0.0000	168 0.0000	169 0.0000	170 0.0000	171 0.0000	172 0.0000	173 0.0000	174 0.0000	175 0.0000	176 0.0000	177 0.0000	178 0.0000	179 0.0000	180 0.0000	181 0.0000	182 0.0000	183 0.0000	184 0.0000	185 0.0000	186 0.0000	187 0.0000
199 0.0000	200 0.0000	201 0.0000	202 0.0000	203 0.0000	204 0.0000	205 0.0000	206 0.0000	207 0.0000	208 0.0000	209 0.0000	210 0.0000	211 0.0000	212 0.0000	213 0.0000	214 0.0000	215 0.0000	216 0.0000	217 0.0000	218 0.0000	219 0.0000	220 0.0000

Figure 5.2: Prediction Equivalent to 1 Point

Figure 5.3 represents the damage case of Element 62. The model predicts the damage location correctly, but there is a wrong damage prediction (false positive) on Element 29. Since this element is a neighbor of the original element, this false positive is disregarded and 1 point is awarded.

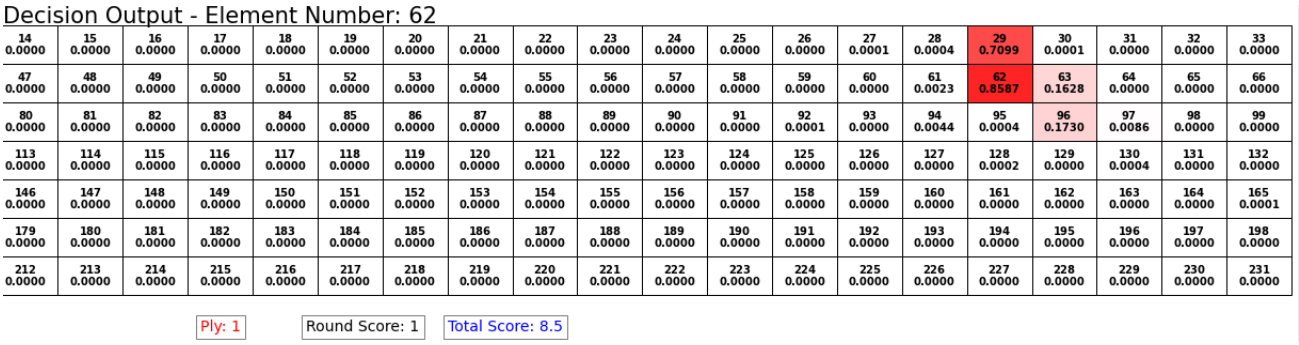

Figure 5.3: Prediction Equivalent to 1 Point

In the following figure, the damage is located at Element 92. Even it seems the prediction is correct, the required threshold of 0.5 is not achieved. Therefore, the prediction is wrong (false negative), and results in a 1 point deduction.

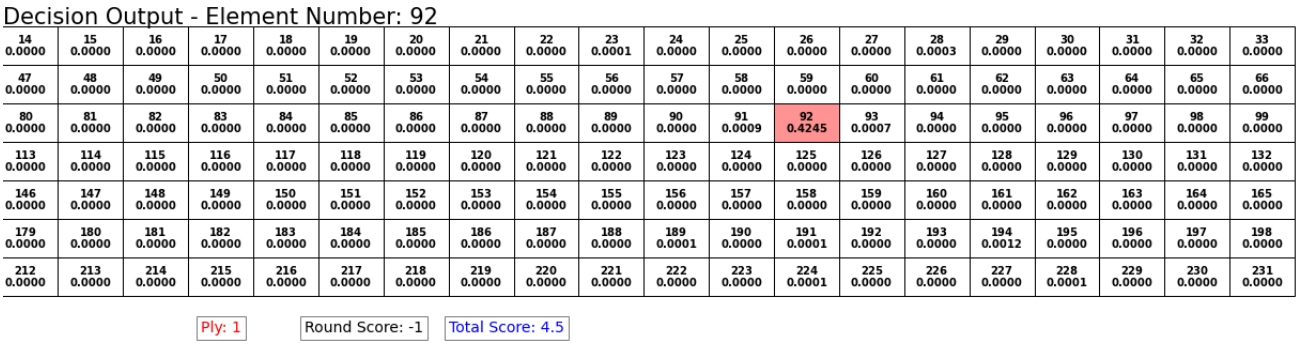

Figure 5.4: Prediction Equivalent to -1 Point

Figure 5.5 shows the damage case of Element 168. The model fails to detect the damage at the original element but identifies damage at Element 204 (false poisitive). Therefore a deduction of 1 point is applied.

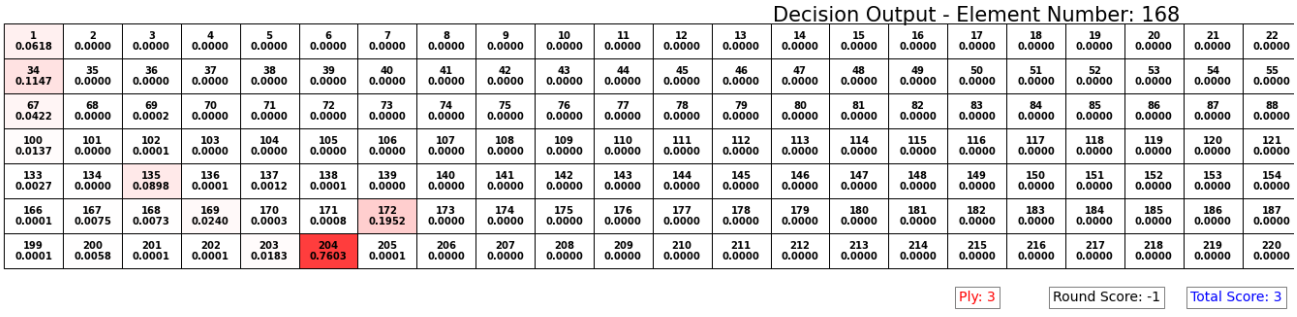

Figure 5.5: Prediction Equivalent to -1 Point

Figure 5.6 represents the damage case of Element 37. As seen, the original element

is identified as damaged but Element 39 is also identified as damaged, which is not a neighbor of the original element. In this case, 0.5 point is awarded to the system, since the prediction would be useful in real-life application.

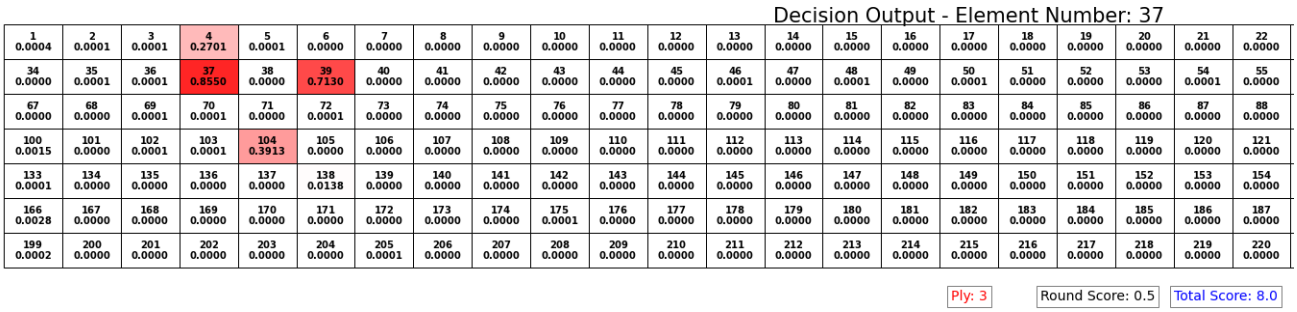

Figure 5.6: Prediction Equivalent to 0.5 Point

5.2 Results of Numerical Case 1

For the Numerical Case 1, Model 1 is used as base, and GNN is employed as the machine learning algorithm. As the testing method, 30 random elements are selected from the model, and considered as damaged individually. The elements, where the learning data is obtained, are excluded from the selection. The predictions of the model is scored according to the custom scoring function given in the previous section. Later, the same technique is repeated with 50 samples instead of 30. For the 30 sample test, the maximum score possible is 30 and the minimum score possible is -30. For the 50 sample test, maximum possible score is 50, and the minimum possible score is -50. The test is conducted for damage cases in each ply individually.

Table 5.1: Results with 30 Samples

Damaged Ply	Run 1	Run 2	Run 3	Run 4	Run 5	Run 6	Run 7	Run 8	Run 9	Run 10	Average(30 Max)
1	-30	-27	-28.5	-28.5	-30	-30	-28.5	-28.5	-28.5	-30	-28.95
2	-28.5	-28.5	-30	-30	-30	-28.5	-28.5	-28.5	-28.5	-27	-28.8
3	-30	-30	-30	-30	-30	-28.5	-30	-28.5	-30	-30	-29.7

Table 5.2: Results with 50 Samples

Damaged Ply	Run 1	Run 2	Run 3	Run 4	Run 5	Run 6	Run 7	Run 8	Run 9	Run 10	Average(50 Max)
1	-50	-50	-48.5	-45.5	-45.5	-50	-50	-50	-48.5	-50	-48.8
2	-48.5	-50	-48.5	-47	-47	-48.5	-47	-48.5	-47	-50	-48.2
3	-50	-50	-50	-48.5	-48.5	-47	-48.5	-50	-48.5	-48.5	-48.95

The obtained results with 30 samples are given in Table 5.1, while results with 50 samples are given in Table 5.2. The results show that the model can not predict the damage location or the damaged ply. More explanation regarding the results is given in the following sections.

5.3 Results of Numerical Case 2

For the Numerical Case 2, Model 1 is used as base, and the ensemble method consisting of Random Forest models is utilized as the machine learning algorithm. The testing method is identical with the previous one, where two test runs, one with 30 samples and other with 50 samples is considered. Again, the test is conducted for damage cases in each ply individually. Unlike the previous application, the damage localization and ply-level identification scores are given separately since the process runs in two-steps.

Table 5.3: Damage Localization Results with 30 Samples

Damaged Ply	Run 1	Run 2	Run 3	Run 4	Run 5	Run 6	Run 7	Run 8	Run 9	Run 10	Average	Success %
1	27	26	23.5	28	26	29	25	28	27.5	29	26.9	89.67
2	22	18	20	24	18	22	16	20	24	20	20.4	68
3	27.5	21	26	27	26	19	25	19	30	23.5	23.5	78.33

Table 5.4: Damage Localization Results with 50 Samples

Damaged Ply	Run 1	Run 2	Run 3	Run 4	Run 5	Run 6	Run 7	Run 8	Run 9	Run 10	Average	Success %
1	46.5	44.5	46	44.5	45.5	47	46	44.5	47	47	45.85	91.7
2	34	36	36	30	40	36	32	28	28	32	33.2	66.4
3	40.5	42.5	40.5	43	45	44.5	42	44	45	39.5	42.65	85.3

The damage localization results are given in Table 5.3 and 5.4, both for 30 samples and 50 samples. Considering the scores of both tests, the ensemble model has around 79-81% success rate on average for damage localization.

Table 5.5: Ply-Level Identification Results with 30 Samples

Damaged Ply	Run 1	Run 2	Run 3	Run 4	Run 5	Run 6	Run 7	Run 8	Run 9	Run 10	Average	Success %
1	30	30	30	30	30	29	30	30	29	30	29.8	99.33
2	26	27.5	25.5	24.5	27	23.5	25.5	26	24.5	26.5	25.65	85.5
3	28	28	27.5	29	30	28	27.5	28.5	28	28	28.25	94.1

Table 5.6: Ply-Level Identification Results with 50 Samples

Damaged Ply	Run 1	Run 2	Run 3	Run 4	Run 5	Run 6	Run 7	Run 8	Run 9	Run 10	Average	Success %
1	50	50	50	50	49	50	50	49	48	49	49,5	99
2	44.5	42.5	41.5	42.5	42	40.5	39	46.5	40.5	46.5	42.6	85.52
3	49	48	47,5	47.5	46	49.5	47.5	46.5	47	46	47.45	94.9

The results for ply-level identification are given in Table 5.5 and 5.6, both for 30 samples and 50 samples. The success rate of ply-level identification is found out to be around 92-93% on average. More comments about the case are given on the following parts.

5.4 Results of Numerical Case 3

For the Numerical Case 3, Model 2 is used as the base, and an ensemble method consisting of different XGBoost models is used as the machine learning algorithm. The same testing method, utilized in the previous cases, is applied. The results are given separately as damage localization and ply-level identification.

Table 5.7: Damage Localization Results with 30 Samples

Damaged Ply	Run 1	Run 2	Run 3	Run 4	Run 5	Run 6	Run 7	Run 8	Run 9	Run 10	Average	Success %
1	29	27	25	29	29.5	27	30	27.5	29	28.5	28.2	93.91
2	20	27.5	24	22	19.5	19.5	18	18	21.5	19.5	20.95	69.83
3	17.5	23.5	15.5	22.5	18.5	18	20	13	9	15	17.25	57.50

Table 5.8: Damage Localization Results with 50 Samples

Damaged Ply	Run 1	Run 2	Run 3	Run 4	Run 5	Run 6	Run 7	Run 8	Run 9	Run 10	Average	Success %
1	47	44	44	44	47	48.5	47.5	47.5	48	48.5	46.6	93.2
2	38	37.5	40	38	44	32	32	34	39.5	36	37.1	74.2
3	43	34.5	33	19.5	22.5	27	25	18	29	31	28.25	56.50

Considering the results in Table 5.7 and 5.8, the average success for the damage localization is found out to be around 73-74%. The results for ply-level identification are given in Table 5.9 and 5.10. According to the results, the model presents a success rate around 78-80%.

Table 5.9: Ply-Level Identification Results with 30 Samples

Damaged Ply	Run 1	Run 2	Run 3	Run 4	Run 5	Run 6	Run 7	Run 8	Run 9	Run 10	Average	Success %
1	25.5	26.5	26	27	29	27.5	29	26	27	27.5	27.1	90.32
2	28.5	25.5	23.5	24	26.5	28	26.5	26	26.5	22.5	25.75	85.82
3	22.5	18	14.5	15.5	18	16	17	15.5	20	16.5	17.35	57.83

Table 5.10: Ply-Level Identification Results with 50 Samples

Damaged Ply	Run 1	Run 2	Run 3	Run 4	Run 5	Run 6	Run 7	Run 8	Run 9	Run 10	Average	Success %
1	47	44.5	45	47.5	47	44	45.5	45.5	48	44.5	45.85	91.7
2	45	47	46	44	45.5	45	44	41.5	45	45	44.8	89.6
3	34	28	26.5	30	29	34	29.5	28	29.5	31	29.95	59.9

5.5 Interpretation and Comparison of Results

The results obtained for each numerical case are given in the previous sections. It is important to remark that each run is done with 5% noise added into the test data.

Examining the results individually, one can see the results obtained in Numerical Case 1 are nothing but poor. It is clear that the system is predicting the damage location completely random. Although the working principle of GNN, based-on neighbor relations, was thought to be suitable for the job, it performed poorly in for damage localization. Therefore, the reasons behind this low performance are investigated. It is discovered that the results get better with increasing datasize, but even those results were far worse than the success achieved in other numerical cases. It is concluded that the low performance of the model is caused by the low datasize. In order to achieve a high performing GNN for damage localization, greater data in terms of size is required.

Numerical Case 2, yields good results in both in damage localization and ply-level identification. The success rate of the prediction drops as the distance from the first ply increases. This is expected, since the data is gathered from the first ply. As the damage occurs in deeper plies, the effect caused by the damage becomes less sensible at the first ply. The success rate of the ensemble model is around 80% considering damage localization. Interestingly, the model shows a really high success rate of 92% in ply-level identification. Unlike in localization, the success rate does not decrease with increasing damage depth in ply-level identification. This might be due to the patterns created in strain, stress, and displacement fields by damages in different plies being more recognizable for ML algorithms. Finally, considering the strain distribution on the part, in order to achieve this success rate, strain gauges with minimum precision of $10\mu\varepsilon$ would be required in real-world application. Most strain gauges are capable of satisfying this precision.

Numerical Case 3, presents similar but relatively worse results compared to previous case. The average success rate for damage localization is around 73% and the steady decrease is seen as the damage occurs on deeper plies. For ply-level identification, the average success rate is around 79%. Although the obtained results are slightly worse than the previous numerical case, the complexity of the model due to the stiffeners must be taken into the account. Even though the distribution of the strain, stress, and displacement fields is more complex, the model achieves to maintain a success rate around 75% for both damage localization and ply-level identification. It should be noted that due to the complexity of the so told fields, high precision strain gauges, at least up to precision of $1\mu\varepsilon$, would be required in order to produce this result in real-world application.

Chapter 6

Conclusion and Implications

6.1 General Conclusions

A novel approach for damage localization and ply-level identification for composite structures has been developed in this study. Two FEM models are produced and three numerical studies are performed. The data is generated through FEM software and processed with Python. As part of the feature engineering process, key features were extracted from the original datasets, and additional derived features were constructed to enhance the discriminative power of the input data. These features were then used to train various machine learning models, some implemented within ensemble structures, under a supervised learning framework. The proposed numerical studies are tested with different test data, and the results are provided.

After testing the models, valuable insights are obtained regarding the predictive capability, robustness under noise, and generalizability of different machine learning models. Some machine learning models are discovered to be better at predicting and localizing damages in composite structures. On the other hand, a limitation is acknowledged on the first numerical study. Although, the machine learning model GNN thought to be a perfect fit for the damage localization process, it is found out that bigger datasets are required to train this model.

Other two numerical cases produced valuable results in terms of advanced damage localization in composite materials. The ensemble method in second numerical case achieved 80% success rate at damage localization and 92% success rate at identifying the damaged ply. Similarly, the third numerical case achieved a success rate of 73% at localization and 79% at ply-level identification. Even though the success rates are slightly lower than the second numerical case, more complex distribution of strain, stress, and displacement fields due to stiffeners must be considered. This numerical case demonstrates the proposed methodology's ability to localize the damages.

Compiling the results obtained, the technical feasibility of the proposed strategy in

detecting and localizing the damages in composite structures to a ply-level degree is proven with this study.

6.2 Practical Implications

The study provides several practical implications for the real-world implementation of damage detection and localization strategies in composite structures. While the proposed methodology demonstrates high potential for Structural Health Monitoring (SHM) systems, it should be noted that not all input features used in this study are directly measurable in practical settings. For example, when using only strain gauges, displacement and stress data are generally not directly measurable and often require numerical reconstruction or model-based estimation techniques. Nevertheless, with the development of digital twin approaches or real-time simulation tools, such parameters can be approximated with sufficient accuracy. Therefore, the methodology remains promising for practical deployment, especially in high-value applications where enhanced sensing and modeling infrastructure is available.

Considering such limitations are addressed through different techniques, the proposed methodology of ensemble structure demonstrates strong potential for integration into Structural Health Monitoring (SHM) systems. Since the model operates based on strain, stress, and displacement field data, which are obtainable by embedded sensors and inverse techniques, it can be used in real-time monitoring scenarios for aerospace, automotive, or civil engineering applications. The advanced ability to localize the damage down to ply-level allows for more accurate and efficient repair and maintenance decisions.

Also, the use of FEM simulations combined with supervised machine learning techniques offers a robust framework for data-driven diagnostics. This can be applied in the early design stages of composite materials, enabling virtual testing and reducing the need for costly physical experiments.

Furthermore, the comparison of different machine learning models provide valuable guidance for model selection in future SHM applications. The proposed ensemble method have shown high performance, even in complex scenarios. On the other hand, graph-based neural networks were found to require greater datasets in terms of size to reach their full potential.

Finally, the successful implementation of the idea in a complex case with stiffeners proves the generalizability of the methodology. This opens the door to applying the technique across a wide variety of composite structures with different geometries and loading conditions.

In summary, this study not only validates a novel damage localization methodology but also lays the theoretical groundwork for practical deployment in real-world engineering systems where safety, reliability, and precision are critical.

6.3 Suggestions for Future Work

For future studies, the limitations of this study can provide a starting point. First and foremost, an experimental study verifying the real-world applicability of the proposed methodology is required. Furthermore, the displacement and stress fields, which are critical for machine learning, cannot be directly measured in practice and thus require indirect estimation through different methods (inverse methods, numerical modeling etc.), which introduces additional complexity and potential sources of error. Another study focusing on reducing this error would be valuable.

More emphasis can be given to other machine learning algorithms. Although, the proposed models provide a high performance in terms of localization of the damage, much better systems in terms of precision, prediction speed, robustness under noisy conditions might be developed. Different structures, including ensemble methods, can be examined, and more efficient solutions might be discovered.

Higher importance should be given to graph-neural networks (GNNs) in the future studies. Although the results obtained in this study are poor, the working principle of the GNNs is a good fit for advanced damage localization. Bigger datasets must be obtained and the performance of GNNs for damage localization should be studied. Also, a study focusing on hyper-parameter optimization could be considered.

More complex geometries must be studied and tested with different machine learning algorithms embedded in the ensemble structure. Since the classification capacity of the machine learning models differ, an optimization study focusing on the relation between the model complexity and the required classification capacity would be helpful to the literature.

Chapter 7

References

[1] H. Speckmann, "Structural health monitoring (shm) – overview on airbus activities," in *16th World Conference on Nondestructive Testing (WCNDT)*. Montreal, Canada: e-Journal of Nondestructive Testing, 2004. [Online]. Available: https://www.ndt.net/?id=2084

[2] E. Figueiredo and J. Brownjohn, "Three decades of statistical pattern recognition paradigm for shm of bridges," *Structural Health Monitoring*, vol. 21, no. 6, pp. 3018–3054, 2022. [Online]. Available: https://doi.org/10.1177/14759217221075241

[3] N. J. Dodda, "Many-to-one: Transformer-based unsupervised anomaly detection and localization on industrial images," Electronic Theses and Dissertations, University of South Florida, 2023. [Online]. Available: https://digitalcommons.usf.edu/etd/9269

[4] Inspectioneering, "How machine learning is changing the data organization game," June 2022, accessed: 2025-04-10. [Online]. Available: https://inspectioneering.com/blog/2022-06-13/10152/how-machine-learning-is-changing-the-data-organization-game

[5] K. Senthil, A. Arockiarajan, R. Palaninathan, B. Santhosh, and K. Usha, "Defects in composite structures: Its effects and prediction methods – a comprehensive review," *Composite Structures*, vol. 106, pp. 139–149, 2013. [Online]. Available: https://www.sciencedirect.com/science/article/pii/S0263822313002845

[6] Composite Materials Hub, "Defects in composite materials," https://compositematerialshub.com/defects-composite-materials/, 2025, accessed: 2025-06-13.

[7] R. Talreja, *On Failure Theories for Composite Materials*, 05 2016, vol. 60, pp. 379–388.

[8] J. Shi, S. Liu, F. Liu, and G. Xun, "Multi-mode ultrasonic visualization of

porosity in composites using a focused transducer with high sensitivity and near-surface resolution," *Composites Part C: Open Access*, vol. 4, p. 100104, 2021. [Online]. Available: https://www.sciencedirect.com/science/article/pii/S2666682020301043

[9] V. S. and H. Murthy, "Damage characterization and fatigue modeling of cfrp subjected to cyclic loading," *Composite Structures*, vol. 202, 06 2018.

[10] R. B. Heslehurst, *Defects and Damage in Composite Materials and Structures*, 1st ed. CRC Press, 2014. [Online]. Available: https://doi.org/10.1201/b16765

[11] C. González, J. Vilatela, J. Molina-Aldareguía, C. Lopes, and J. LLorca, "Structural composites for multifunctional applications: Current challenges and future trends," *Progress in Materials Science*, vol. 89, pp. 194–251, 2017. [Online]. Available: https://www.sciencedirect.com/science/article/pii/S0079642517300415

[12] M. Bhong, T. K. Khan, K. Devade, B. Vijay Krishna, S. Sura, H. Eftikhaar, H. Pal Thethi, and N. Gupta, "Review of composite materials and applications," *Materials Today: Proceedings*, 2023. [Online]. Available: https://www.sciencedirect.com/science/article/pii/S2214785323049313

[13] M. Nachtane, M. Tarfaoui, M. a. Abichou, A. Vetcher, M. Rouway, A. Aâmir, H. Mouadili, H. Laaouidi, and H. Naanani, "An overview of the recent advances in composite materials and artificial intelligence for hydrogen storage vessels design," *Journal of Composites Science*, vol. 7, no. 3, 2023. [Online]. Available: https://www.mdpi.com/2504-477X/7/3/119

[14] Hussain, Laeth, Praveen, Ragavu, Sreerench, Pahwa, Shilpa, Jain, Alok, R J, Anandhi, and Praveena, K., "The development of composites materials: From conventional to innovative uses," *E3S Web of Conf.*, vol. 529, p. 01050, 2024. [Online]. Available: https://doi.org/10.1051/e3sconf/202452901050

[15] M. Mollineaux and R. Rajagopal, "Structural health monitoring of progressive damage," *Earthquake Engineering & Structural Dynamics*, vol. 44, no. 4, pp. 583–600, 2015. [Online]. Available: https://onlinelibrary.wiley.com/doi/abs/10.1002/eqe.2562

[16] S. Hassani, M. Mousavi, and A. H. Gandomi, "Structural health monitoring in composite structures: A comprehensive review," *Sensors*, vol. 22, no. 1, 2022. [Online]. Available: https://www.mdpi.com/1424-8220/22/1/153

[17] C. R. Farrar, S. W. Doebling, and D. A. Nix, "Vibration-based structural damage identification," *Philosophical Transactions: Mathematical, Physical and Engineering Sciences*, vol. 359, no. 1778, pp. 131–149, 2001. [Online]. Available: http://www.jstor.org/stable/3066397

[18] Y. Liu and S. Nayak, "Structural health monitoring: State of the art and perspectives," *JOM*, vol. 64, no. 7, pp. 789–792, Jul 2012. [Online]. Available:

https://doi.org/10.1007/s11837-012-0370-9

[19] G. Ding, W. Song, X. Gao, and H. Cao, "Damage detection in holed carbon fiber composite laminates using embedded fiber bragg grating sensors based on strain information," *Shock and Vibration*, vol. 2020, pp. 1–11, 12 2020.

[20] J. Holmes, S. Sommacal, R. Das, Z. Stachurski, and P. Compston, "Digital image and volume correlation for deformation and damage characterisation of fibre-reinforced composites: A review," *Composite Structures*, vol. 315, p. 116994, 2023. [Online]. Available: https://www.sciencedirect.com/science/article/pii/S0263822323003380

[21] M. M. Azad, O. Munyaneza, J. Jung, J. W. Sohn, J. W. Han, and H. S. Kim, "Damage localization and severity assessment in composite structures using deep learning based on lamb waves," *Sensors (Basel, Switzerland)*, vol. 24, 2024. [Online]. Available: https://api.semanticscholar.org/CorpusID:274861585

[22] S. Ručevskis, T. Rogala, and A. Katunin, "Monitoring of damage in composite structures using an optimized sensor network: A data-driven experimental approach," *Sensors*, vol. 23, no. 4, 2023. [Online]. Available: https://www.mdpi.com/1424-8220/23/4/2290

[23] Y. Li and Z. Sharif-Khodaei, "A novel damage detection method for carbon fibre reinforced polymer structures based on distributed strain measurements with fibre optical sensor," *Mechanical Systems and Signal Processing*, vol. 208, p. 110954, 2024. [Online]. Available: https://www.sciencedirect.com/science/article/pii/S0888327023008622

[24] M. J. M. Fikry, Y. Arai, R. Inoue, V. Vinogradov, K. T. Tan, and S. Ogihara, "Damage behavior in unidirectional cfrp laminates with ply discontinuity," *Applied Composite Materials*, Mar 2025. [Online]. Available: https://doi.org/10.1007/s10443-025-10320-w

[25] V. R. Gharehbaghi, E. Noroozinejad Farsangi, M. Noori, T. Y. Yang, S. Li, A. Nguyen, C. Málaga-Chuquitaype, P. Gardoni, and S. Mirjalili, "A critical review on structural health monitoring: Definitions, methods, and perspectives," *Archives of Computational Methods in Engineering*, vol. 29, no. 4, pp. 2209–2235, Jun 2022. [Online]. Available: https://doi.org/10.1007/s11831-021-09665-9

[26] C. Farrar and K. Worden, *Structural Health Monitoring A Machine Learning Perspective*, 01 2013.

[27] J. L. Beck and L. S. Katafygiotis, "Probabilistic System Identification and Health Monitoring of Structures," Aug. 2023.

[28] A. Mita, "Emerging needs in japan for health monitoring technologies in civil and building structures," 1999. [Online]. Available: https://api.semanticscholar.org/CorpusID:54704957

[29] F. Semperlotti, "Structural damage detection via nonlinear system identification and structural intensity methods," Doctoral Dissertation, The Pennsylvania State University, 2009.

[30] B. Basu, O. S. Bursi, F. Casciati, S. Casciati, A. E. Del Grosso, M. Domaneschi, L. Faravelli, J. Holnicki-Szulc, H. Irschik, M. Krommer, M. Lepidi, A. Martelli, B. Ozturk, F. Pozo, G. Pujol, Z. Rakicevic, and J. Rodellar, "A european association for the control of structures joint perspective. recent studies in civil structural control across europe," *Structural Control and Health Monitoring*, vol. 21, no. 12, pp. 1414–1436, 2014. [Online]. Available: https://onlinelibrary.wiley.com/doi/abs/10.1002/stc.1652

[31] E. Aydin, B. Ozturk, E. Noroozinejad Farsangi, and A. Bogdanovic, "Editorial: New trends and developments on Structural Control & Health Monitoring," *Frontiers in Built Environment*, vol. 6, 2020. [Online]. Available: https://www.frontiersin.org/articles/10.3389/fbuil.2020.00053

[32] K. Worden and G. Manson, "The application of machine learning to structural health monitoring," *Philosophical Transactions of the Royal Society A: Mathematical, Physical and Engineering Sciences*, vol. 365, no. 1851, pp. 515–537, 2007. [Online]. Available: https://royalsocietypublishing.org/doi/abs/10.1098/rsta.2006.1938

[33] M. I. Friswell, "Damage identification using inverse methods," *Philosophical Transactions of the Royal Society A: Mathematical, Physical and Engineering Sciences*, vol. 365, no. 1851, pp. 393–410, 2007. [Online]. Available: https://royalsocietypublishing.org/doi/abs/10.1098/rsta.2006.1930

[34] T. Marwala, "Finite element model updating using wavelet data and genetic algorithm," *Journal of Aircraft*, vol. 39, no. 4, pp. 709–711, 2002. [Online]. Available: https://doi.org/10.2514/2.2985

[35] H. Sohn, C. R. Farrar, F. M. Hemez, and J. J. Czarnecki, "A review of structural health review of structural health monitoring literature 1996-2001." Los Alamos National Laboratory (LANL), Los Alamos, NM (United States), 01 2002. [Online]. Available: https://www.osti.gov/biblio/976152

[36] P. Cao, Q. Shuai, and J. Tang, "Structural damage identification using piezoelectric impedance measurement with sparse inverse analysis," *Smart Materials and Structures*, vol. 27, 02 2018.

[37] E. Z. Moore, J. M. Nichols, and K. D. Murphy, "Model-based shm: Demonstration of identification of a crack in a thin plate using free vibration data," *Mechanical Systems and Signal Processing*, vol. 29, pp. 284–295, 2012. [Online]. Available: https://www.sciencedirect.com/science/article/pii/S0888327011003906

[38] R. Zhao, R. Yan, Z. Chen, K. Mao, P. Wang, and R. X. Gao, "Deep learning and its applications to machine health monitoring," *Mechanical*

Systems and Signal Processing, vol. 115, pp. 213–237, 2019. [Online]. Available: https://www.sciencedirect.com/science/article/pii/S0888327018303108

[39] Q.-A. Wang, Y. Dai, Z.-G. Ma, Y.-Q. Ni, J.-Q. Tang, X.-Q. Xu, and Z.-Y. Wu, "Towards probabilistic data-driven damage detection in shm using sparse bayesian learning scheme," *Structural Control and Health Monitoring*, vol. 29, no. 11, p. e3070, 2022. [Online]. Available: https://onlinelibrary.wiley.com/doi/abs/10.1002/stc.3070

[40] M. Döhler, F. Hille, and L. Mevel, *Vibration-Based Monitoring of Civil Structures with Subspace-Based Damage Detection*. Cham: Springer International Publishing, 2018, pp. 307–326. [Online]. Available: https://doi.org/10.1007/978-3-319-68646-2_14

[41] B. Xu, G. Song, and S. Masri, "Damage detection for a frame structure model using vibration displacement measurement," *Structural Health Monitoring*, vol. 11, pp. 281–292, 04 2012.

[42] T. Huang, M. Chaves-Vargas, J.-S. Yang, and K.-U. Schröder, "A baseline-free structural damage indicator based on node displacement of structural mode shapes," *Journal of Sound and Vibration*, vol. 433, pp. 366–384, 10 2018.

[43] R. Ono, T. Ha, and S. Fukada, "Analytical study on damage detection method using displacement influence lines of road bridge slab," *Journal of Civil Structural Health Monitoring*, vol. 9, 09 2019.

[44] F. Huseynov, C.-W. Kim, E. OBrien, J. Brownjohn, D. Hester, and K. Chang, "Bridge damage detection using rotation measurements - experimental validation," *Mechanical Systems and Signal Processing*, vol. 135, 12 2019.

[45] Z. S. Z. Wu, J. Zhang, and M. Noori, *Fiber-optic sensors for infrastructure health monitoring. Volume I, Introduction and fundamental concepts*, 1st ed., ser. Momentum Press sustainable structural systems collection. New York, New York: Momentum Press, LLC, 2019.

[46] Z. J. Wu, Z. S. (Zhishen) and M. Noori, *Fiber-optic sensors for infrastructure health monitoring. Volume II, Methodology and case*, 1st ed., ser. Momentum Press sustainable structural systems collection. New York, New York: Momentum Press, LLC, 2019.

[47] S. Jang, S.-H. Sim, and B. Spencer, "Structural damage detection using static strain data," in *World Forum on Smart Materials and Smart Structures Technology*, 1st ed. CRC Press, 2008, p. 1, eBook.

[48] Y. Zhao, M. Noori, W. A. Altabey, R. Ghiasi, and Z. Wu, "Deep learning-based damage, load and support identification for a composite pipeline by extracting modal macro strains from dynamic excitations," *Applied Sciences*, vol. 8, no. 12, 2018. [Online]. Available: https://www.mdpi.com/2076-3417/8/12/2564

[49] A. Rageh, D. Linzell, and Y. Eftekhar Azam, "Automated, strain-based, output-only bridge damage detection," *Journal of Civil Structural Health Monitoring*, vol. 8, 11 2018.

[50] B. Glišić, D. Hubbell, D. Sigurdardottir, and Y. Yao, "Damage detection and characterization using long-gauge and distributed fiber optic sensors," *Optical Engineering*, vol. 52, pp. 7101–, 08 2013.

[51] G. Tondreau and A. Deraemaeker, "Automated data-based damage localization under ambient vibration using local modal filters and dynamic strain measurements: Experimental applications," *Journal of Sound and Vibration*, vol. 333, no. 26, pp. 7364–7385, 2014. [Online]. Available: https://www.sciencedirect.com/science/article/pii/S0022460X14006737

[52] N. A. J. Lieven, D. J. Ewins, C. R. Farrar, S. W. Doebling, and D. A. Nix, "Vibration–based structural damage identification," *Philosophical Transactions of the Royal Society of London. Series A: Mathematical, Physical and Engineering Sciences*, vol. 359, no. 1778, pp. 131–149, 2001. [Online]. Available: https://royalsocietypublishing.org/doi/abs/10.1098/rsta.2000.0717

[53] K. He and W. Zhu, "Structural damage detection using changes in natural frequencies: Theory and applications," *Journal of Physics: Conference Series*, vol. 305, p. 012054, 07 2011.

[54] B. Monavari, "Shm-based structural deterioration assessment," Doctoral Dissertation, Queensland University of Technology, 2019.

[55] T. Salter and I. Mayes, "Use of vibration analysis in the power generation industry," in *IEE Colloquium on Advanced Vibration Measurements, Techniques and Instrumentation for the Early Prediction of Failure*, 1992, pp. 7/1–711.

[56] P. GAO, T. YU, Y. ZHANG, J. WANG, and J. ZHAI, "Vibration analysis and control technologies of hydraulic pipeline system in aircraft: A review," *Chinese Journal of Aeronautics*, vol. 34, no. 4, pp. 83–114, 2021. [Online]. Available: https://www.sciencedirect.com/science/article/pii/S1000936120303265

[57] S. Neild, "Using non-linear vibration techniques to detect damage in concrete bridges," Doctoral Dissertation, University of Oxford., 2001.

[58] Z. Jassim, N. Ali, F. Mustapha, and N. Abdul Jalil, "A review on the vibration analysis for a damage occurrence of a cantilever beam," *Engineering Failure Analysis*, vol. 31, pp. 442–461, 2013. [Online]. Available: https://www.sciencedirect.com/science/article/pii/S1350630713000770

[59] T. Chu, T. Nguyen, H. Yoo, and J. Wang, "A review of vibration analysis and its applications," *Heliyon*, vol. 10, no. 5, p. e26282, 2024. [Online]. Available: https://www.sciencedirect.com/science/article/pii/S2405844024023132

[60] O. Salawu, "Detection of structural damage through changes in frequency: a

review," *Engineering Structures*, vol. 19, no. 9, pp. 718–723, 1997. [Online]. Available: https://www.sciencedirect.com/science/article/pii/S0141029696001496

[61] B. J. Morgan and R. G. Oesterle, "On-site modal analysis – a new powerful inspection technique," in *Proceedings of the 2nd International Bridge Conference*, Pittsburgh, Pennsylvania, 1994, pp. 108–114.

[62] S. G. Creed, "Assessment of large engineering structures using data collected during in-service loading," in *Structural Assessment*, F. K. Garas, J. L. Clarke, and G. S. T. Armer, Eds. London: Butterworths, 1990, pp. 55–62.

[63] M. Haroon, "Free and forced vibration models," in *Encyclopedia of Structural Health Monitoring*, C. Boller, F.-K. Chang, and Y. Fujino, Eds. Chichester, UK: John Wiley & Sons, 2009, pp. 1–28.

[64] J.-T. Kim, Y.-S. Ryu, H.-M. Cho, and N. Stubbs, "Damage identification in beam-type structures: frequency-based method vs mode-shape-based method," *Engineering Structures*, vol. 25, no. 1, pp. 57–67, 2003. [Online]. Available: https://www.sciencedirect.com/science/article/pii/S0141029602001189

[65] V. Mohan, S. Parivallal, K. Kesavan, B. Arunsundaram, A. K. F. Ahmed, and K. Ravisankar, "Studies on damage detection using frequency change correlation approach for health assessment," *Procedia Engineering*, vol. 86, pp. 503–510, 2014, structural Integrity. [Online]. Available: https://www.sciencedirect.com/science/article/pii/S1877705814020335

[66] L. Kannappan, "Damage detection in structure susing natural frequency measurements," Doctoral Dissertation, University of New South Wales, 2008.

[67] S. W. Doebling, C. R. Farrar, M. B. Prime, and D. W. Shevitz, "Damage identification and health monitoring of structural and mechanical systems from changes in their vibration characteristics: A literature review," Los Alamos National Lab. (LANL), Los Alamos, NM (United States), Tech. Rep., 05 1996. [Online]. Available: https://www.osti.gov/biblio/249299

[68] V. M. Karbhari and F. Ansari, Eds., *Structural Health Monitoring of Civil Infrastructure Systems*. Cambridge, UK: Woodhead Publishing, 2009. [Online]. Available: https://www.sciencedirect.com/book/9781845693923/structural-health-monitoring-of-civil-infrastructure-systems

[69] G. Sha, M. Radzienski, R. Soman, M. Cao, W. Ostachowicz, and W. Xu, "Multiple damage detection in laminated composite beams by data fusion of teager energy operator-wavelet transform mode shapes," *Composite Structures*, vol. 235, p. 111798, 2020. [Online]. Available: https://www.sciencedirect.com/science/article/pii/S0263822319315144

[70] W. Fan and P. Qiao, "Vibration-based damage identification methods: A review and comparative study," *Structural Health Monitoring*, vol. 10, no. 1, pp. 83–111, 2011. [Online]. Available: https://doi.org/10.1177/1475921710365419

[71] "Changes in an orbiter test specimen," in *Proceedings of the Air Force Conference on Aircraft Structural Integrity*, unspecified, pp. 1–6.

[72] A. Gandomi, M. Sahab, A. Rahaei, and M. Gorji, "Development in mode shape-based structural fault identification technique," vol. 5, 01 2008.

[73] M. Pástor, M. Binda, and T. Harčarik, "Modal assurance criterion," *Procedia Engineering*, vol. 48, p. 543–548, 12 2012.

[74] J. G. Chen and O. Büyüköztürk, "A symmetry measure for damage detection with mode shapes," *Journal of Sound and Vibration*, vol. 408, pp. 123–137, 2017. [Online]. Available: https://www.sciencedirect.com/science/article/pii/S0022460X17305461

[75] L. Khoo, P. Mantena, and P. Jadhav, "Structural damage assessment using vibration modal analysis," *Structural Health Monitoring*, vol. 3, pp. 177–194, 06 2004.

[76] Y. An, E. Chatzi, S.-H. Sim, S. Laflamme, B. Blachowski, and J. Ou, "Recent progress and future trends on damage identification methods for bridge structures," *Structural Control and Health Monitoring*, vol. 26, no. 10, p. e2416, 2019, e2416 STC-18-0435.R3. [Online]. Available: https://onlinelibrary.wiley.com/doi/abs/10.1002/stc.2416

[77] P. C. Chang, A. Flatau, and S. C. Liu, "Review paper: Health monitoring of civil infrastructure," *Structural Health Monitoring*, vol. 2, no. 3, pp. 257–267, 2003. [Online]. Available: https://doi.org/10.1177/1475921703036169

[78] K. Roy, "Structural damage identification using mode shape slope and curvature," *Journal of Engineering Mechanics*, vol. 143, no. 9, p. 04017110, 2017. [Online]. Available: https://ascelibrary.org/doi/abs/10.1061/%28ASCE%29EM.1943-7889.0001305

[79] Y. Shokrani, V. K. Dertimanis, E. N. Chatzi, and M. N. Savoia, "On the use of mode shape curvatures for damage localization under varying environmental conditions," *Structural Control and Health Monitoring*, vol. 25, no. 4, p. e2132, 2018, e2132 stc.2132. [Online]. Available: https://onlinelibrary.wiley.com/doi/abs/10.1002/stc.2132

[80] S. Wang and M. X. and, "Modal strain energy-based structural damage identification: A review and comparative study," *Structural Engineering International*, vol. 29, no. 2, pp. 234–248, 2019. [Online]. Available: https://doi.org/10.1080/10168664.2018.1507607

[81] Z. Shi, S. Law, and L. Zhang, "Structural damage localization from modal strain energy change," *Journal of Sound and Vibration*, vol. 218, no. 5, pp. 825–844, 1998. [Online]. Available: https://www.sciencedirect.com/science/article/pii/S0022460X98918788

[82] K.-D. Nguyen, T. H. Chan, D. P. Thambiratnam, and A. Nguyen, "Damage identification in a complex truss structure using modal characteristics correlation method and sensitivity-weighted search space," *Structural Health Monitoring*, vol. 18, no. 1, pp. 49–65, 2019. [Online]. Available: https://doi.org/10.1177/1475921718809471

[83] A. Messina, E. Williams, and T. Contursi, "Structural damage detection by a sensitivity and statistical-based method," *Journal of Sound and Vibration*, vol. 216, no. 5, pp. 791–808, 1998. [Online]. Available: https://www.sciencedirect.com/science/article/pii/S0022460X9891728X

[84] Z. Tan, D. Thambiratnam, T. Chan, and H. Abdul Razak, "Detecting damage in steel beams using modal strain energy based damage index and artificial neural network," *Engineering Failure Analysis*, vol. 79, pp. 253–262, 2017. [Online]. Available: https://www.sciencedirect.com/science/article/pii/S1350630717300523

[85] M. Frizzarin, M. Q. Feng, P. Franchetti, S. Soyoz, and C. Modena, "Damage detection based on damping analysis of ambient vibration data," *Structural Control and Health Monitoring*, vol. 17, no. 4, pp. 368–385, 2010. [Online]. Available: https://onlinelibrary.wiley.com/doi/abs/10.1002/stc.296

[86] D. Montalvão, A. Ribeiro, and J. Duarte-Silva, "A method for the localization of damage in a cfrp plate using damping," *Mechanical Systems and Signal Processing*, vol. 23, no. 6, pp. 1846–1854, 2009, special Issue: Inverse Problems. [Online]. Available: https://www.sciencedirect.com/science/article/pii/S0888327008002100

[87] S. Law, J. Li, and Y. Ding, "Structural response reconstruction with transmissibility concept in frequency domain," *Mechanical Systems and Signal Processing*, vol. 25, no. 3, pp. 952–968, 2011. [Online]. Available: https://www.sciencedirect.com/science/article/pii/S0888327010003195

[88] X. Fang, H. Luo, and J. Tang, "Structural damage detection using neural network with learning rate improvement," *Computers & Structures*, vol. 83, no. 25, pp. 2150–2161, 2005. [Online]. Available: https://www.sciencedirect.com/science/article/pii/S004579490500177X

[89] S. K. Thyagarajan, M. J. Schulz, P. F. Pai, and J. Chung, "Detecting Structural Damage Using Frequency Response Functions," *Journal of Sound Vibration*, vol. 210, no. 1, pp. 162–170, Feb. 1998.

[90] S. Hassani and F. Shadan, "Using incomplete frf measurements for damage detection of structures with closely-spaced eigenvalues," *Measurement*, vol. 188, p. 110388, 2022. [Online]. Available: https://www.sciencedirect.com/science/article/pii/S0263224121012793

[91] R. P. Bandara, T. H. Chan, and D. P. Thambiratnam, "Structural

damage detection method using frequency response functions," *Structural Health Monitoring*, vol. 13, no. 4, pp. 418–429, 2014. [Online]. Available: https://doi.org/10.1177/1475921714522847

[92] A. Tomaszewska, "Influence of statistical errors on damage detection based on structural flexibility and mode shape curvature," *Computers & Structures*, vol. 88, no. 3, pp. 154–164, 2010. [Online]. Available: https://www.sciencedirect.com/science/article/pii/S0045794909002302

[93] W. R. Wickramasinghe, D. P. Thambiratnam, and T. H. Chan, "Damage detection in a suspension bridge using modal flexibility method," *Engineering Failure Analysis*, vol. 107, p. 104194, 2020. [Online]. Available: https://www.sciencedirect.com/science/article/pii/S1350630717307823

[94] D. Luckey, H. Fritz, D. Legatiuk, K. Dragos, and K. Smarsly, "Artificial intelligence techniques for smart city applications," in *Proceedings of the 18th International Conference on Computing in Civil and Building Engineering: ICCCBE 2020*. Springer, 2021, pp. 3–15.

[95] M. Awad and R. Khanna, "Machine learning in action: Examples," in *Efficient learning machines: Theories, concepts, and applications for engineers and system designers*. Springer, 2015, pp. 209–240.

[96] A. C. Müller and S. Guido, *Introduction to machine learning with Python: a guide for data scientists*. " O'Reilly Media, Inc.", 2016.

[97] O. Avci, O. Abdeljaber, S. Kiranyaz, M. Hussein, M. Gabbouj, and D. J. Inman, "A review of vibration-based damage detection in civil structures: From traditional methods to machine learning and deep learning applications," *Mechanical Systems and Signal Processing*, vol. 147, p. 107077, 2021. [Online]. Available: https://www.sciencedirect.com/science/article/pii/S0888327020304635

[98] M. Dusseault and K. Gray, "Mechanisms of stress-induced wellbore damage," 02 1992.

[99] J.-H. Chou and J. Ghaboussi, "Genetic algorithm in structural damage detection," *Computers & Structures*, vol. 79, no. 14, pp. 1335–1353, 2001. [Online]. Available: https://www.sciencedirect.com/science/article/pii/S004579490100027X

[100] A. Rytter, "Vibrational based inspection of civil engineering structures," Aalborg, 1993, ph.D.-Thesis defended publicly at the University of Aalborg, April 20, 1993 PDF for print: 206 pp.

[101] K. Worden and J. Dulieu-Barton, "An overview of intelligent fault detection in systems and structures," *Structural Health Monitoring*, vol. 3, no. 1, pp. 85–98, 2004. [Online]. Available: https://eprints.soton.ac.uk/22716/

[102] C. Farrar and N. Lieven, "Damage prognosis: The future of structural health monitoring," *Philosophical transactions. Series A, Mathematical, physical, and engineering sciences*, vol. 365, pp. 623–32, 12 2006.

[103] B. Rajoub, *Supervised and unsupervised learning*, 01 2020, pp. 51–89.

[104] V. Nasteski, "An overview of the supervised machine learning methods," *HORIZONS.B*, vol. 4, pp. 51–62, 12 2017.

[105] Q. Liu and Y. Wu, "Supervised learning," 01 2012.

[106] R. Caruana and A. Niculescu-Mizil, "An empirical comparison of supervised learning algorithms," *Proceedings of the 23rd international conference on Machine learning - ICML '06*, vol. 2006, pp. 161–168, 06 2006.

[107] S. Kotsiantis, "Supervised machine learning: A review of classification techniques." *Informatica (Slovenia)*, vol. 31, pp. 249–268, 01 2007.

[108] M. J. Rahaman, "A comprehensive review to understand the definitions, advantages, disadvantages and applications of machine learning algorithms," *International Journal of Computer Applications*, vol. 186, pp. 43–47, 07 2024.

[109] C. R. Farrar and K. Worden, "An introduction to structural health monitoring," *Philosophical Transactions of the Royal Society A: Mathematical, Physical and Engineering Sciences*, vol. 365, no. 1851, pp. 303–315, 2007. [Online]. Available: https://royalsocietypublishing.org/doi/abs/10.1098/rsta.2006.1928

[110] S. Naeem, A. Ali, S. Anam, and M. Ahmed, "An unsupervised machine learning algorithms: Comprehensive review," *IJCDS Journal*, vol. 13, pp. 911–921, 04 2023.

[111] M. Usama, J. Qadir, A. Raza, H. Arif, K.-l. A. Yau, Y. Elkhatib, A. Hussain, and A. Al-Fuqaha, "Unsupervised machine learning for networking: Techniques, applications and research challenges," *IEEE Access*, vol. 7, pp. 65 579–65 615, 2019.

[112] P. Rizzo, M. Cammarata, D. Dutta, and K. Harries, "Unsupervised learning algorithm for fatigue crack detection in waveguides," *Smart Materials and Structures*, vol. 18, p. 025016, 01 2009.

[113] H. Sohn, "Effects of environmental and operational variability on structural health monitoring," *Philosophical Transactions of the Royal Society A: Mathematical, Physical and Engineering Sciences*, vol. 365, no. 1851, pp. 539–560, 2007. [Online]. Available: https://royalsocietypublishing.org/doi/abs/10.1098/rsta.2006.1935

[114] C. Farrar, P. Cornwell, S. Doebling, and M. Prime, "Structural health monitoring studies of the alamosa canyon and i-40 bridges," 07 2000.

[115] Y. Ding, A. Li, and T. Liu, "Environmental variability study on the measured responses of runyang cablestayed bridge using wavelet packet analysis," *Science*

in China Series E: Technological Sciences, vol. 51, no. 5, pp. 517–528, May 2008. [Online]. Available: https://doi.org/10.1007/s11431-008-0043-7

[116] F. Magalhães, A. Cunha, and E. Caetano, "Vibration based structural health monitoring of an arch bridge: From automated oma to damage detection," *Mechanical Systems and Signal Processing*, vol. 28, pp. 212–228, 2012, interdisciplinary and Integration Aspects in Structural Health Monitoring. [Online]. Available: https://www.sciencedirect.com/science/article/pii/S0888327011002330

[117] E. Figueiredo, I. Moldovan, A. Santos, P. Campos, and J. C. W. A. Costa, "Finite element–based machine-learning approach to detect damage in bridges under operational and environmental variations," *Journal of Bridge Engineering*, vol. 24, no. 7, p. 04019061, 2019. [Online]. Available: https://ascelibrary.org/doi/abs/10.1061/%28ASCE%29BE.1943-5592.0001432

[118] E. Figueiredo, G. Park, C. R. Farrar, K. Worden, and J. Figueiras, "Machine learning algorithms for damage detection under operational and environmental variability," *Structural Health Monitoring*, vol. 10, no. 6, pp. 559–572, 2011. [Online]. Available: https://doi.org/10.1177/1475921710388971

[119] Y. Lee, H. Kim, S. Min, and H. Yoon, "Structural damage detection using deep learning and fe model updating techniques," *Scientific Reports*, vol. 13, no. 1, p. 18694, Oct 2023. [Online]. Available: https://doi.org/10.1038/s41598-023-46141-9

[120] Dhiraj, A. Agarwal, A. Agrawal, V. Meruane, and K. Sangwan, "Development of a machine learning based model for damage detection, localization and quantification to extend structure life," *Procedia CIRP*, vol. 98, pp. 199–204, 2021, the 28th CIRP Conference on Life Cycle Engineering, March 10 – 12, 2021, Jaipur, India. [Online]. Available: https://www.sciencedirect.com/science/article/pii/S2212827121000536

[121] M. Azimi, A. D. Eslamlou, and G. Pekcan, "Data-driven structural health monitoring and damage detection through deep learning: State-of-the-art review," *Sensors*, vol. 20, no. 10, 2020. [Online]. Available: https://www.mdpi.com/1424-8220/20/10/2778

[122] I. Bayane, J. Leander, and R. Karoumi, "An unsupervised machine learning approach for real-time damage detection in bridges," *Engineering Structures*, vol. 308, p. 117971, 2024. [Online]. Available: https://www.sciencedirect.com/science/article/pii/S0141029624005339

[123] J.-H. Park, J.-T. Kim, D.-S. Hong, D.-D. Ho, and J.-H. Yi, "Sequential damage detection approaches for beams using time-modal features and artificial neural networks," *Journal of Sound and Vibration*, vol. 323, no. 1, pp. 451–474, 2009. [Online]. Available: https://www.sciencedirect.com/science/article/pii/

S0022460X08010109

[124] W. Yeung and J. Smith, "Damage detection in bridges using neural networks for pattern recognition of vibration signatures," *Engineering Structures*, vol. 27, no. 5, pp. 685–698, 2005. [Online]. Available: https://www.sciencedirect.com/science/article/pii/S0141029605000155

[125] F. Parisi, A. Mangini, M. Fanti, and J. M. Adam, "Automated location of steel truss bridge damage using machine learning and raw strain sensor data," *Automation in Construction*, vol. 138, p. 104249, 2022. [Online]. Available: https://www.sciencedirect.com/science/article/pii/S0926580522001224

[126] C. Bigoni and J. S. Hesthaven, "Simulation-based anomaly detection and damage localization: An application to structural health monitoring," *Computer Methods in Applied Mechanics and Engineering*, vol. 363, p. 112896, 2020. [Online]. Available: https://www.sciencedirect.com/science/article/pii/S0045782520300785

[127] D. Kim and M. Philen, "Damage classification using adaboost machine learning for structural health monitoring," in *Sensors and Smart Structures Technologies for Civil, Mechanical, and Aerospace Systems 2011*, vol. 7981. SPIE, 2011, pp. 659–673.

[128] Y. Ying, J. H. Garrett Jr, I. J. Oppenheim, L. Soibelman, J. B. Harley, J. Shi, and Y. Jin, "Toward data-driven structural health monitoring: application of machine learning and signal processing to damage detection," *Journal of Computing in Civil Engineering*, vol. 27, no. 6, pp. 667–680, 2013.

[129] W. Nick, K. Asamene, G. Bullock, A. Esterline, and M. Sundaresan, "A study of machine learning techniques for detecting and classifying structural damage," *International Journal of Machine Learning and Computing*, vol. 5, no. 4, p. 313, 2015.

[130] G. Gui, H. Pan, Z. Lin, Y. Li, and Z. Yuan, "Data-driven support vector machine with optimization techniques for structural health monitoring and damage detection," *KSCE Journal of Civil Engineering*, vol. 21, no. 2, pp. 523–534, Feb 2017. [Online]. Available: https://doi.org/10.1007/s12205-017-1518-5

[131] K. Smarsly, K. Dragos, and J. Wiggenbrock, "Machine learning techniques for structural health monitoring," in *Proceedings of the 8th European workshop on structural health monitoring (EWSHM 2016), Bilbao, Spain*, 2016, pp. 5–8.

[132] R. Hsissou, R. Seghiri, Z. Benzekri, M. Hilali, M. Rafik, and A. Elharfi, "Polymer composite materials: A comprehensive review," *Composite Structures*, vol. 262, p. 113640, 2021. [Online]. Available: https://www.sciencedirect.com/science/article/pii/S026382232100101X

[133] Y. Yan, B. Liu, Y. Xing, E. Carrera, and A. Pagani, "Free vibration analysis of variable stiffness composite laminated beams and plates by novel

hierarchical differential quadrature finite elements," *Composite Structures*, vol. 274, p. 114364, 2021. [Online]. Available: https://www.sciencedirect.com/science/article/pii/S0263822321008266

[134] G. G. Lozano, A. Tiwari, C. Turner, and S. Astwood, "A review on design for manufacture of variable stiffness composite laminates," *Proceedings of the Institution of Mechanical Engineers, Part B: Journal of Engineering Manufacture*, vol. 230, no. 6, pp. 981–992, 2016.

[135] B. Loyola, "Fiber reinforced polymer composite materials: Design application and shm." Sandia National Lab.(SNL-CA), Livermore, CA (United States), Tech. Rep., 2014.

[136] V. V. Bolotin, "Delaminations in composite structures: its origin, buckling, growth and stability," *Composites Part B: Engineering*, vol. 27, no. 2, pp. 129–145, 1996.

[137] D. J. Wilkins, J. R. Eisenmann, R. A. Camin, W. S. Margolis, and R. A. Benson, "Characterizing delamination growth in graphite-epoxy," in *ASTM Special Technical Publication 775*. ASTM International, 1982, pp. 168–183.

[138] A. C. Garg, "Delamination—a damage mode in composite structures," *Engineering Fracture Mechanics*, vol. 29, no. 5, pp. 557–584, 1988. [Online]. Available: https://www.sciencedirect.com/science/article/pii/0013794488901816

[139] P. Patel and V. Chaudhary, "Delamination evaluation in drilling of composite materials – a review," *Materials Today: Proceedings*, vol. 56, pp. 2690–2695, 2022, 3rd International Conference on Contemporary Advances in Mechanical Engineering. [Online]. Available: https://www.sciencedirect.com/science/article/pii/S2214785321061265

[140] E. Pliusys and P. T. Mativenga, "Reducing delamination in micro drilling of carbon composite materials," in *Proceedings of the 38th International MATADOR Conference*, S. Hinduja, P. J. da Silva Bartolo, L. Li, and W.-Y. Jywe, Eds. Cham: Springer International Publishing, 2022, pp. 337–356.

[141] Q. Saghir, A. ur Rehman Shah, S. Kamran Afaq, T. Ahmed, and J.-i. Song, "Effect of machining parameters on surface quality and delamination of carbon/glass/epoxy hybrid composite material during end milling operation," *Journal of Mechanical Science and Technology*, vol. 37, no. 5, pp. 2319–2324, May 2023. [Online]. Available: https://doi.org/10.1007/s12206-023-0408-7

[142] H. Chai, W. Knauss, and C. Babcock, "Observation of damage growth in compressively loaded laminates: The phenomenological aspects of composite-panel-failure under compressive in-plane loading and low-velocity transverse impact are studied experimentally via real-time recording of the failure-propagation event," *Experimental Mechanics*, vol. 23, pp. 329–337, 1983.

[143] K.-S. Kim, A. Segall, and G. S. Springer, "The use of strain measurements for

detecting delaminations in composite laminates," *Composite Structures*, vol. 23, no. 1, pp. 75–84, 1993. [Online]. Available: https://www.sciencedirect.com/science/article/pii/0263822393900763

[144] D. Sarvanos, V. Birman, and D. Hopkins, "Detection of delaminations in composite beams using piezoelectric sensors," in *Adaptive structures forum*, 1994, p. 1754.

[145] A. Muc and A. Stawiarski, "Identification of damages in composite multilayered cylindrical panels with delaminations," *Composite Structures*, vol. 94, no. 5, pp. 1871–1879, 2012. [Online]. Available: https://www.sciencedirect.com/science/article/pii/S0263822311004405

[146] D. Aggelis, N.-M. Barkoula, T. Matikas, and A. Paipetis, "Acoustic structural health monitoring of composite materials : Damage identification and evaluation in cross ply laminates using acoustic emission and ultrasonics," *Composites Science and Technology*, vol. 72, no. 10, pp. 1127–1133, 2012. [Online]. Available: https://www.sciencedirect.com/science/article/pii/S0266353811003770

[147] R. Roy and M. Gherlone, "Delamination and skin-spar debond detection in composite structures using the inverse finite element method," *Materials*, vol. 16, no. 5, 2023. [Online]. Available: https://www.mdpi.com/1996-1944/16/5/1969

[148] R. TALREJA, "Damage mechanics of composite materials," *Composite Materials Series, 9*, 1994.

[149] J. Nairn and S. Hu, "Matrix microcracking," *Composite materials series*, pp. 187–187, 1994.

[150] J. Varna, R. Joffe, N. Akshantala, and R. Talreja, "Damage in composite laminates with off-axis plies," *Composites Science and Technology*, vol. 59, no. 14, pp. 2139–2147, 1999.

[151] M. Kashtalyan and C. Soutis, "Analysis of composite laminates with intra-and interlaminar damage," *Progress in Aerospace Sciences*, vol. 41, no. 2, pp. 152–173, 2005.

[152] S. Abrate, "Matrix cracking in laminated composites: A review," *Composites Engineering*, vol. 1, no. 6, pp. 337–353, 1991. [Online]. Available: https://www.sciencedirect.com/science/article/pii/096195269190039U

[153] J. A. Nairn, "Matrix microcracking in composites," *Polymer matrix composites*, vol. 2, no. 10.1016, pp. B0–08, 2000.

[154] A. Parvizi, K. W. Garrett, and J. E. Bailey, "Constrained cracking in glass fibre-reinforced epoxy cross-ply laminates," *Journal of Materials Science*, vol. 13, no. 1, pp. 195–201, Jan 1978. [Online]. Available: https://doi.org/10.1007/BF00739291

[155] P. Pawar and R. Ganguli, "Matrix crack detection in thin-walled composite beam using genetic fuzzy system," *Journal of Intelligent Material Systems and Struc-*

tures, vol. 16, pp. 395–409, 05 2005.

[156] A. Todoroki, K. Omagari, Y. Shimamura, and H. Kobayashi, "Matrix crack detection of cfrp using electrical resistance change with integrated surface probes," *Composites Science and Technology*, vol. 66, no. 11, pp. 1539–1545, 2006. [Online]. Available: https://www.sciencedirect.com/science/article/pii/S0266353805004537

[157] A. Mardanshahi, V. Nasir, S. Kazemirad, and M. Shokrieh, "Detection and classification of matrix cracking in laminated composites using guided wave propagation and artificial neural networks," *Composite Structures*, vol. 246, p. 112403, 2020. [Online]. Available: https://www.sciencedirect.com/science/article/pii/S0263822319345684

[158] W. H. Prosser, K. E. Jackson, S. Kellas, B. T. Smith, J. McKeon, and A. Friedman, "Advanced waveform-based acoustic emission detection of matrix cracking in composites," *Materials Evaluation*, vol. 53, no. 9, 09 1995. [Online]. Available: https://www.osti.gov/biblio/116140

[159] X. Liu, B. Wang, F. Ai, D. Wei, and L. Bo, "Evaluation of matrix cracking in composite laminates based on anomaly indices," *International Journal of Fatigue*, vol. 140, p. 105841, 2020. [Online]. Available: https://www.sciencedirect.com/science/article/pii/S0142112320303728

[160] S. N. A. B. Safri, M. Sultan, and M. Jawaid, "7 - damage analysis of glass fiber reinforced composites," in *Durability and Life Prediction in Biocomposites, Fibre-Reinforced Composites and Hybrid Composites*, ser. Woodhead Publishing Series in Composites Science and Engineering, M. Jawaid, M. Thariq, and N. Saba, Eds. Woodhead Publishing, 2019, pp. 133–147. [Online]. Available: https://www.sciencedirect.com/science/article/pii/B9780081022900000076

[161] B. Vieille, V. M. Casado, and C. Bouvet, "About the impact behavior of woven-ply carbon fiber-reinforced thermoplastic-and thermosetting-composites: a comparative study," *Composite structures*, vol. 101, pp. 9–21, 2013.

[162] T. Mitrevski, I. H. Marshall, and R. Thomson, "The influence of impactor shape on the damage to composite laminates," *Composite Structures*, vol. 76, no. 1-2, pp. 116–122, 2006.

[163] A. Groszek, "Composite in-service damage assessment," in *Aircraft Airworthiness and Sustainment Conference*. QinetiQ Australia, 2017.

[164] Y. Ma, Y. Yang, T. Sugahara, and H. Hamada, "A study on the failure behavior and mechanical properties of unidirectional fiber reinforced thermosetting and thermoplastic composites," *Composites Part B: Engineering*, vol. 99, pp. 162–172, 2016.

[165] A. Engelbrecht-Wiggans and S. L. Phoenix, "A stochastic model based on fiber breakage and matrix creep for the stress-rupture failure of unidirectional

continuous fiber composites," *International Journal of Fracture*, vol. 217, no. 1, pp. 1–34, Jun 2019. [Online]. Available: https://doi.org/10.1007/s10704-019-00359-9

[166] N. Ativitavas, T. Fowler, and T. Pothisiri, "Identification of fiber breakage in fiber reinforced plastic by low-amplitude filtering of acoustic emission data," *Journal of Nondestructive Evaluation*, vol. 23, pp. 21–36, 01 2004.

[167] S. A. Malik, L. Wang, P. T. Curtis, and G. F. Fernando, "Self-sensing composites: In-situ detection of fibre fracture," *Sensors*, vol. 16, no. 5, 2016. [Online]. Available: https://www.mdpi.com/1424-8220/16/5/615

[168] R. T. Kidangan, C. V. Krishnamurthy, and K. Balasubramaniam, "Identification of the fiber breakage orientation in carbon fiber reinforced polymer composites using induction thermography," *NDT & E International*, vol. 122, p. 102498, 2021. [Online]. Available: https://www.sciencedirect.com/science/article/pii/S0963869521000979

[169] D. J. Pasadas, M. Barzegar, A. L. Ribeiro, and H. G. Ramos, "Locating and imaging fiber breaks in cfrp using guided wave tomography and eddy current testing," *Sensors*, vol. 22, no. 19, 2022. [Online]. Available: https://www.mdpi.com/1424-8220/22/19/7377

[170] G. Fernlund, J. Wells, L. Fahrang, J. Kay, and A. Poursartip, "Causes and remedies for porosity in composite manufacturing," *IOP Conference Series: Materials Science and Engineering*, vol. 139, no. 1, p. 012002, jul 2016. [Online]. Available: https://dx.doi.org/10.1088/1757-899X/139/1/012002

[171] C. Mobuchon, C. Keulen, K. Hsiao, G. Fernlund, and A. Poursartip, "Development of a structured approach to porosity management in composites manufacturing," *International SAMPE Technical Conference*, 01 2014.

[172] A. M. Rubin and K. L. Jerina, "Evaluation of porosity in composite aircraft structures," *Mechanics of Composite Materials*, vol. 30, no. 6, pp. 587–600, Nov 1994. [Online]. Available: https://doi.org/10.1007/BF00821276

[173] E. A. Birt and R. A. Smith, "A review of nde methods for porosity measurement in fibre-reinforced polymer composites," *Insight - Non-Destructive Testing and Condition Monitoring*, vol. 46, no. 11, pp. 681–686, Nov. 2004. [Online]. Available: https://www.ingentaconnect.com/content/bindt/insight/2004/00000046/00000011/art00011

[174] R. Garrett, "Effect of defects on aircraft composite structures," in *AGARD Conference on Characterisation, Analysis and Significance of Defects in Composite Materials*, 1983.

[175] X. Lu, Y. Shen, T. Xu, H. Sun, L. Zhu, J. Zhang, T. Chang, and H.-L. Cui, "Accurate detection of porosity in glass fiber reinforced polymers by terahertz spectroscopy," *Composites Part B: Engineering*, vol. 242, p. 110058,

2022. [Online]. Available: https://www.sciencedirect.com/science/article/pii/S1359836822004346

[176] S. Bayat, A. Jamzad, N. Zobeiry, A. Poursartip, P. Mousavi, and P. Abolmaesumi, "Temporal enhanced ultrasound: A new method for detection of porosity defects in composites," *Composites Part A: Applied Science and Manufacturing*, vol. 164, p. 107259, 2023. [Online]. Available: https://www.sciencedirect.com/science/article/pii/S1359835X22004407

[177] V. Ajith and S. Gopalakrishnan, "Wave propagation in a porous composite beam: Porosity determination, location and quantification," *International Journal of Solids and Structures*, vol. 50, no. 3, pp. 556–569, 2013. [Online]. Available: https://www.sciencedirect.com/science/article/pii/S0020768312004453

[178] T. B. Hudson, P. J. Follis, J. J. Pinakidis, T. Sreekantamurthy, and F. L. Palmieri, "Porosity detection and localization during composite cure inside an autoclave using ultrasonic inspection," *Composites Part A: Applied Science and Manufacturing*, vol. 147, p. 106337, 2021. [Online]. Available: https://www.sciencedirect.com/science/article/pii/S1359835X21000622

[179] W. Kurz, "Debonding along a fiber/matrix interface in a composite," Technische Universiteit Eindhoven, Tech. Rep. 1993.109, 1993.

[180] F. Li, H. Murayama, K. Kageyama, G. Meng, I. Ohsawa, and T. Shirai, "A fiber optic doppler sensor and its application in debonding detection for composite structures," *Sensors*, vol. 10, no. 6, pp. 5975–5993, 2010. [Online]. Available: https://www.mdpi.com/1424-8220/10/6/5975

[181] J. Ahmed, B. Gao, G. Y. Tian, Y. Yang, and Y. C. Fan, "Sparse ensemble matrix factorization for debond detection in cfrp composites using optical thermography," *Infrared Physics & Technology*, vol. 92, pp. 392–401, 2018. [Online]. Available: https://www.sciencedirect.com/science/article/pii/S1350449518302287

[182] Z. Hamam, N. Godin, C. Fusco, A. Doitrand, and T. Monnier, "Acoustic emission signal due to fiber break and fiber matrix debonding in model composite: A computational study," *Applied Sciences*, vol. 11, no. 18, 2021. [Online]. Available: https://www.mdpi.com/2076-3417/11/18/8406

[183] K. Z. Uddin, H. Girard, N. B. Mennie, A. Doitrand, and B. Koohbor, "Simultaneous measurement of fiber-matrix interface debonding and tunneling using a dual-vision experimental setup," *Experimental Mechanics*, vol. 64, no. 9, pp. 1497–1511, Nov 2024. [Online]. Available: https://doi.org/10.1007/s11340-024-01111-8

[184] T. Wierzbicki, "Structural mechanics," Massachusetts Institute of Technology: MIT OpenCourseWare, 2013. [Online]. Available: https://ocw.mit.edu/courses/2-080j-structural-mechanics-fall-2013/

[185] B. D. Leahy, N. Y. Lin, and I. Cohen, "Quantitative light microscopy

of dense suspensions: Colloid science at the next decimal place," *Current Opinion in Colloid & Interface Science*, vol. 34, pp. 32–46, 2018, microscopy Methods: You Can Observe a Lot by Watching. [Online]. Available: https://www.sciencedirect.com/science/article/pii/S1359029417301711

[186] D. Dye, "Continuum mechanics," Imperial College, 2013-14. [Online]. Available: https://dyedavid.com/wp-content/uploads/2014/01/203b-stresstensors-dd-notes.pdf

[187] R. Maclin and D. W. Opitz, "Popular ensemble methods: An empirical study," *CoRR*, vol. abs/1106.0257, 2011. [Online]. Available: http://arxiv.org/abs/1106.0257

[188] Z. Yang and Z. Yang, "6.01 - artificial neural networks," in *Comprehensive Biomedical Physics*, A. Brahme, Ed. Oxford: Elsevier, 2014, pp. 1–17. [Online]. Available: https://www.sciencedirect.com/science/article/pii/B9780444536327011011

[189] C. Bishop, *Pattern Recognition and Machine Learning*, 01 2006, vol. 16, pp. 140–155.

[190] Q. Xu, H. Hofmeyer, J. Maljaars, and R. A. P. van Herpen, "Pyrolysis modelling of insulation material in coupled fire-structure simulations," *Journal of Building Engineering*, vol. 98, p. 110969, 2024.

Chapter 8

Appendix

8.1 Appendix A

Table 8.1: Comparison of SHM Methods Based on Sensor Type, Damage Type, and Layer Detection Capability

Author	**Method**	**Sensor Type**	**Damage Type**	**L2**	**L3**	**Exp. Verified**	**Sensor No Opt.**	**Year**
Xu, Song and Masri	Displacement based	Non-contact laser displacement sensors	Joint connection damages	✓	✓	✓	✗	2012
Huang et al.	Displacement based	Accelerometer	Cracks	✓[1]	✗	✓	✓	2018
Ono, Ha and Fukada	Displacement based	Displacement meter	Unspecified[2]	✓	✗	✗	✗	2019
Huseynov et al.	Displacement based	Inclinometer	Unspecified[2]	✓	✗	✓	✗	2019
Jang, Sim and Spencer Jr.	Strain based	Unspecified	Unspecified[2]	✓	✗	✓	✗	2008
Zhao et al.	Strain based	Long gauge sensors	Unspecified[2]	✓	✓	✗	✗	2018
Rageh, Linzell and Azam	Strain based	Strain gauges	Unspecified[2]	✓	✗	✓	✗	2018
Glišić et al.	Strain based	Fiber Bragg-grating sensors	Crack, ruptures	✓	✗	✓	✗	2013
Tondreau and Deraemaeker	Strain based	PVDF sensors	Crack	✓	✗	✓	✗	2014
Kim et al.	Natural frequency based	Unspecified	Crack	✓	✗	✗	✗	2002
Mohan et al.	Natural frequency based	Unspecified	Material loss	✓	✗	✗	✗	2014

Continued on next page

Author	Method	Sensor Type	Damage Type	L2	L3	Exp. Verified	Sensor No Opt.	Year
Chen and Buyukozturk	Mode-shape based	Accelerometer	Corrosion, material loss	✓	✗	✓	✗	2017
Khoo, Mantena and Jadhav	Mode-shape based	Laser vibrometer	Material loss, termite degradation[3]	✓	✗	✓	✗	2004
Roy	Mode-shape curvature based	Unspecified	Unspecified[2]	✓	✗	✓	✗	2017
Shokrani et al.	Mode-shape curvature based	Unspecified	Unspecified[2]	✓	✓	✗	✗	2016
Zhang, Shi and Law	Modal strain energies based	Unspecified	Unspecified[2]	✓	✗	✗	✗	1998
Nyugen et al.	Modal strain energies based	Accelerometer	Joint connection damages	✓	✓	✓	✗	2018
Tan et al.	Modal strain energies based	Unspecified	Unspecified[2]	✓	✓	✓	✗	2017
Frizzarin et al.	Damping analysis	Accelerometer	Seismic damages	✓	✓	✓	✗	2010
Montalvão, Ribeiro and Silva	Damping analysis	Unspecified	Delamination[4]	✓	✗	✗	✗	2008
Hassani and Shadan	FRFs	Unspecified	Unspecified[2]	✓	✗	✗	✗	2022
Bandara, Chan, Thambiratnam	FRFs	Accelerometer	Unspecified[2]	✓	✓	✓	✗	2014
Tomaszewska	Matrix-based	Unspecified	Unspecified[2]	✓	✓	✗	✗	2010
Wickramasinghe, Thambiratnam, Chan	Matrix-based	Unspecified	Unspecified[2]	✓	✓	✗	✗	2020

1: Localization only on 2D. 2: Damage is modeled as stiffness reduction but type is not specified. 3: This damage is caused by termites. 4: This study works on composites.

8.2 Appendix B

Table 8.2: Comparison of Studies on Machine Learning Approaches for Damage Detection

Author	**Data**	**Machine Learning Model**	**Applied Structure**	**Supervised-Unsupervised**	**L2**	**L3**	**Exp. Verified**	**Year**
Bayane et al.	Strain, acceleration measurements	Anomaly detection algorithms[1]	Bridge	Unsupervised	✗	✗	✓	2024
Park et al.[2]	Acceleration measurements	Artificial neural network (ANN)	Beams	Supervised	✓	✓	✓	2009
Yeung and Smith	Vibration data	Probabilistic resource allocation network (PRAN) and DIGNET network	Bridge	Unsupervised	✗	✗	✗	2004
Parisi et al.	Strain gauges	k-nearest neighbors and convolutional neural network (CNN)	Bridge	Supervised	✓	✓	✗	2022
Bigoni et al.[3]	Guided waves	Support vector machine (SVM)	Beam, complex structures	Semi-supervised	✓	✓	✗	2019
Kim and Philen	Various time-frequency measurements	AdaBoost	Metallic 2D plates	Supervised	✓	✗	✓	2011
Ying et al.	Ultrasonic measurements	Support vector machines (SVM) and AdaBoost	Pipes	Supervised	✗	✗	✓	2012
Smarsly et al.[4]	Acceleration measurements	Artificial neural network (ANN)	Complex steel structure	Supervised	✗	✗	✓	2016

Continued on next page

Author	**Data**	**Machine Learning Model**	**Applied Structure**	**Supervised-Unsupervised**	**L2**	**L3**	**Exp. Verified**	**Year**
Nick et al.[5]	Acoustic emission (AE)	SVM, naïve Bayes, FNN, k-means, and SOMs	Unspecified	Supervised and unsupervised	✓	✓	✗	2015
Gui et al.	Acceleration measurements	SVMs with different optimization methods	Frame structure	Unspecified	✓	✗	✓	2016

1: Isolation forest, one-class support vector machine, local outlier factor, and Mahalanobis distance. 2: Requires training with real data. 3: States undamaged state is labeled, and the rest unlabeled. 4: Focuses on sensor problems and miscalibrations. 5: Damage presence and localization results are not given as accuracy, but as time metrics.

8.3 Appendix C

Table 8.3: Comparison of Studies on Damage Detection in Composites

Author	**Damage Type**	**Damage Cause**	**Sensor Type**	**Material**	**L2**	**L3**	**Exp. Verified**	**Year**
Chai et al.[1]	Delamination	Impact	High speed cameras	Unidirectional carbon/epoxy prepeg	✗	✗	✓	1983
Kim et al.	Delamination	Indentor	Strain gauges	Unidirectional carbon/epoxy prepeg	✓	✗	✓	1993
Saravanos et al.[2]	Delamination	Unspecified	Piezoelectric sensors	T300/934	✓	✗	✓	1994
Muc and Stawiarski[3]	Delamination	Unspecified[4]	Piezoelectric sensors	Unspecified	✓	✗	✓	2011
Aggelis et al.	Delamination, matrix cracking	Small inclusions	Acoustic emission	Unidirectional glass/epoxy	✗	✗	✓	2012
Gherlone and Roy	Delamination	Numerically modeled	Fiber-optic strain sensors	CFRP	✓	✗	✗	2023
Prashant et al.	Matrix cracking	Numerically modeled	Unspecified	Glass/epoxy	✓	✓	✗	2005
Todoroki et al.	Matrix cracking	Tensile loading	Electrical probes	CFRP	✗	✗	✓	2006
Mardanshahi	Matrix cracking	Tensile loading	Digital oscilloscope	Glass/epoxy	✗	✓	✓	2020
Prosser et al.	Matrix cracking	Tensile loading	Acoustic emission	CFRP	✓	✗	✓	1995
Liu et al.	Matrix cracking	Tensile loading	Piezoelectric sensors	CFRP	✗	✓	✓	2020
Ativitavas et al.[5]	Fiber breakage	Tensile loading	Acoustic emission	FRP-vinly ester resin reinforced with glass fibers	✗	✗	✓	2004

Continued on next page

Author	Damage Type	Damage Cause	Sensor Type	Material	L2	L3	Exp. Verified	Year
Malik et al.	Fiber breakage	Tensile loading	R15 Acoustic emission sensor	Epoxy/amine with custom fibers	✓[6]	✗	✓	2016
Kidangan et al.	Fiber breakage	Inclusions	Thermal camera	CFRP	✓	✗	✓	2021
Pasadas et al.	Fiber breakage	Inclusions	Oscilloscope	CFRP	✓	✗	✓	2022
Lu et al.	Porosity[7]	Varying manufacturing conditions	Spectrometer	GFRP	✓	✗	✓	2022
Bayat et al.	Porosity[8]	Varying manufacturing conditions	Digital microscope	AS4/8552	✓	✗	✓	2023
Ajith and Gopalakrishnan	Porosity	Varying curing pressure	Piezoelectric sensors	CFRP	✓	✗	✓	2012
Hudson et al.	Porosity	Unspecified	High temperature transducers	CFRP	✓	✗	✓	2021
Li et al.	Fiber-matrix debonding[9]	Tensile loading	Fiber-optic Doppler (FOD)	CFRP	✗	✗	✓	2010
Ahmed et al.	Debonding[10]	Unspecified	Infrared camera	CFRP	✓	✗	✓	2018
Hamam et al.[11]	Fiber-matrix debonding, fiber breakage	Simulated and tensile loading	Resonant sensors	Epoxy/amine matrix with long carbon fibers	✗	✗	✓	2021
Uddin et al.[12]	Fiber-matrix debonding	Tensile loading	Digital image correlation setup	GFRP	✗	✗	✓	2024

1: Focuses on damage growth, not detection. 2: Based on CLT. 3: Uses only one sensor. 4: Properties given in text. 5: Does not focus on localization. 6: Detects the broken fiber, not location. 7: Predicts porosity density. 8: Predicts porosity density. 9: Only focuses on lap joints. 10: Focuses on multiple subsurface defects, not only fiber-matrix debonding. 11: Optimizes sensor location, not number. 12: Does not focus on localization.

8.4 Appendix D

The data used in the study can be accessed by scanning the QR code below.